Library
TA
1
U58

Journal of Research

of the

National Bureau of Standards

JANUARY 1949

VOLUME 42 NUMBER 1

PERIODICALS OF THE NATIONAL BUREAU OF STANDARDS

Journal of Research

The National Bureau of Standards is the principal agency of the Federal Government for fundamental research in physics, chemistry, and engineering. It has the custody of the national standards of physical measurement in terms of which all working standards in research laboratories and industry are calibrated, and carries on necessary research leading to improvement in such standards and methods of measurement. It also has a general responsibility for basic research in physics, chemistry, and engineering, and for development of improved methods for testing materials and equipment. It determines physical constants and properties of materials, tests and calibrates standard measuring apparatus and reference standards, and studies technical processes. The results of the Bureau's research and investigations are published in the JOURNAL OF RESEARCH.

Research Papers

Reprints of individual articles appearing in the JOURNAL OF RESEARCH. They are made available to serve the needs of research workers, technical groups, and others for the separate papers relating to the special subjects in which they are interested.

Technical News Bulletin

Contains short but complete summaries of research, development, and testing in progress at the Bureau, accounts of the Bureau's national and international activities, scientific and technical announcements of new plans and programs, and a list of publications by members of the staff. It is a prompt and reliable source of official information of value to those who desire to keep in touch with the general activities of the Bureau.

Basic Radio Propagation Predictions

The CRPL-D series, Basic Radio Propagation Predictions, is issued as a monthly publication for those concerned with radio communication in determining the best sky-wave frequencies over any path at any time of day for average conditions for the month of prediction, which is made 3 months in advance. Charts of extraordinary-wave critical frequency for the F2 layer, of maximum usable frequency for a transmission distance of 4,000 km, and of percentage of time occurrence for transmission by sporadic E in excess of 15 Mc, for a distance of 2,000 km, are included.

ANNUAL SUBSCRIPTION Send order, with remittance, to Superintendent of Documents U. S. Government Printing Office, Washington 25, D. C.	United States, Canada, Cuba, Mexico, Newfoundland, Republic of Panama	Other countries
JOURNAL OF RESEARCH of the National Bureau of Standards:		
12 monthly issues (2 volumes), paper covers	$4.50	$5.50
Bound volume (½ year, 1 volume), blue buckram	3.00	3.50
RESEARCH PAPERS	(*)	(*)
TECHNICAL NEWS BULLETIN, 12 monthly issues	1.00	1.25
BASIC RADIO PROPAGATION PREDICTIONS, 12 monthly issues	1.00	1.25

*The prices of the separate Research Papers appearing in this JOURNAL are given in the Contents. If 100 or more copies of any separate are ordered, a discount of 25 per cent is allowed. Those who desire copies of separate Research Papers should send their orders and remittances without delay to the Superintendent of Documents, U. S. Government Printing Office, Washington 25, D. C. This will aid him in determining the number of copies to be printed for sale. Research Papers are not printed from electrotypes and usually no more reprints can be had when the first and only printing is exhausted.

The printing of this publication has been approved by the Director of the Bureau of the Budget, April 23, 1947.

U. S. DEPARTMENT OF COMMERCE
Charles Sawyer, Secretary
NATIONAL BUREAU OF STANDARDS
E. U. Condon, Director

JANUARY 1949
VOLUME 42
NUMBER 1

JOURNAL OF RESEARCH

of the

NATIONAL BUREAU OF STANDARDS

Contents

RP		Page
1946	Response functions for types of vision according to the Müller theory. Deane B. Judd. (Price 10 cents)	1
1947	Rate of shrinkage of tendon collagen: Heat, entropy, and free energy of activation of the shrinkage of untreated tendon; Effect of acid, salt, pickle, and tannage on the activation of tendon collagen. Charles E. Weir. (Price 10 cents)	17
1948	Kinetic study of the reaction of carbon adsorbents with oxygen. William V. Loebenstein, Leland F. Gleysteen, and Victor R. Deitz. (Price 10 cents)	33
1949	Weather resistance of porcelain enamels exposed for seven years. William N. Harrison and Dwight G. Moore. (Price 10 cents)	43
1950	On the precision of a certain procedure of numerical integration. Harry D. Huskey and Douglas R. Hartree. (Price 10 cents)	57
1951	Treatment of leather with synthetic resins. Rene Oehler and Timothy J. Kilduff. (Price 10 cents)	63
1952	Noise spectrum of a diode with a retarding field. Jacob J. Freeman. (Price 10 cents)	75

For sale by the Superintendent of Documents, U. S. Government Printing Office, Washington 25, D. C. - Price 50 cents
$4.50 per year on subscription

UNITED STATES GOVERNMENT PRINTING OFFICE, WASHINGTON : 1949

U. S. Department of Commerce
National Bureau of Standards

Research Paper RP1946
Volume 42, January 1949

Part of the Journal of Research of the National Bureau of Standards

Response Functions for Types of Vision According to the Müller Theory

By Deane B. Judd

According to the Müller theory of vision there are three stages in the visual process, an initial photochemical stage, an intermediate chemical stage relating to the chromatic aspect, and a final stage of excitations of the optic-nerve fibers. By taking advantage of recent precise information regarding the metamers characteristic of normal, protanopic, and deuteranopic vision there have been derived the spectral variations of the responses for each stage as functions of wavelength. These response functions account precisely for the same normal metamers as the ICI standard observer, and closely for the same confusions by color-blind observers as the simpler König theory. Furthermore these functions describe chromatic thresholds of the normal eye (Abney, Priest-Brickwedde) as a gradual approach to tritanopic vision as field size and luminance are decreased.

I. Introduction

In the ninteenth century, two rival theories of vision monopolized most of the interest of investigators. One of these is the Young-Helmholtz three-components formulation; the other is the Hering opponent-colors theory. The discovery of the facts of red-green blindness dealt fatal blows to the then current forms of both of these simple theories, though proponents of the respective theories continued to pump a semblance of life into them with wordy battles. The opponent-colors theory in its original simple form can be made to yield but a single form of red-green blindness, that known as deuteranopia. It must overlook the established fact of a second type of red-green blindness, protanopia, in which the luminosity function is deficient in the long-wave portion of the spectrum and in which the chromaticity confusions are consistently different from those of deuteranopia. The three-components theory explains the confusions made by both types perfectly but in its original simple form has to predict that deuteranopic vision consists of mixtures of red and violet and protanopic vision consists of mixtures of green and violet. When cases of unilateral red-green blindness showed consistently that the perceptions of red-green-blind observers have the hues blue and yellow and no others, the original simple three-components formulation became obsolete. Some advocates of this simple theory took refuge in a suggestion by Fick [1][1] that red-green confusion is the result, not of the nonfunctioning of either the red or the green receptor system, but rather of the two receptor systems having identical photosensitive substances, either that for red (deuteranopia) or that for green (protanopia). By this suggestion, the responses from the red cones combine with those from the green, regardless of the photosensitive substance in either, to give yellow. This combination can take place in the postretinal portion of the nervous system, as emphasized by Hecht [2], for binocular fusion of colors, and it is permissible to assume that it always takes place there even in binary stimulation of one eye alone. From this view it is only a step to the theoretical position originally proposed by Donders [3] and later espoused by König [4], von Kries [5], and Adams [6] that the three-components formulation holds for processes in one stage of the visual mechanism (perhaps the photosensitive-substance stage), while the opponent-colors theory holds for

[1] Figures in brackets indicate the literature references at the end of this paper.

processes in a later stage (perhaps the optic nerve). This view may be called the stage or "zone" theory of vision. Furthermore, a very able advocate of the opponent-colors theory, G. E. Müller, adopted a theoretical view [7] that, although divergent in detail and elaborated to include an additional stage, was essentially in agreement with the stage theories favored by Donders, König, von Kries, and Adams.

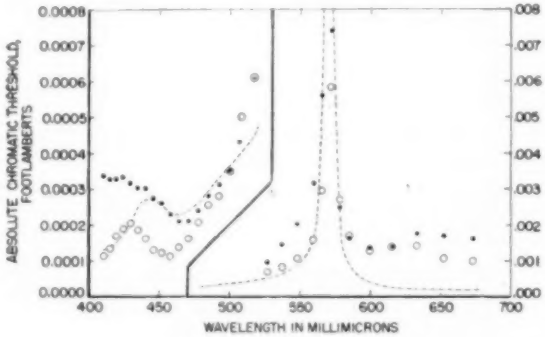

FIGURE 1. *Absolute chromatic thresholds for homogeneous light as a function of wavelength.*

The dotted curve is based on the Müller theory; see section VII. ●, Observed Abney; ○, observed Watson; — — — —, $\frac{0.0020\ (w-s)}{[(gR)^2+(0.04gY)^2]^{1/2}}$.

It was shown by Abney [8] in 1910, by Priest and Brickwedde [9] in 1926, by Guild [10] in 1928, by Holmes [11] in 1941, by MacAdam [12] in 1942, and probably by others, that the nearly achromatic color of noon sunlight is more confusible with

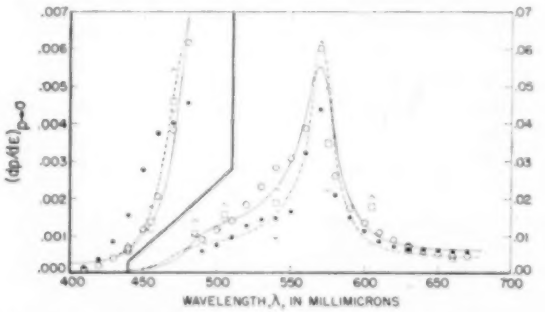

FIGURE 2. *Least fraction of spectrum light detectable as a chromatic difference in a mixture with sunlight, 2° observing field.*

The solid line is an empirical representation of these data based on the uniform-chromaticity-scale triangle (Judd); the dotted curve is based on the Müller theory; see section VII.

○, Mean observed Priest; ●, mean observed Brickwedde; ∧, □, ∨, observed Purdy; ————, from triangle; — — — —, $\frac{0.05\ (w-s)}{[(gR)^2+(0.5gY)^2]^{1/2}}$.

the greenish yellow color of spectrum light at 570 mμ by a normal observer than with any other nearby portion of the spectrum, definitely more than with the yellow portion (575 to 585 mμ). Figure 1 shows the brightness in foot lamberts found by Abney to be required to produce the perception of a chromatic color noticeably distinct from the achromatic color of light from the carbon arc. Figure 2 shows the Priest-Brickwedde determination of minimum perceptible colorimetric purity. In both of these figures the maximum near 570 mμ is outstanding. Similar results were found by Guild, Holmes, and MacAdam. This outstanding maximum might suggest that pigmentation of the eye media of the normal eye absorbs a large fraction of the short-wave (violet) portion of the spectrum, or for small fields it could mean that because of the chromatic aberration of the eye, the short-wave portion of the sunlight spectrum is out of focus and largely lost. But the most likely explanation is that the normal eye, at least in the fovea, has some of the characteristics of a tritanopic eye; a tritanope has a neutral point in the spectrum near 570 mμ where the normal observer has this quasi-neutral point. Furthermore, for very small fields subtending 20′ or less, it has been shown by König [4], Willmer [13], Hartridge [15], and Wright [14] that the fovea is tritanopic.

In an attempt to describe the chromaticity sensibility of the normal observer in terms of an approach to tritanopia, Judd [16] derived a transformation of the OSA "excitations" corresponding to an 80-percent dilution of the violet excitation with red and green. Figure 3 shows the resulting excitation curves and Maxwell triangle, and Figure 4 shows how this formulation corresponds with Priest's data on minimum perceptible colorimetric purity. This formulation corresponds to a theoretical suggestion similar to Fick's proposal to account for red-green confusion; it suggests that in the fovea the red and green substance from the red and green cones has leaked into the violet cones to a serious degree (80% leakage). A similar degree of success was demonstrated by Hecht [17] in another development of the Young-Helmholtz theory. Both explantions suffer, however, from a failure to permit an account of dichromatic vision, as do various coordinate systems empirically derived to represent in a simple way the facts of chromaticity sensibility [18, 19, 20].

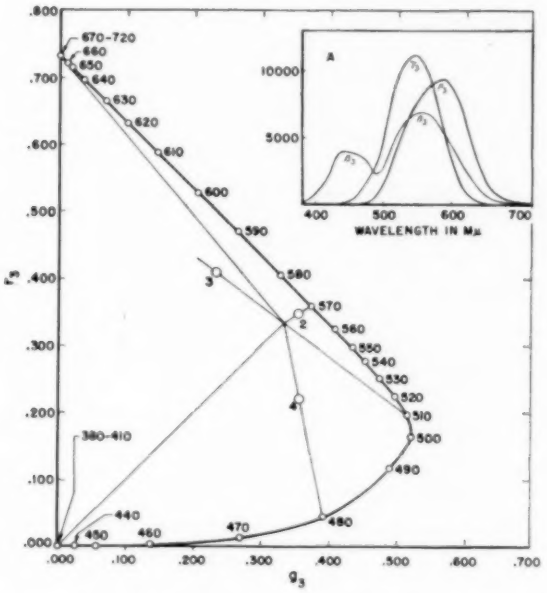

FIGURE 3. *The response functions and Maxwell triangle corresponding to a three-components explanation (Judd) of the data shown in figure 2.*

The suggested explanation is that segregation of photosensitive substances specific for long-wave energy is poor, violet cones having nearly as much (80%) as the red and green cones. Chromaticity coordinates of the spectrum referred to a set of stimulus primaries that have been found useful in deriving the "minimum purity perceptible." (See BS J. Research **4**, 515 (1930) RP163 also J. Opt. Soc. Am. and Rev. Sci. Instr. **16**, 115 (1928)). A, The three "distribution" curves which give the mixture diagram shown.

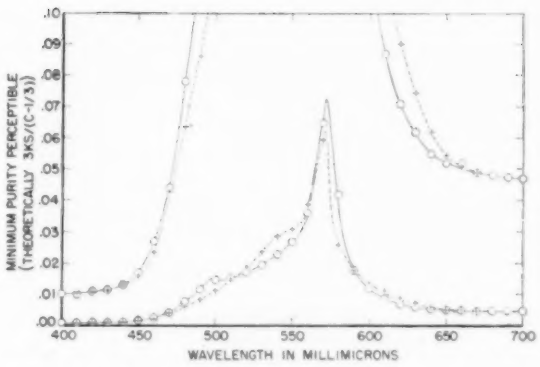

FIGURE 4. *Least fraction of spectrum light detectable as a chromatic difference in a mixture with sunlight, 2° observing field.*

The dotted line represents a part of the data shown in figure 2; the solid line is based on a three-components explanation (Judd, see fig. 3) of the tendency of the normal eye under these conditions to make tritanopic confusions. ○ $3KS/(c-1/3)$; $K=0.0024$, 0.8 blue deficient; +, $(dp/dE)_{p\to\infty}$. Irwin G Priest, observer.

There are, however, two accounts of chromaticity sensibility that do seem also to permit good explanations of dichromatic vision, that by Adams [21] and the recent excellent treatment of chromaticity sensibility by Stiles [22]. An account of protanopia and tritanopia by the Adams theory has not yet been worked out in detail.

An outstanding defect of the three-component accounts of chromaticity sensibility is that there is no satisfactory explanation of the primary character of the spectrum in the neighborhood of 475 mμ. Most normal observers (though not all) see this portion of the spectrum as blue, and they see the short-wave extreme as binary in character, a mixture of red and blue. In commenting on this difficulty, it was remarked by Judd [23] in 1932, "The most satisfactory solution yet offered is Müller's theory which ascribes primacy to both blue and violet, the latter in the retinal processes, and the former in the optic nerve."

As a prerequisite to a quantitative explanation in terms of the Müller theory for the confusibility of sunlight with the spectrum at 570 mμ and for chromaticity sensibility generally, there must be derived the colorimetric coordinate systems corresponding to the two additional stages, the retinal and the optic nerve stages, of the Müller theory. They have so far been described only qualitatively, or at least semiquantitatively. Since the theory has been adjusted to correspond qualitatively with the facts of colorblindness, and since those facts have recently become known quantitatively (chiefly through the work of Pitt [33]), it is now possible to evaluate these coordinate systems, and so lay the ground work for a possible explanation of chromaticity sensibility based on the Müller theory.

II. Formulation for Normal Vision

According to the Müller theory,[2] light stimuli can elicit three different primary sensitizing processes (P-processes) in the cone mechanism, whose strengths are determined according to wavelength of the incident radiant energy according to functions similar to those defining the three components of the Young-Helmholtz theory. The P_1-process is aroused by the spectral region 475

[2] Acknowledgment is made to Michael J. Zigler, Department of Psychology, Wellesley College, who kindly supplied a very helpful translation into English of these parts of Müller's discussion of color-blindness [7].

mμ up to the long-wave visible extreme. The P_2-process is aroused by the spectral region between the long-wave end stretch (770 mμ to a wavelength greater than 655 mμ) and the short-wave end stretch (380 mμ to a wavelength less than 450 mμ). The P_3-process is aroused by the spectral region between 540 mμ and the short-wave visible extreme. From this description, the distribution curves of the P-processes are seen to resemble closely the OSA excitation curves [24]. The best modern evaluation of these distribution curves based upon the ICI standard observer [25] is to be obtained [26] by the following transformation:

$$\left.\begin{aligned} P_1 &= 3.1956X + 2.4478Y - 0.6434Z \\ P_2 &= -2.5455X + 7.0492Y + 0.4963Z \\ P_3 &= 0.0000X + 0.0000Y + 5.0000Z \end{aligned}\right\}, \quad (1)$$

which are graphed in figure 5. The reverse transformation [27] is given by

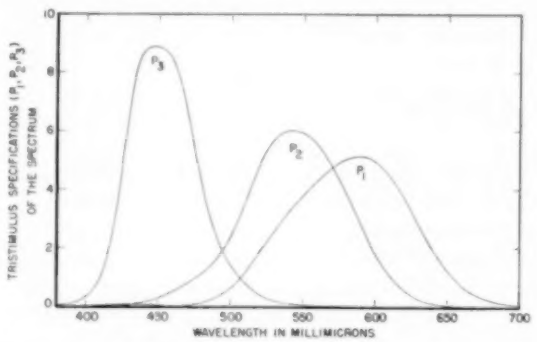

FIGURE 5. *Rates of decomposition of the photosensitive substances of the three-components theory as functions of wavelength.*

These functions are suited to the first stage of the Müller theory.

$$\left.\begin{aligned} X &= 0.24513P_1 - 0.08512P_2 + 0.03999P_3 \\ Y &= 0.08852P_1 + 0.11112P_2 + 0.00036P_3 \\ Z &= 0.00000P_1 + 0.00000P_2 + 0.20000P_3 \end{aligned}\right\}, \quad (1a)$$

Except for the small secondary maximum of the P_1 curve in the neighborhood of 430 mμ, these functions conform essentially to the description by Müller of the primary sensitizing processes. These processes contribute immediately to excitation of a black-white "substance" of the optic-nerve fibers in the sense of producing white. They also act upon certain assumed chromatic sensory substances in the cones of the normal eye as follows: the P_1-process acts to produce a major yellowish red (yR) process in a yellowish red-bluish green (yR-bG) substance and a minor greenish yellow (gY) process in a greenish yellow-reddish blue (gY-rB) substance. The P_2-process acts to produce a major bluish green (bG) process in the yR-bG substance and a minor greenish yellow (gY) process in the gY-rB substance. The P_3-process acts to produce a reddish blue (rB) process in the gY-rB substance. It is further assumed that the processes within each of these chromatic sensory substances are antagonistic so that a yR-process cancels completely a bG-process of equal strength; and a gY-process may cancel completely an rB-process. The wavelengths at which stimulation by homogeneous radiant energy would produce these cancellations are between 560 and 570 mμ for yR to cancel bG, and near 495 mμ for gY to cancel rB.

From this description it would seem that the transformation from the amounts of the primary sensitizing processes to the amounts of the chromatic sensory processes might take on the simple form:

$$\left.\begin{aligned} yR &= -bG = a_1P_1 - a_2P_2 \\ gY &= -rB = b_1P_1 + b_2P_2 - b_3P_3 \end{aligned}\right\}, \quad (2)$$

where a_1, a_2, b_1, b_2, and b_3 are constants greater than zero, with a_1 greater than b_1, and a_2 greater than b_2.

In addition to the primary sensitizing processes (P_1, P_2, P_3) and the chromatic sensory processes (yR-bG, gY-rB), there are six different excitations of the optic nerve (w, s, r, g, y, b), which correlate with the introspectively pure white, black, red, green, yellow, and blue sensations, respectively. The chromatic excitations are assumed to arise from the chromatic sensory processes alone, the yR-process arousing a major r-excitation and a minor y-excitation as indicated by the notation yR. Similar major and minor excitations are aroused by the bG, gY, and rB processes. The white-excitation of the optic nerve comes from the immediate effect of the primary sensitizing processes (P_1, P_2, P_3) to which secondary contributions from the yR- and gY-processes are added. The black-excitation comes chiefly by induction [7a, p. 85], from a white

surrounding field or from a white preexposure field, but a secondary contribution comes from the bG and rB processes. Like the chromatic sensory processes, the four chromatic excitations of the optic nerve make antagonistic pairs, an amount of r-excitation cancelling a like amount of g-excitation, and the same cancellations for y- and b-excitation. For stimulation by homogeneous radiant energy, the one cancellation occurs at the wavelength for arousing unitary yellow, which is probably between 575 and 582 mμ under usual observing conditions for an average normal observer. A second (r,g)-cancellation occurs at the wavelength for arousing unitary blue, and a (y,b)-cancellation occurs at the wavelength for unitary green.

For self-luminous areas with a neutral surrounding field the s-excitation acts as negative w-excitation; however, they do not cancel, but combine to give gray. From this description it would appear that the excitations of the optic nerve could be found for the normal observer by the following transformations:

$$\left.\begin{aligned} r &= -g = c_1 yR + c_2 rB = -c_1 bG - c_2 gY \\ y &= -b = d_1 gY + d_2 yR = -d_1 rB - d_2 bG \\ w &= e_1 P_1 + e_2 P_2 + e_3 P_3 + e_4 yR + e_5 gY \\ s &= e_4 bG + e_5 rB \end{aligned}\right\}, \qquad (3)$$

where the luminance of the area is given by the difference, $w-s$, between the white and black excitation, and the symbols with subscripts represent constants evaluated so far only by the conditions that c_1 is greater than d_2, and d_1 is greater than c_2.

Equation 3 is similar to those set up by Schrödinger [28] in accord with the theoretical views of von Kries [5], and by Adams [21] in accord with his own theory [6]. Adams has, moreover, pointed out the advantages and theoretical plausibility of the view that the various stages are not linearly connected. For simplicity in the present derivation, attention will be confined to the assumption represented in eq 2 and 3 that the connection is linear and homogeneous.

III. Dichromatic Vision

According to the Müller theory, protanopia corresponds to the failure of the (yR, bG)-chromatic substance; and on this account, it is called by him outer red-green blindness. Thus, for protanopia, $yR=bG=0$, and we may write from eq 3:

$$\left.\begin{aligned} r_p &= -g_p = c_2 rB = -c_2 gY \\ y_p &= -b_p = d_1 gY = -d_1 rB \\ w_p &= e_1 P_1 + e_2 P_2 + e_3 P_3 + e_5 gY \\ s_p &= e_3 rB \end{aligned}\right\}. \qquad (4)$$

From eq 4 one might think that the Müller theory predicts for protanopia simply the sensations of black and white plus the two chromatic sensations greenish yellow and reddish blue, since a given amount of blue excitation is always bound up inextricably with the same minor red excitation. This is indeed the simplest prediction from the formulation and corresponds fairly well with reports of unilaterally protanopic observers. Müller, however, points out that although failure of the (yR, bG) chromatic process is sufficient to produce the symptoms of protanopia completely, this failure could be accompanied by a failure of some of the chromatic processes in the optic nerve, which combination of circumstances could give rise to an observer having protanopic vision by all tests actually sensing only the hues yellow and blue, or even only the hues red and green. Such observers could be distinguished from each other only if one eye had trichromatic, and the other, protanopic vision.

Deuteranopia, on the other hand, is ascribed by Müller to failure of the (r, g)-sense of the optic nerve and is called inner red-green blindness. Thus, for deuteranopia, $r_d=-g_d=0$, and we may write from eq 3:

$$\left.\begin{aligned} y_d &= -b_d = d_1 gY + d_2 yR \\ w_d &= e_1 P_1 + e_2 P_2 + e_3 P_3 + e_4 yR + e_5 gY \\ s_d &= e_4 bG + e_5 rB \end{aligned}\right\}. \qquad (5)$$

From eq 5 it is plain that the predicted sensations of deuteranopes must be black, white, yellow, and blue; there are no alternatives.

Tritanopia, like protanopia, is ascribed to a retinal defect. It corresponds to failure of the (gY, rB)-chromatic substance and is called outer yellow-blue blindness. Thus, for tritanopia, $gY=rB=0$, and we may write from eq 3:

$$\left.\begin{aligned} r_t &= -g_t = c_1 yR = -c_1 bG, \\ y_t &= -b_t = d_2 yR = -d_2 bG, \\ w_t &= e_1 P_1 + e_2 P_2 + e_3 P_3 + e_4 yR, \\ e_t &= e_4 bG \end{aligned}\right\}. \qquad (6)$$

The sensations of tritanopes are seen to be predicted as black, white, and either yellow and blue, or red and green, or some fixed combination such as yellowish red and bluish green. The latter hues correspond to the simplest prediction, since the (yR, bG) chromatic sensory process is unaffected. These hues agree well with the reports of tritanopes who have acquired the defect through a disease of the retina.

IV. Evaluation of the Constants

Response functions for normal and dichromatic vision according to the Müller theory can be evaluated from eq 1, 2, and 3, for all three stages of excitation, provided the 14 constants of eq 2 and 3 be evaluated. For the normal mechanism adapted to a stimulus yielding an achromatic color, the stimuli for the unitary hues, red, yellow, green, and blue, are known [29, 30] within limits; these stimuli must excite only the respective *r*-, *y*-, *g*-, and *b*-processes of the optic nerve. The stimulus yielding the achromatic color, itself, must cause the chromatic sensory processes yR, gY, bG, and rB to vanish, and also reduce to zero the chromatic *r*-, *y*-, *g*-, and *b*-processes of the optic nerve. The colors confused with gray by the typical protanope, deuteranope, and tritanope must conform to the yR-process, the *g*-process, the rB-process, and their complements, respectively. The difference between the spectral luminosity function of the typical protanope and the same function for the normal observer must be a constant fraction of the (yR, bG)-process in order to conform to Müller's proposal; and similarly the difference between normal and tritanopic luminosity must be a constant fraction of the (gY, rB)-process.

There are many more than 14 conditions to be satisfied, including several that are set down by Müller only in qualitative terms, and some that relate to sensibility to chromaticity differences. In evaluating these constants, the best determined conditions (marked by asterisks in the next sections) have been satisfied perfectly; and from the resulting excitation curves it may be seen to what extent the less well-determined conditions are satisfied. For example, of the data for the normal stimuli for the unitary hues, only those for unitary yellow have been used, since they were specifically mentioned by Müller as indicating the stimulus to be between 575 and 582 μ. Unitary blue has necessarily to be taken as the complement of unitary yellow relative to the stimulus for white or gray; and unitary red and green were taken as the confusion colors for typical deuteranopia.

1. Hueless Point and Unitary Yellow

For an achromatic color, both the chromatic processes of the optic nerve and the chromatic sensory processes must cancel to zero. It is known [31] that stimulation of the normal eye by a source of equal energy results under ordinary conditions of observation in a closely achromatic, or hueless color. For such a source, $X=Y=Z$, and from eq 1, $P_1=P_2=P_3$; hence we may write with sufficient accuracy from eq 2

$$yR = a_1 P_1 - a_2 P_2 = 0,$$

whence:

$$a_1/a_2 = 1.000; \qquad (7)^*$$

and similarly

$$gY = b_1 P_1 + b_2 P_2 - b_3 P_3 = 0,$$

whence we find

$$b_1 + b_2 = b_3. \qquad (8)^*$$

By setting $r=g=y=b=0$ in eq 3, and substituting eq 7 and 8, the expressions vanish, and no further relation is found.

For the *r*-*g* cancellation point between 575 and 582 mμ, we may take somewhat arbitrarily for simplicity the crossing point of X and Y at 578.1 mμ. For stimulation by homogeneous energy of this wavelength we may write

$$\begin{aligned} r = -g &= c_1 yR + c_2 rB = 0 \\ &= c_1(a_1 P_1 - a_2 P_2) - c_2(b_1 P_1 + b_2 P_2 - b_3 P_3) = 0 \\ &= (a_1 c_1 - b_1 c_2)(3.1956X + 2.4478Y - 0.6434Z) - \\ &\quad (a_2 c_1 + b_2 c_2)(-2.5455X + 7.0492Y + 0.4963Z) + \\ &\quad b_3 c_2 (5.0000Z) = 0 \end{aligned}$$

By substituting $X=Y=0.4996$, $Z=0.0008$, which refer closely to 578.1 mμ, we obtain

$$2.8189(a_1c_1-b_1c_2)-2.2505(a_2c_1+b_2c_2)+0.0040b_3c_2=0. \quad (9)^*$$

2. Dichromatic Copunctal Points

The chromaticity confusions of dichromatic vision may be represented on the Maxwell triangle by families of straight lines, all lines of one family intersecting at a common point, known as the copunctal point [32]. These copunctal points have been evaluated from recent determinations, chiefly by Pitt [33], and expressed in terms of the ICI standard coordinate system. They embody the essential information regarding the chromaticity confusions of dichromats and lead to a convenient expression of four conditions affecting the unknown constants.

According to the Müller theory, protanopia corresponds to the failure of the (yR,bG)-chromatic substance. For certain stimuli the (gY,rB)-process is also reduced to zero. These stimuli are the equal-energy stimulus and all of those confused with it by the protanope. These chromaticity confusions are indicated on the Maxwell triangle by a straight line passing through the equal-energy point, and for every point on this line, $gY=-rB=0$. In particular, since all of the chromaticity confusion lines pass through a single point, these conditions must hold for the protanopic copunctal point defined by $x=X/(X+Y+Z)=0.747$, $y=Y/(X+Y+Z)=0.253$, $z=Z/(X+Y+Z)=0$. Hence we may write from eq 2

$$b_1P_1+b_2P_2-b_3P_3=$$
$$b_1(3.1956X+2.4478Y-0.6434Z)+$$
$$b_2(-2.5455X+7.0492Y+0.4963Z)-$$
$$b_3(5.0000Z)=0;$$

whence we find

$$b_1/b_2=0.0393. \quad (10)^*$$

Similarly, from the less well-determined tritanopic copunctal point, $x=0.18$, $y=0.00$, $z=0.82$, we may write

$$yR=-bG=a_1P_1-a_2P_2=0,$$
$$=a_1(3.1956X+2.4478Y-0.6434Z)-$$
$$a_2(-2.5455X+7.0492Y+0.4963Z)=0;$$

whence we find $a_1/a_2=-0.0512/0.0476=-1.07$, a value contradictory to eq 7 based upon the achromatic stimulus for the normal observer, which is much more reliably established than the tritanopic copunctal point. By setting $a_1=a_2$ in conformity with eq 7, we find that a condition for the tritanopic copunctal point by the Müller formulation is that $P_1=P_2$, which from eq 1 is equivalent to $y=1.987x-0.327$. This line intersects the x-axis of the chromaticity diagram at $x=0.165$, $y=0.000$, which is in as good agreement with the facts as the approximate evaluation of the copunctal point ($x=0.18$, $y=0.00$) estimated with the help of the König theory [32]. The latter accords with Müller's view that tritanopia is characterized by a single neutral point in the spectrum (near 570 mμ); the former places a second neutral point near the violet extreme of the spectrum (430 mμ) and arises from application of the Müller theory to the properties of the standard observer. As already noted, P_1 evaluated by this means has a small secondary maximum in the neighborhood of 430 mμ, causing it to cross the P_2-curve at this point, a result quite unanticipated by Müller. Actual reports of tritanopic vision are fairly well divided in this respect; for example, the cases reported by König [4] and Köllner [34] yielded a single neutral point; those by Collin and Nagel [35] and Piper [36] had neutral points or areas in the neighborhood of 430 mμ. Willmer and Wright [14] found an indication of such a neutral region for small fields in the normal fovea, and Pitt [37] considers this to be typical of tritanopia. The difference in chromaticity between 430 mμ and the short-wave end of the spectrum is small, and it is possible that individual variations among tritanopes can account for the slight discrepancy in the report between no short-wave neutral point and one near 430 mμ. On the other hand, it seems to be fairly frequent that tritanopes have ocular media pigmented heavily with brown pigment, and it is also possible that this pigmentation would cause the spectrum to become invisible to many tritanopes at a wavelength greater than 430 mμ as in a case reported by Farnsworth [38]. The formulation could be made to accord strictly with the Müller view on this point by choosing constants in eq 1, so that the representation of P_2 is everywhere higher than P_1 for wavelengths less than 500 mμ, such as that found by Stiles [22], but such a wavelength dis-

815197—49——2

tribution of P_2 is itself contrary to Müller's view. It seems more useful to proceed with an account of tritanopia involving a second neutral point near 430 mμ. Take therefore $a_1=a_2$ as in eq 7.

By the same argument given for protanopia, we may set $y=-b=0$, for the deuteranopic copunctal point defined by $Y=Z=0$. For eq 1, 2, and 3 we may write

$$y=-b=d_1gY+d_2yR=d_1(b_1P_1+b_2P_2-b_3P_3)+d_2(a_1P_1-a_2P_2)=0,$$

$$=(b_1d_1+a_1d_2)(3.1956X+2.4478Y-0.6434Z)+(b_2d_1-a_2d_2)(-2.5455X+7.0492Y+0.4963Z)-b_3d_1(5.0000Z);$$

whence we find, since $Y=Z=0$,

$$3.1956(b_1d_1+a_1d_2)-2.5455(b_2d_1-a_2d_2)=0. \quad (11)^*$$

Two other conditions may be derived from the protanopic and deuteranopic copunctal points. It has been shown [32] that the deuteranopic copunctal point lies on the deuteranopic alychne, that is, the line on the Maxwell triangle associated with zero deuteranopic luminosity; and the protanopic copunctal point lies on the protanopic alychne. Hence for the respective copunctal points we may set $(w-s)_d$ and $(w-s)_p$ equal to zero, and from eq 1, 2, and 3 there are found:

$$e_1-0.0393e_2+2e_5(b_1-0.0393b_2)=0, \quad (12)^*$$

and

$$3.1956(e_1+2e_4a_1+2e_5b_1)-2.5455(e_2-2e_4a_2+2e_5b_2)=0. \quad (13)^*$$

3. Dichromatic Luminosity Functions

It has been shown that the luminosity functions of red-green-blind observers can be expressed as functions of X, Y, and Z [39] by eq 14 and 15, in which W_p is the protanopic luminosity and W_d, the deuteranopic

$$W_p=0.460X+1.359Y+0.101Z, \quad (14)$$

$$W_d=Y. \quad (15)$$

From eq 1a, these functions may be written in terms of the primary processes, P_1, P_2, and P_3:

$$W_p=0.00754P_1+0.19017P_2+0.00229P_3, \quad (14a)$$

$$W_d=0.08852P_1+0.11112P_2+0.00036P_3. \quad (15a)$$

But from eq 2, 4, and 5, we may write

$$W_p=(w-s)_p=(e_1+2b_1e_5)P_1+(e_2+2b_2e_5)P_2+(e_3-2b_3e_5)P_3, \quad (14b)$$

$$W_d=(w-s)_d=(w-s)=(e_1+2a_1e_4+2b_1e_5)P_1+(e_2-2a_2e_4+2b_2e_5)P_2+(e_3-2b_3e_5)P_3. \quad (15b)$$

By equating the coefficients of P_1, P_2, and P_3 in eq 14a and 14b, we obtain three additional conditions to be satisfied by the constants:

$$e_1+2b_1e_5=0.00754, \quad (16)$$

$$e_2+2b_2e_5=0.19017, \quad (17)$$

$$e_3-2b_3e_5=0.00229. \quad (18)$$

Similarly, by equating the coefficients in eq 15a and 15b we obtain three more conditions:

$$e_1+2a_1e_4+2b_1e_5=0.08852, \quad (19)$$

$$e_2-2a_2e_4+2b_2e_5=0.11112, \quad (20)^*$$

$$e_3-2b_3e_5=0.00036. \quad (21)^*$$

Equations 16 to 21 are not entirely independent of the conditions previously found, nor are they all congruent. From eq 16 and 17 there may be derived eq 12; and from eq 19 and 20 there may be derived eq 13. Furthermore, eq 7, 10, 12, 19, and 20 combine to give eq 16 and 17. Equations 18 and 21 are contradictory. Since it is an essential part of the Müller theory that the deuteranopic luminosity function be the same as the normal, we must accept eq 21 and reject eq 18. This choice will prevent $(w-s)_p$ in eq 14b from being exactly equal to W_p in eq 14. It remains to be found whether the resulting evaluation of $(w-s)_p$ is as representative of available data on the protanopic luminosity function as is W_p. Thus, we have obtained only two additional independent conditions from protanopic and deuteranopic luminosity functions, eq 20 and 21.

If it be assumed for the moment that tritanopic luminosity is the same as deuteranopic and nor-

mal luminosity, as it may well be judging from the available information [7a, pp 53 and 102; 34, 36, 40, 41, 42, 43], then from eq 2 and 6 we obtain eq 22:

$$(w-s)=(w-s)_t=e_1P_1+e_2P_2+e_3P_3+2e_4\ (a_1P_1-a_2P_2). \tag{22}$$

By comparing the coefficients of P_1, P_2, and P_3 in eq 15b and 22 we see from each of the three comparisons that e_5 must be zero; that is, there can be no darkening effect from the gY-process, such as implied by eq 3. The Müller theory thus cannot abide having equality between tritanopic and normal luminosity. Müller was well aware that his theory required the tritanopic luminosity function to be different from normal and remarks [7a, p. 63] "In regard to spectral luminosity distribution in tritanopia, there must be, if no complications exist, because of the absence of the w value of the gY process, a decrease in the luminosity of yellow and yellowish lights in comparison to normal. . . . Unfortunately there have been up to now no investigations of the spectral luminosity characteristic of tritanopia." Since the present purpose is to find the coordinate systems implied by the Müller theory, we must disregard the rather inconclusive indications that there is no difference between tritanopic and normal luminosity; hence no attention can be paid to eq 22 in evaluating the constants, and e_5 must be given a positive, though small value. Take arbitrarily, then:

$$e_5=0.03\ e_4. \tag{23}*$$

4. Chromaticity Sensibility and Theory

We may now take stock of the conditions that must be satisfied by the 14 constants:

Criterion	Resulting condition
Hueless point	Eq 7 and 8
Unitary yellow	Eq 9
Protanopic copunctal point	Eq 10 and 12
Deuteranopic copunctal point	Eq 11 and 13
Dichromatic luminosity	Eq 20, 21, and 23.

These 10 equations have been marked with asterisks to show that they were used in the derivation of the constants.

There remain four conditions to be set up before the 14 constants can be evaluated. Three of the four conditions refer to the relative sizes of a_1 and b_3, c_1 and d_1, and a_1 and c_1.

The first ratio, a_1/b_3, has to do with the relative sensibility of the eye to yellowish red-bluish green differences on the one hand and greenish yellow-reddish blue differences on the other. Empirical studies on large fields [20, 21] indicate that a_1/b_3 is about 2.5, that is, the normal eye detects (yR, bG)-differences more readily by about a factor of 2.5 than would be judged from the relatively great overlap of P_1 and P_2. By setting $c_1/d_1=1.0$, this greater sensibility to (yR, bG)-differences is preserved in the optic-nerve stage.

The ratio of a_1/c_1 has to do with the comparative amounts of the chromatic sensory process and the chromatic excitations of the optic nerve. There does not seem to be any fundamental meaning to this comparison. It has merely to do with a relation between the units expressing the rate of a chemical process in the retinal receptors and those expressing the frequency of the resulting impulses in the fibers of the optic nerve. This ratio may be set arbitrarily, and for simplicity we set $a_1/c_1=1$.

The final condition refers to the size of the arbitrary units in which the chromatic responses are to be expressed; for simplicity take $a_1=1$.

Solution of these 14 equations simultaneously gives the values of the constants:

$$a_1=1.0000, a_2=1.0000,$$

$$b_1=0.0151, b_2=0.3849, b_3=0.40000,$$

$$c_1=1.0000, c_2=0.6265,$$

$$d_1=1.0000,\ d_2=0.1622,$$

$$e_1=0.0075, e_2=0.1912, e_3=0.0013, e_4=0.0405, e_5=0.0012$$

It will be noted that, as required by eq 2, a_1 is greater than b_1, and a_2 is greater than b_2. Furthermore, as required by eq 3, c_1 is greater than d_2, and d_1 is greater than c_2. This correspondence with the Müller description indicates how thorough was his grasp of the facts from purely qualitative data, though probably $c_2=0.6265$ is not as small compared to $d_1=1.0000$ as would be expected from Müller's designation of d_1gY and

c_2gY as a major y-excitation and a minor g-excitation, respectively, resulting from the gY process. The value of c_2 would be reduced somewhat by taking a higher value for the wavelength of the spectrum stimulus for unitary yellow, say 582 mμ instead of 578 mμ; see eq 9.

V. Definition of the Coordinate Systems

We may now insert these constants into eq 2 and 3, and so give explicit definitions of the two new coordinate systems implied in the Müller theory. The coordinate system applying to the chromatic sensory processes of the retinal receptors is defined by eq 2a:

$$\left.\begin{aligned} yR &= -bG = P_1 - P_2, \\ gY &= -rB = 0.0151P_1 + 0.3849P_2 - 0.4000P_3 \end{aligned}\right\} \quad (2a)$$

The coordinate system applying to the processes in the optic nerve fibers is defined by eq 3a;

$$\left.\begin{aligned} r &= -g = yR + 0.6265rB = -bG - 0.6265gY, \\ y &= -b = gY + 0.1622yR = -rB - 0.1622bG, \\ w &= 0.0075P_1 + 0.1912P_2 + 0.0013P_3 + 0.0405 \\ &\quad yR + 0.0012gY, \\ s &= 0.0405bG + 0.0012rB. \end{aligned}\right\} \quad (3a)$$

These two coordinate systems may also be defined in terms of the standard 1931 ICI coordinate system for colorimetry from eq 1. Equation 2b gives the definition of the colorimetric coordinate system for normal observers corresponding to the chromatic sensory processes combined with the luminosity function Y; and eq 2c gives the reverse transformation from this coordinate system to the standard ICI system:

$$\left.\begin{aligned} yR = -bG &= 5.741X - 4.601Y - 1.140Z, \\ gY = -rB &= -0.932X + 2.750Y - 1.819Z, \\ Y &= 1.000Y; \end{aligned}\right\} \quad (2b)$$

$$\left.\begin{aligned} X &= 0.1581yR - 0.0991gY + Y, \\ Y &= Y, \\ Z &= -0.0810yR - 0.4991gY + Y, \end{aligned}\right\} \quad (2c)$$

Equation 3b gives the definition of the colorimetric coordinate system for normal observers corresponding to the excitations of the optic nerve, and eq 3c gives the reverse transformation from this coordinate system to the standard ICI system:

$$\left.\begin{aligned} r = -g &= 6.325X - 6.325Y \\ y = -b &= 2.004Y - 2.004Z \\ (w-s) &= 1.000Y \end{aligned}\right\} \quad (3b)$$

$$\left.\begin{aligned} X &= 0.1581r + (w-s) \\ Y &= (w-s) \\ Z &= -0.4991y + (w-s) \end{aligned}\right\} \quad (3c)$$

Table 1 gives the response functions of the normal, protanopic, deuteranopic, and tritanopic types of vision derived from the ICI standard observer according to the Müller theory (eq 1, 2b, 3b, 4, 5, and 6).

The very simple transformation equations between the chromatic excitations of the optic nerve according to the Müller theory and the standard 1931 ICI coordinate system for colorimetry arise, of course, from the fact that the X-primary of the ICI system corresponds to a stimulus for unitary red, and the Z-primary corresponds to unitary blue. The r,y $(w\text{-}s)$ system corresponds to the central stage of the Adams theory [6], and coordinate systems closely resembling that described by eq 3b have been used by Adams with considerable success to explain chromaticity spacing for large fields, chiefly studies of the spacing of the Munsell colors [21].

The coordinate system set up by Schrödinger [44] in 1925 resembles closely that defined by eq 3b except that it was not adjusted to correspond to the same balance between (y,b)-excitation and the (r,g)-excitation ($a_1/b_3 = 2.5$, $c_1/d_1 = 1.0$). Schouten [45] made use of conditions derived from the hueless point (eqs 7 and 8), the deuteranopic neutral point (eq 11) and the unitary yellow point (eq 9) to compute response functions for assumed central r-, y-, g-, and b-processes. These functions bear a considerable resemblance to r and y evaluated from eq 3b. Thus it is seen that the essence of eq 3b is neither new nor confined to the Müller theory; it arises from the opponent-colors theory of Hering and has been used in at least three theoretical studies since 1925.

Figure 6 shows as functions of wavelength P_1, P_2, P_3; yR and gY; r and y; and finally in the

TABLE 1. *Response functions of the normal, protanopic, deuteranopic, and tritanopic types of vision derived from the ICI standard observer according to the Müller theory*

[Spectrum: equienergy]

Wave length	Primary sensitizing processes (possessed by all types of vision)				Chromatic sensory processes		Optic-nerve excitation				
	P_1	P_2	P_3	Normal vision Protanopic vision Deuteranopic vision Tritanopic vision	$yR\text{-}bG$ ..... $(yR\text{-}bG)_d$ $(yR\text{-}bG)_t$	$gY\text{-}rB$ $(gY\text{-}rB)_p$ $(gY\text{-}rB)_d$	$r\text{-}g$ (a) ..... (a)	$y\text{-}b$ (a) $(y\text{-}b)_d$ (a)	$w\text{-}s$ ..... $(w\text{-}s)_d$	..... $(w\text{-}s)_p$	.... $(w\text{-}s)_t$
mμ											
380	.....	.....	32	.....	.....	−13	+8	−13	.....	.....	.....
390	1	.....	100	.....	+1	−40	+26	−40	0.1	.....	0.2
400	3	.....	340	.....	+3	−136	+88	−135	.4	0.1	.6
410	8	1	1,037	.....	+8	−414	+267	−413	1.2	.5	2.1
420	24	6	3,228	.....	+17	−1,288	+824	−1,286	4.0	2.5	7.0
430	44	47	6,928	.....	−3	−2,752	+1,722	−2,753	11.6	12	18.1
440	45	143	8,736	.....	−97	−3,439	+2,057	−3,454	23	31	31.1
450	27	292	8,860	.....	−264	−3,432	+1,886	−3,475	38	59	46
460	2	511	8,346	.....	−509	−3,142	+1,489	−3,224	60	100	67
470	19	783	6,438	.....	−764	−2,274	+660	−2,398	91	152	96
480	123	1,140	4,065	.....	−1,017	−1,185	−275	−1,350	139	220	142
490	312	1,616	2,326	.....	−1,304	−304	−1,113	−515	208	312	208
500	631	2,390	1,360	.....	−1,768	+389	−2,012	+102	323	464	322
510	1,159	3,600	791	.....	−2,441	+1,087	−3,122	+691	503	699	501
520	1,890	4,883	391	.....	−2,993	+1,751	−4,090	+1,266	710	949	706
530	2,612	5,676	211	.....	−3,064	+2,140	−4,405	+1,643	862	1,107	857
540	3,235	5,996	102	.....	−2,746	+2,316	−4,197	+1,871	954	1,174	948
550	3,815	5,915	44	.....	−2,100	+2,317	−3,552	+1,976	995	1,163	990
560	4,333	5,503	20	.....	−1,170	+2,176	−2,533	+1,986	995	1,089	990
570	4,764	4,772	10	.....	−8	+1,904	−1,201	+1,903	952	953	948
580	5,057	3,801	8	.....	+1,255	+1,536	+293	+1,710	870	770	866
590	5,132	2,724	6	.....	+2,408	+1,124	+1,704	+1,514	757	564	754
600	4,938	1,745	4	.....	+3,194	+744	+2,728	+1,263	631	376	629
610	4,435	994	2	.....	+3,441	+449	+3,160	+1,003	503	228	502
620	3,663	510	1	.....	+3,152	+252	+2,994	+763	381	129	380
630	2,702	233	.....	.....	+2,469	+130	+2,387	+531	265	68	265
640	1,860	94	.....	.....	+1,766	+64	+1,726	+351	175	34	175
650	1,168	33	.....	.....	+1,135	+30	+1,116	+214	107	16	107
660	676	10	.....	.....	+666	+14	+657	+122	61	8	61
670	358	3	.....	.....	+354	+7	+350	+64	32	4	32
680	191	1	.....	.....	+190	+3	+188	+34	17	2	17
690	93	.....	.....	.....	+93	+1	+92	+16	8.2	1	8
700	46	.....	.....	.....	+46	+1	+46	+8	4.1	.....	4.1
710	24	.....	.....	.....	+24	.....	+23	+4	2.1	.....	2.1
720	12	.....	.....	.....	+11	.....	+11	+2	1.0	.....	.9
730	6	.....	.....	.....	+6	.....	+6	+1	.5	.....	.4
740	3	.....	.....	.....	+3	.....	+3	.....	.3	.....	.3

[a] For protanopic and tritanopic vision the Müller theory does not state rigidly that the optic nerve excitation must follow eq 4 and 6, though this is the simplest prediction. Either $r\text{-}g$ or $y\text{-}b$, but not both, may be zero. If they are not zero, they have wavelength distributions proportional to the chromatic sensory processes.

lower left quadrant the deuteranopic luminosity according to eq 3b, the protanopic luminosity according to eq 4 together with the luminosity contributions of the chromatic sensory processes yR and gY.

VI. Protanopic Luminosity Function

In the ICI system the standard luminosity function is represented by the second function, Y; and from eq 3b it may be seen that the Müller

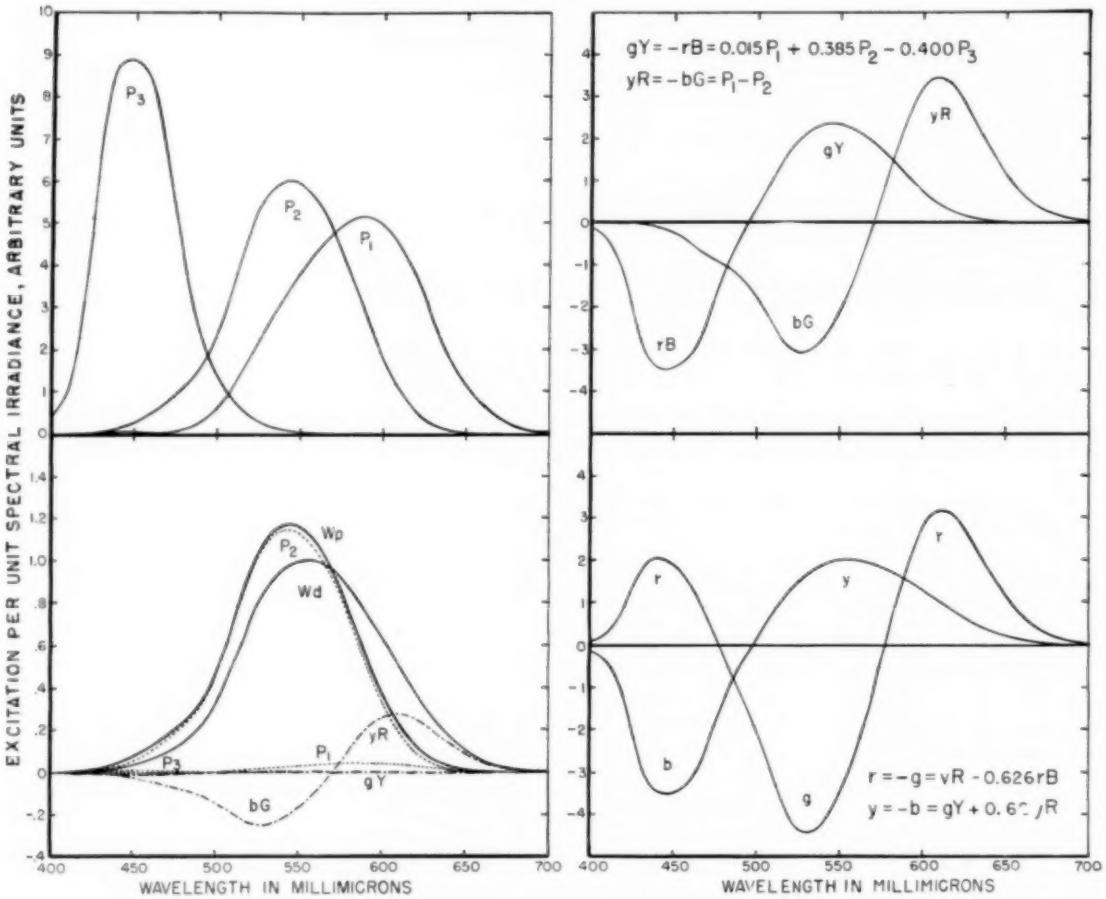

FIGURE 6. *Response functions according to the three stages of the Müller theory.*

Upper left: Processes in the initial photosensitive stage (same as Young theory, see eq 1 and fig. 5); lower left: components in the luminosity function ($w-s$) both for normal and deuteranopic, W_d, and protanopic, W_p, vision (see eq 3a); upper right: chromatic retinal sensory processes (see eq 2a); lower right: chromatic processes in the optic-nerve fiber stage (same as the Hering theory, see eq 3a).

theory can be formulated, as he claimed, in such a way that the difference between the w-excitation and the s-excitation gives the normal luminosity function. This function has already been shown to be as satisfactory a representation of deuteranopic luminosity as it is for some normal luminosity functions, because the deuteranopic luminosity functions fall within normal limits [32]. In these two respects this formulation of the Müller theory conforms exactly to that previously worked out in accord with the König theory [4, 32]. However, it was noted previously that eq 21 contradicts eq 18; so it remains to be seen whether the prediction of protanopic luminosity by this formulation of the Müller theory is as acceptable as that by the König theory. By inserting the constants in eq 4 it is found that this formulation of the Müller theory requires protanopic luminosity to be given by:

$$(w\text{-}s)_p = 0.0075\ P_1 + 0.1921\ P_2 + 0.0003\ P_3. \quad (4a)$$

The previous formulation of the König theory yielded the equation:

$$W_p = 0.0075\ P_1 + 0.1902\ P_2 + 0.0023\ P_3. \quad (14a)$$

Figure 7 is a plot of these functions adjusted approximately to unit maximum, together with upper and lower limits of available data on luminosity functions of protanopic and protanom-

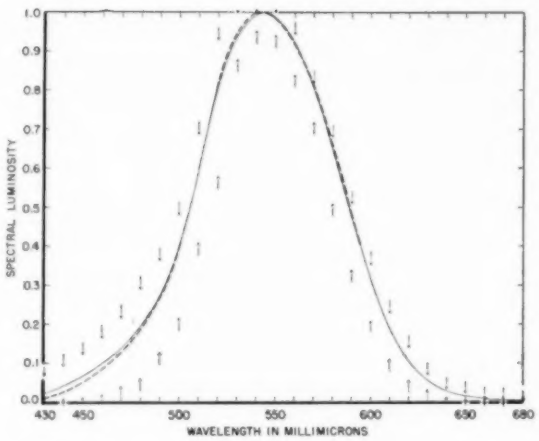

FIGURE 7. *Protanopic and protanomalous luminosity functions.*

The solid curve, W_p, corresponds to a wavelength function derived in accord with the later Kŏnig form of three-components formulation for protanopic luminosity [32]; the dotted curve, $(w-s)_p$, is based on the Müller theory. The arrows indicate maximum and minimum luminosities of 12 protanomalous and six protanopic observers. Note that these data support both functions about equally well.

alous observers [32]. It will be seen that these data support both functions about equally well.

VII. Chromatic Thresholds, Normal and Tritanopic

We are now in position to inquire whether the Müller theory offers a basis for explaining the chromatic-threshold data of Abney [8] and Priest Brickwedde [9] referred to earlier. According to the Müller theory the ability of an observer to detect a slight variation in chromaticity from a central chromaticity, such as that of the light from a carbon arc, would depend upon the excitation of the chromatic sensory processes. The amounts of the excitation of these processes corresponding to any color specified in terms (X, Y, Z) of the 1931 ICI standard observer can be found from eq 2b. And, in particular, they have been found for the spectrum colors for unit irradiance and are plotted in the upper right quadrant of figure 6. Both of the above sets of data are given, however, in luminous units (luminance of the field just yielding a chromatic difference from carbon-arc light in Abney's work, or luminance fraction required to be mixed with sunlight to produce a color just noticeably different from sunlight in the work of Priest and Brickwedde). We should expect to compare with them, therefore, the excitations of the chromatic sensory processes corresponding to the colors of a spectrum of constant luminance; that is, we should expect to find the chromatic thresholds in luminance terms to correspond to the reciprocal of some combination of $yR/(w-s)$ and $gY/(w-s)$. The exact form of combination would seem to be expressible in terms of the probability of a chromaticity difference being discriminated as a function of the probabilities of each of the two independent chromatic processes becoming effective considered separately. For the present purpose it is sufficient to take tentatively the combination as the square root of the sum of the squares; that is, assume, for the moment, that the effective chromatic excitation for large fields and high luminance is proportional to: $[(yR)^2+(gY)^2]^{1/2}/(w-s)$. For experimental conditions, such as restricted angular size of field or low luminance, that make the normal eye respond more or less like a tritanopic eye, the effective chromatic excitation may be assumed to be proportional to $[(yR)^2+f^2\ (gY)^2]^{1/2}/(w-s)$, where f is the relative effectiveness of the gY-rB process compared to the yR-bG process. In general, we would compare to the chromatic thresholds dB/dE, expressed in luminous terms, the reciprocals of these assumed effective chromatic excitations so as to study the validity of the relation

$$dB/dE=k(w-s)/[(yR)^2+f^2\ (gY)^2]^{1/2}, \qquad (24)$$

where k is the constant required to adjust the theoretical function to the units in which the chromatic threshold is expressed.

Abney's data have been found to agree fairly well with eq 24 for $k=0.0020$ and $f=0.04$; see dotted curve of figure 1. The course of the experimentally determined function is followed well, except for wavelengths greater than 590 mμ where the predicted threshold is considerably lower than that found experimentally. As far as is known, no explanation of these data has previously been suggested. It should be pointed out also that more recent determinations of the chromatic threshold by Purdy [46], and Otero, Plaza, and Casero [47] are quite at variance with these data, and indeed with each other. They show neither the sharp peak at 570 mμ nor the decline to small values near 450 mμ. Needless to say, they are quite unexplainable by the Müller theory. The data by Abney and Watson, how-

ever, may be summarized by saying that they conform fairly well to the Müller theory for a retinal region in which the normal gY, rB process is 96 percent ineffective. Tritanopia corresponds to complete ineffectiveness of this process.

The data of Priest and Brickwedde have been found to agree well with eq 24 for $k=0.05$, and $f=0.5$; see dotted curve on figure 2. The degree of agreement is quite comparable to that obtained by a coordinate system adjusted empirically to represent such data [18]; see solid curve. In this case, the less complete data by Purdy are in substantial agreement and are also shown. It should be pointed out, however, that these data have been corrected to refer to the standard luminosity function by multiplying them by the ratio of the standard luminosity function to that found by Gibson and Tyndall. It is probable that an improvement in the theoretical account of other psychophysical data by means of the Müller theory would result from revaluation in terms of an observer based on the Gibson-Tyndall experimental mean [18] luminosity function instead of on the standard observer. However, we may say that the Priest-Brickwedde data correspond well to the Müller theory for a retinal region in which the normal gY-rB-process is 50 percent effective.

It is concluded that the Müller theory affords a good explanation of chromatic thresholds in terms of a gradual approach to tritanopic vision. A thorough study of the implications of the Müller theory for chromaticity sensibility of all types such as that carried out by Stiles [22] for the three-components theory would seem to be worth while.

VIII. Summary and Conclusion

By taking into account the metamers known to be characteristic of protanopic, deuteranopic, and normal vision as well as data on the stimulus for a neutral color and the stimulus for a color of unitary yellow hue, the spectral variations of the responses for each of the three stages of the Müller theory of vision have been evaluated as functions of wavelength.

These response functions are shown to yield an account of normal, protanopic, and deuteranopic vision that differs in no essential respect from the simpler explanation yielded by the König form of three-components theory. They differ in their explanation of tritanopic vision by requiring the tritanopic luminosity function to be slightly higher in the short-wave end of the spectrum than normal; the three-components explanation requires it to be slightly lower in this part of the spectrum.

The chromatic response functions of the second stage of the Müller theory are shown to lead to a satisfactory and convenient account of the approach to tritanopia exhibited by the normal eye in viewing small fields or fields of luminance near the chromatic threshold.

It is concluded that the qualitative ideas of Müller lead to admissible and consistent coordinate systems. The Müller theory shows how the three-components formulation of Young, Helmholtz, and König (first stage) and the opponent-colors formulation of Hering (third stage) may both be accepted, and the explaining power of both be simultaneously utilized. The intermediate stage is also a promising and powerful theoretical tool. The quantitative consistency of the Müller ideas and the success demonstrated in accounting for tritanopic confusions made by normal observers does not, of course, prove the Müller theory to be completely, or even basically, correct. Alternate explanations are possible. There are important gaps in our knowledge of retinal chemistry and conduction and integration of nerve impulses that, if filled, might disprove the Müller theory and require adoption of an alternate account. Furthermore, several aspects of the Müller explanation, though admissible in the present state of our knowledge, seem implausible and unlikely to be born out by future work. At the very least, however, the Müller theory must be viewed as a forward step, and the coordinate system suggested by the second stage has practical value regardless of any of these future theoretical developments.

IX. References

[1] A. Fick, Die Lehre von der Lichtempfindung, Hermann's Handbuch der Physiologie **3,** Part 1, 139 (Leipzig, 1879).

[2] S. Hecht, On the binocular fusion of colors and its relation to theories of color vision, Proc. Nat. Acad. Sci. **14,** 237 (1928).

[3] F. C. Donders, Ueber Farbensysteme, Arch. Ophthalmol. **27,** 155 (1881).

[4] A. König, Ueber "Blaublindheit," Sitz. Akad. Wiss. Berlin, p. 718 (July 8, 1897); also Gesammelte Abhandlungen, p. 396 (Barth, Leipzig, 1903).

[5] J. von Kries, Die Gesichtsempfindungen, Handbuch der Physiologie des Menschen **3,** 260 (Braunschweig, 1905).

[6] E. Q. Adams, A theory of color vision, Psychol. Rev. **30,** 56 (1923).

[7] G. E. Müller, Darstellung und Erklärung der verschiedenen Typen der Farbenblindheit (Vandenhoeck-Ruprecht, Göttingen, 1924); G. E. Müller, Ueber die Farbenempfindungen, Z. Psychol. Ergänzungsbände **17** and **18** (1930).

[8] W. de W. Abney, On the extinction of colour by reduction of luminosity, Proc. Roy. Soc. [A] **83,** (1910); Researches in colour vision and the trichromatic theory, p. 151 (Longmans-Green, London, 1913).

[9] I. G. Priest and F. G. Brickwedde, The minimum perceptible colorimetric purity as a function of dominant wavelength with sunlight as neutral standard, J. Opt. Soc. Am. **13,** 306 (1926); **28,** 133 (1938).

[10] J. Guild, On the selection of a suitable yellow glass for railway signals, Proc. Intern. Comm. Illum., p. 862, 7th session, Saranac, 1929 (Chemical Pub. Co., Easton, Pa., 1929).

[11] J. G. Holmes, The recognition of coloured light signals, Trans. Illum. Eng. Soc. **6,** 71 (1941).

[12] D. L. MacAdam, Visual sensitivities to color differences in daylight, J. Opt. Soc. Am. **32,** 247 (1942).

[13] E. N. Willmer, Colour of small objects, Nature **153,** 774 (June 24, 1944).

[14] E. N. Willmer and W. D. Wright, Colour sensitivity of the fovea centralis, Nature **156,** 119 (1945).

[15] H. Hartridge, The visual perception of fine detail, Phil. Trans. Roy. Soc., London [B], **232,** 535 (1947); Nature **155,** 391, 657 (1945).

[16] D. B. Judd, Sensibility to color change determined from the visual response functions; extension to complete and partial dichromasy, J. Opt. Soc. Am. **16,** 115 (1928); Reduction of data on mixture of color stimuli, BS J. Research **4,** 515 (1930) RP163.

[17] Selig Hecht, A quantitative formulation of colour-vision, Report of a joint discussion on vision, physical and optical societies (Univ. Press, Cambridge, June 1932).

[18] D. B. Judd, A Maxwell triangle yielding uniform chromaticity scales, J. Research NBS **14,** 41 (1935); RP756; J. Opt. Soc. Am. **25,** 24 (1935).

[19] R. H. Sinden, A further search for the ideal color system, II. A reconsideration of the Helmholtz line element, J. Opt. Soc. Am. **28,** 339 (1938).

[20] F. Scofield, D. B. Judd, and R. S. Hunter, A proposed method of designating color, Am. Soc. Testing Materials Bull., p. 19 (May 1941).

[21] E. Q. Adams, X-Z planes in the 1931 ICI system of colorimetry, J. Opt. Soc. Am. **32,** 168 (1942).

[22] W. S. Stiles, A modified Helmholtz line-element in brightness-colour space, Proc. Phys. Soc. (London) **58,** 41 (1946).

[23] D. B. Judd, Chromaticity sensibility to stimulus differences, J. Opt. Soc. Am. **22,** 72 (1932).

[24] L. T. Troland, Report of Committee on Colorimetry for 1920–21, J. Opt. Soc. Am. **6,** 548 (1922).

[25] Proceedings of the Eighth Session, Commission Internationale de l'Éclairage, Cambridge, Eng., pp. 19–29 (Sept. 1931).

[26] D. B. Judd, Color systems and their interrelation, Illum. Eng. **36,** 347 (March 1941).

[27] D. B. Judd, Reduction of data on mixture of color stimuli, BS J. Research **4,** 515 (1930) RP163.

[28] E. Schrödinger, Ueber das Verhältnis der Vierfarben- zur Dreifarben theorie, Sitz. Akad. Wiss. (Wien) IIa **134,** 471 (1925).

[29] F. L. Dimmick and M. R. Hubbard, The spectral components of psychologically unique red, Am. J. Psychol. **52,** 348 (1939).

[30] F. C. Breckenridge and W. R. Schaub, Rectangular uniform-chromaticity-scale coordinates, J. Opt. Soc. Am. **29,** 370 (1939).

[31] I. G. Priest, An experiment bearing on the adoption of a standard neutral stimulus in colorimetry: the choice as between "sun" and "equal energy," J. Opt. Soc. Am. and Rev. Sci. Instr. **13,** 306 (1926).

[32] D. B. Judd, Standard response functions for protanopic and deuteranopic vision, J. Research NBS **33,** 407 (1944).

[33] F. H. G. Pitt, Characteristics of dichromatic vision, Medical Research Council, Report of the Committee on the Physiology of vision, XIV, Special Report Series, No. 200 (London, 1935).

[34] H. Köllner, Die Störungen des Farbensinnes, p. 48 (Karger, Berlin, 1912).

[35] Collin and W. A. Nagel, Erworbene Tritanopie (Violettblindheit), Z. Sinnesphysiol. **41,** 74 (1907).

[36] H. Piper, Beobachtungen an einem Fall von totaler Farbenblindheit des Netzhautzentrums im einen und von Violettblindheit des anderen Auges, Z. Psychol. **38,** 155 (1905).

[37] F. H. G. Pitt, The nature of normal trichromatic and dichromatic vision, Proc. Roy. Soc. [B], **132,** 101 (1944).

[38] D. Farnsworth, Description of a subject congenitally deficient in violet-yellow vision, J. Opt. Soc. Am. **33,** 350 (1943).

[39] D. B. Judd, Standard response functions for protanopic and deuteranopic vision, J. Research NBS **33,** 407 (1944) RP1618; J. Opt. Soc. Am. **35,** 199 (1945).

[40] F. C. Donders, Remarques sur les couleurs et la cécité des couleurs, Arch. Ophthalmal. **84,** 205 (1880); Brit. Med. J. No. 13 (1880); Ann. d'oculistique **84,** 212 (1880).

[41] A. Kirschmann, Beiträge zur Kenntnis der Farbenblindheit, Wundt's Philos. Studien. **8,** 173, 407 (1892–93).

[42] H. Köllner, Erworbene totale farbenblindheit mit Bericht über einen weiteren Fall, Z. Augenh. **21,** 193, 309 (1909).

[43] H. Köllner, Anleitung zür Prüfung des Farbenunterscheidungsvermögens mittels des Anomaloskopes für Bahnaugenärzte, Physikalisch-medizin, Ges. Würzburg (1913).

[44] E. Schrödinger, Uber das Verhältnis der Vierfarben- zur Dreifarbentheorie, Sitz. Akad. Wiss. Wien, IIa **134,** 471 (1925).

[45] J. F. Schouten, Grundlagen einer quantitativen Vierfarbentheorie, I. Proc. Koninklijke Akad. v. Wetenschappen (Amsterdam) **38,** 3 (1935).

[46] D. McL. Purdy, On the saturations and chromatic thresholds of the spectral colours, Brit. J. Psychol. Gen. Sec. **21,** 283 (1930–31).

[47] J. M. Otero, L. Plaza, and L. Casero, El intervalo acromatico y las sensaciones fundamentales en la zona media del espectro, Anales. Fisica Quimica[A], **16** (1948).

WASHINGTON, July 9, 1948.

U. S. Department of Commerce
National Bureau of Standards

Research Paper RP1947
Volume 42, January 1949

Part of the Journal of Research of the National Bureau of Standards

Rate of Shrinkage of Tendon Collagen: Heat, Entropy, and Free Energy of Activation of the Shrinkage of Untreated Tendon; Effect of Acid, Salt, Pickle, and Tannage on the Activation of Tendon Collagen

By Charles E. Weir

From isothermal measurements of the rate of shrinkage of tendon collagen, it is concluded that shrinkage is a rate process involving a reaction of first order. The effects of tension and length of soaking before shrinkage are studied. Average values of heat, entropy, and free energy of shrinkage of untreated tendon are obtained by application of the theory of absolute reaction rates to the data. These values are found to be 141 kcal/mole, 349 cal/mole deg, and 24.7 kcal/mole at 60° C, respectively, with standard deviations of 15 kcal/mole, 43 cal/mole deg, and 0.6 kcal/mole at 60° C, respectively. Measurements of shrinkage temperatures are discussed. The effects of pH, salt, tanning, and pretannage treatments on the activation process are studied. Heat, entropy, and free energy decrease in acid and alkaline media. Salt solutions cause a decrease in heat and entropy but an increase in free energy in concentrated solutions. The effect of salt and acid in combination is complex, but in concentrated salt solutions an increase in free energy is observed. All tannages investigated, with the exception of chrome tanning, appear to reduce the entropy more than the heat, thereby increasing the free energy. Chrome tanning increases heat, entropy, and free energy markedly. An interpretation of the results is given.

I. Introduction

The shrinkage of leather and collagen, when heated in an aqueous medium, has been the subject of extensive investigations. The history of such studies is outlined adequately by McLaughlin and Theis [1][1] and Hobbs [2]. The measurement of shrinkage temperatures consists of heating a water bath containing the specimen and observing the temperature at which initial shrinkage occurs. The dimensions of the test specimen and the rate of heating are prescribed [3]. Theis and Schaffer [4], lacking a reliable analytical method for determining formaldehyde combined with collagen, proposed the measurement of the temperature of initial shrinkage as a measure of the degree of "leathering." Recent investigations by Bowes and coworkers [5] have shown that increased chrome content results in increased shrinkage temperature.

Theis and coworkers [6, 7, 8] and Chater [9, 10] have investigated many factors that influence shrinkage temperature but, as far as can be ascertained, all investigations, with one exception, were concerned with the initial appearance of shrinkage under conditions of continually increasing temperature. The shrinkage temperature of chrome-tanned leather is generally found to be above 100° C, and therefore it cannot be attained with an ordinary water bath. Chater [11], Harnly and Parker [12], and Merry [13] have published data showing that chrome-tanned leather having a shrinkage temperature exceeding 100° C will shrink progressively if the temperature of the bath is maintained at 100° C for a period of time. Chater [14] has presented evidence that the amount of shrinkage is a function of the initial temperature of the bath. Critical examination

[1] Figures in brackets indicate the literature references at the end of this paper.

of the foregoing results tends to indicate that shrinkage does not occur at a fixed temperature, although shrinkage has been regarded as analogous to a phase change occurring at a fixed temperature [15].

Recent measurements at this Bureau [16] of the expansivity of leather and collagen showed that shrinkage occurred at a temperature many degrees lower than that ordinarily measured as the shrinkage temperatures of the specimens tested. These measurements proved that the apparent shrinkage is a result of anistropy of the material and that the net change results in an increase in real volume. One measurement made during shrinkage showed that the volume change approximately followed the first-order rate equation. This investigation was performed by observing specimens in thermal equilibrium with water over long periods of time. The results indicated that there was no fixed temperature that might be called the shrinkage temperature, but rather that shrinkage was a rate process occurring over a range of temperatures. In the previous investigation involving dilatometric techniques, it was not possible to determine the temperature coefficient and the related thermodynamic quantities of the rate process, and the present series of studies was initiated.

The present investigation, utilizing tendon collagen as the experimental material, shows that the shrinkage phenomenon is a rate process having an extremely high temperature coefficient, measurements being possible over a temperature interval of approximately 10 to 15 deg C. The heat, entropy, and free energy of activation of the shrinkage process have been evaluated for untreated tendons and for tendons subjected to processes commonly used in the tannery.

II. Apparatus and Method of Measurement

The equipment required for the measurements consisted of a temperature-controlled water bath, suitable devices for suspending the specimen, and a cathetometer for measuring the length of the specimen.

The water bath was improvised from a cylindrical glass aquarium, 12 in. in diameter and 18 in. in depth. The bath was equipped with a controlled intermittent heater of 500-watt capacity, a variable continuous heater of 1,000-watt capacity, a thermoregulator of the toluene-mercury type, and an electrically driven stirrer. The thermostat was capable of maintaining any desired temperature between 30° and 95° C to within ±0.1° C. At temperatures exceeding 65° C, the surface of the water was covered with a layer of light mineral oil to reduce excessive evaporation.

A glass cylinder, closed at the lower end, was clamped in the bath in an upright position. The cylinder was a 500-ml graduate and was closed at the top with a two-hole stopper containing a thermometer and a glass rod. The thermometer, which was graduated to 0.2° C, was placed to record the average temperature of the specimen during shrinkage. The specimen was bound to the glass rod by fine copper wire and was placed under tension by the addition of a weight at the lower end. The weight was made up of an "alligator" clip to which was fastened a brass weight. The weight was essential to prevent curling of the specimen during the initial stages of the shrinkage. The effect of the weight will be described later.

Measurements of length were obtained with a cathetometer graduated to 0.05 mm. Readings were made of the heights of the wire at the top of the specimen and the jaw of the "alligator" clip where it clamped the specimen.

Test specimens consisted of kangaroo tail tendons, which were approximtely 1 mm in diameter. These tendons represent nearly pure collagen in a highly oriented form [17]. The tendons had been subjected to no chemical treatment. A confining sheath, which is occasionally found on some tendons, was found to restrict shrinkage and was therefore removed prior to test.

Measurements were made as follows. The graduate was filled with distilled water, and the bath was adjusted to the desired temperature. A length of tendon (approximately 10 cm and excluding ends of tendons, which give erratic results) was fastened to the glass rod, and the alligator clip with its appended weight was clamped to the bottom of the specimen. The assembly, consisting of rod, tendon, stopper, and thermometer, was then inserted into the graduate, and the stopper was seated securely. At the same instant a stopwatch was started. An initial reading of the position of the jaw of the "alligator" clip was made as rapidly as possible, that is, within 5 sec. This

reading represents the position of the bottom of the specimen at zero time. The position of the top of the specimen was then recorded, and further readings were made of the position of the alligator clip until shrinkage ceased. The rate of shrinkage varies with time and temperature, and the interval between readings was varied. Numerous readings were made in the region of half-shrinkage to permit accurate interpolation of the data.

III. Results and Discussion of Measurements on Untreated Tendon

1. Shrinkage Curve

Routine measurements were made on specimens that had been soaked in water at 5° C prior to testing. The results obtained on shrinkage at 60° C of specimens soaked for varying periods of time are shown in figure 1. In this figure the residual lengths in centimeters, that is, the lengths, l, at time, t, minus the fully shrunken length, l_∞, are plotted as ordinate and the time in minutes as the abscissa. Coordinates of this nature were chosen in analogy with applications of the first-order reaction equation. The curves illustrate the effect of varying the length of soaking period prior to shrinkage. It is observed that the dry

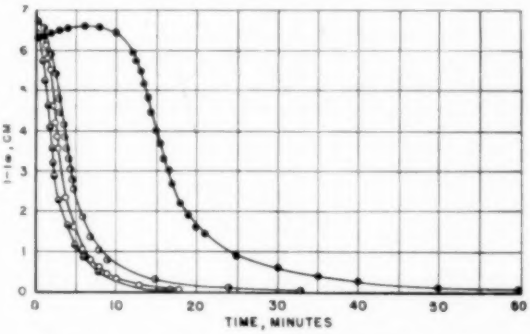

FIGURE 1. *Effect of length of soaking on shrinkage.*

●, Soaked 0 hr; ◑, soaked 1 hr; ◒, soaked 2 hr; ○, soaked 24 hr.

specimen elongates before shrinkage occurs, probably because of absorption of water. No preliminary elongation is observed after soaking for 1 hr or longer. Relatively little change is to be noted in either shape or position of the curve after the 1-hr soaking period. All subsequent measurements were made on tendons that were soaked in distilled water at 5° C for 24 hr prior to test. This procedure was adopted for convenience, since equilibrium appears to be attained in this period, and specimens prepared one day may be tested the following day.

In figure 2, typical shrinkage curves at various temperatures are shown. The effect of a few degrees variation in temperature is pronounced. In general, it has been found that a 2-deg rise in temperature results in approximately a twofold increase in rate of shrinkage. This behavior differs from that of most ordinary chemical reactions in which a temperature rise of 10 deg C approximately doubles the speed of the reaction.

The curves of figure 2 indicate that shrinkage is not a simple process. The shrinkage is seen to accelerate initially, to reach an approximately constant rate, and then to decelerate. As shown by the figure, the periods of acceleration and deceleration are shortened as the temperature increases.

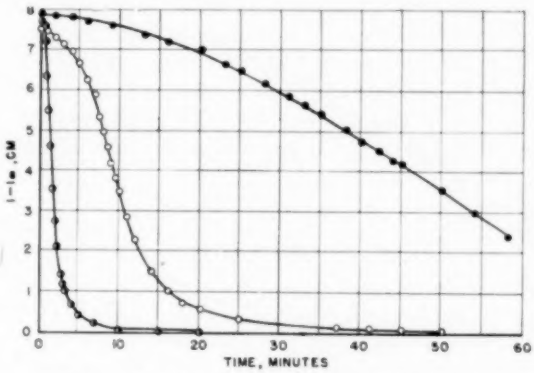

FIGURE 2. *Effect of temperature on shrinkage.*

●, 58.4°C; ○, 60.1°C; ◑, 62.0°C.

Following complete shrinkage another process occurs, which is not shown in the figure, since it is beyond the scope of this investigation. This process involves reelongation of the shrunken collagen and is presumably associated with solution of the shrunken material, weakening of the structure, and resultant stretching. This process is of concern only in that it seriously limits the range of measurements, rendering impractical any measurements requiring more than a few hours.

2. Characteristics of Shrinkage

The mechanism of shrinkage, as related to the structure of collagen, is of great theoretical interest but is beyond the scope of this investigation. Observations made during shrinkage may give a

clue to the mechanism. A tendon, when first immersed with the bath at a temperature that causes a moderate rate of shrinkage, is completely quiescent. The finely corrugated regular surface of the original tendon gradually becomes slightly distorted at fixed points, the distortion being caused by tiny nodules that are formed inside the tendon. The formation of nodules marks the onset of shrinkage. A nodule grows internally, produces a large lump, and then appears to gelatinize and form a gelatinous ring around the tendon. The gelatinous ring is invariably oriented at an angle of approximately 30° with the axis of the tendon and is of a much larger diameter (two to three times) than that of the tendon. Tendon adjacent to the gelatinous ring appears to be pulled into the ring from both directions. Nodules, which appear to be formed at a rate proportional to the temperature, grow, coalesce, and thus cause shrinkage. Most shrinkage is associated with nodule formation and growth, and it is most probable that the transformation of the adjacent tendon into gelatinous material is of minor importance in causing shrinkage. The drawings in figure 3 illustrate the course of the

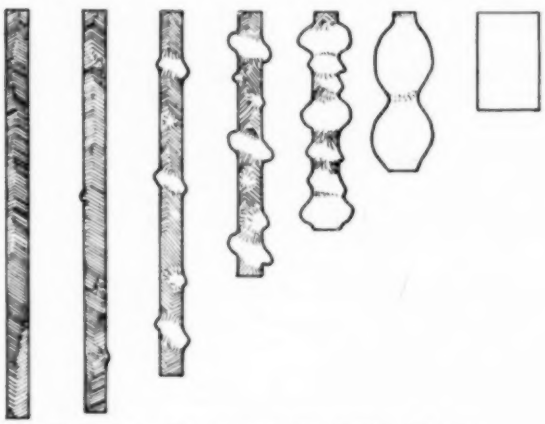

FIGURE 3. *Behavior of tendon during shrinkage.*

shrinkage. These observations are remarkably similar to photographs made of shrinkage of fibrils of submicroscopic dimensions by Nutting and Borasky [18].

3. Effect of Tension on Shrinkage

Measurements were made to determine the effect of tension on the experimental results. Shrinkage tests were made by using weights of 3.6, 14.4, and 40.2 g. on the tendons. The results of these measurements at 65.3° C are shown in figure 4, measurements at other temperatures yielding comparable results. It is noted that increasing tension apparently causes decreased rate of shrinkage and an increasing induction period. This effect will be discussed subsequently.

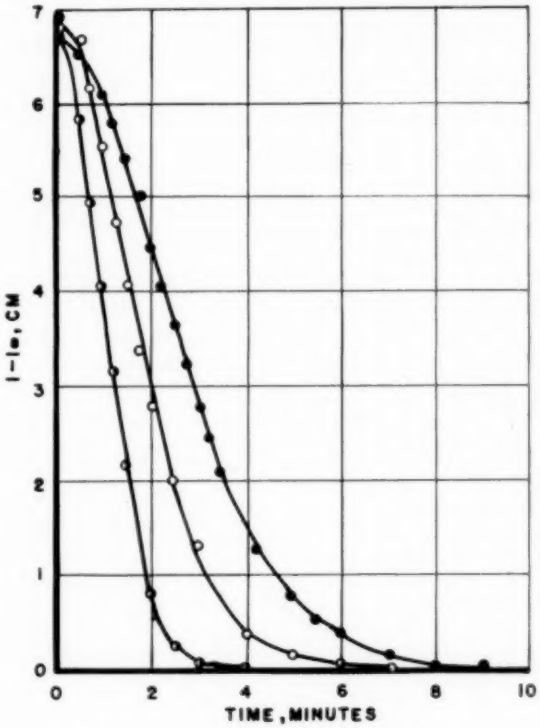

FIGURE 4. *Effect of tension on shrinkage.*

◑, Load 3.6 g, 65.3°C; ○, load 14.4 g, 65.2°C; ●, load 40.2 g, 65.4°C.

4. Mathematical Treatment of Results

(a) Rate Constants and Heat of Activation

The results shown in figures 1, 2, and 4 indicate that, except at low temperatures, where shrinkage is quite slow, the shrinkage follows approximately an exponential function of the time after a period of induction. Such a relationship may be written

$$l=(l_0-l_\infty)e^{-Kt}+l_\infty, \qquad (1)$$

where l is the length of tendon at time t, l_∞ is the completely shrunken length, l_0 is the initial length, and K is the rate constant for the shrinkage. Equation 1 is of the form of a first-order equation [19]. If such a process is investigated, a graph of log $(l-l_\infty)$ as ordinate and t as abscissa will yield

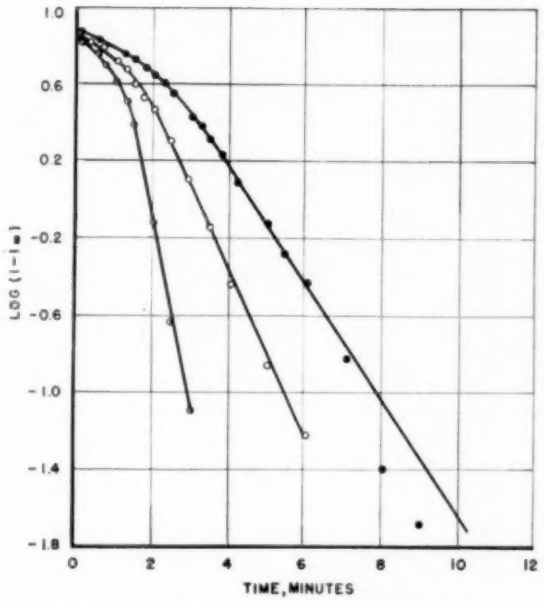

FIGURE 5. *First-order plot of shrinkage data.*
◑, Load 3.6 g, 65.3°C; ○, load 14.4 g, 65.2°C; ●, load 40.2 g, 65.4°C.

a straight line of slope $-K$. Figure 5 shows the results given in figure 4 plotted in this manner, and it is seen that following a period of nonconformity, approximate linearity is obtained.

Objections to the use of rate constants obtained in this manner are as follows: (1) Graphs of data at lower temperatures show negligible linearity and, therefore, do not yield values of K. This behavior is probably related to the fact that a physical measurement of length is being utilized to follow a complex chemical process that probably involves consecutive reactions. (2) At higher temperatures adequate linearity is attained, but shrinkage occurs so rapidly that it is difficult to obtain sufficient data to permit accurate evaluation of K. Therefore a more useful measure of the rate of the reaction has been utilized, the time of half-shrinkage, designated by $t_{1/2}$ and defined as the time, t, at which the length of the tendon, l, is equal to $(l_0+l_\infty)/2$.

Let the energy, or heat, of the activation process be ΔH. Then the temperature dependence of K [19] is given by the equation

$$\ln K=\frac{\Delta H}{RT}+C, \qquad (2)$$

where in addition to previously defined terms, R is the gas constant, T is the absolute temperature, and C is a constant. A similar relationship holds if $\ln(1/t^*)$ is substituted in eq 2 for $\ln K$, where t^* is defined to be any corresponding time in the course of the reaction. The corresponding time is taken to be a measure of the extent of the reaction, and in the present study the time corresponding to half-shrinkage $t_{1/2}$ is used. Since the evidence that has been presented indicates that the shrinkage follows, in part, the law of a first-order reaction and, since it has been found that in general protein denaturation follows this law [21], it is assumed that the shrinkage process is a denaturation reaction of first order and that the times of half-shrinkage obtained from experimental data represent times of half-chemical reaction. It is seen from eq 2 that the latter portion of the assumption is unnecessary to obtain correct values of ΔH. It will be required, however, in the theory of absolute reaction rates to obtain entropy and free-energy values.

The validity of use of $t_{1/2}$ is justified by linearity of graphs obtained by plotting log $(1/t_{1/2})$ as ordinate and $1/T$ as abscissa. The linearity obtained implies either that $t_{1/2}$ is a true measure of a corresponding point in the reaction or that ΔH and $t_{1/2}$ vary in a complicated manner to produce linearity. The latter possibility is remote and therefore rejected as improbable. Values of $t_{1/2}$ may be obtained readily by interpolation of data and will be used hereafter to characterize the reaction velocity. Values of ΔH will be obtained as the slopes of lines obtained from graphs of log $(1/t_{1/2})$ and $1/T$ as described later.

(b) Entropy and Free Energy of Activation

The shrinkage process can be measured only over a short temperature range, which implies a large heat of activation. On the basis of the theory of absolute reaction rates [20], in order for such a process to occur with measurable velocity at ordinary temperatures, a large entropy *increase*, ΔS, must be associated with activation. In other words, the free energy of activation, ΔF, defined by the relationship,

$$\Delta F=\Delta H-T\Delta S, \qquad (3)$$

must be of a much smaller magnitude than ΔH. To obtain these quantities from the experimental data, use was made of the theory of absolute

reaction rates. The fundamental equation of this theory is

$$K=\frac{kT}{h}\kappa K', \tag{4}$$

where K is the reaction velocity constant, k, Boltzmann's constant, h, Planck's constant, T, the absolute temperature, K', the equilibrium constant of the reaction involving formation of an "activated complex," and κ, the transmission coefficient. This factor will be constant under the conditions of this experiment, and in the absence of information concerning its magnitude, will be assumed to be unity. As this reaction involves disorganization of the structure of collagen and therefore may be considered to be a decomposition, κ probably is approximately 1 [20]. If the term in κ is included it will represent an uncertainty in ΔS but will have no effect on ΔH, as will be seen by a consideration of later equations.

Substituting for K' in eq 4 from the relationship

$$\Delta F=-RT\ln K' \tag{5}$$

we obtain an equation relating K and F,

$$K=\frac{kT}{h}e^{-\Delta F/RT}. \tag{6}$$

Substituting for ΔF from eq 3,

$$K=\frac{kT}{h}e^{-(\Delta H/RT-\Delta S/R)}. \tag{7}$$

To obtain a relationship involving $t_{1/2}$ in place of K for reasons previously enumerated, assume the equation

$$K=\frac{0.6932}{t_{1/2}}. \tag{8}$$

The constant 0.6932 corresponds to the numerical relationship between K and $t_{1/2}$ for first-order reactions [19]. Substituting into eq 7 and rearranging, the following relationships are obtained:

$$\frac{0.6932h}{kTt_{1/2}}=e^{-\Delta F/RT}=e^{-(\Delta H/RT-\Delta S/R)}. \tag{9}$$

By taking logarithms of these equations, it is seen that a graph of $\log 0.6932h/kTt_{1/2}$ and $1/T$ yields a line that has a slope and intercept proportional to ΔH and ΔS, respectively.

Solving eq 9 and 7 for ΔS the two following results are obtained:

$$\Delta S=2.303R\left[\log\frac{h}{kT}+\log\frac{1}{t_{1/2}}+\log 0.6932\right]+\frac{\Delta H}{T} \tag{10}$$

$$\Delta S=2.303R\left[\log\frac{h}{kT}+\log K\right]+\frac{\Delta H}{T}. \tag{11}$$

Equation 11 will yield the absolute value of $\triangle S$ for the activation. The essential difference between eq 10 and 11 lies in the proportionality factor 0.6932 of eq 10. Assuming the value of 0.6932 is in error by a factor of 1,000, an uncertainty of only 13.8 cal/mole deg in ΔS results. A corresponding uncertainty of only 4.6 kcal/mole in values of ΔF at 60° C is obtained. Derived values of ΔH will be unaffected by uncertainties in the relationship between K and $t_{1/2}$. It seems, therefore, that ΔS and ΔF obtained through use

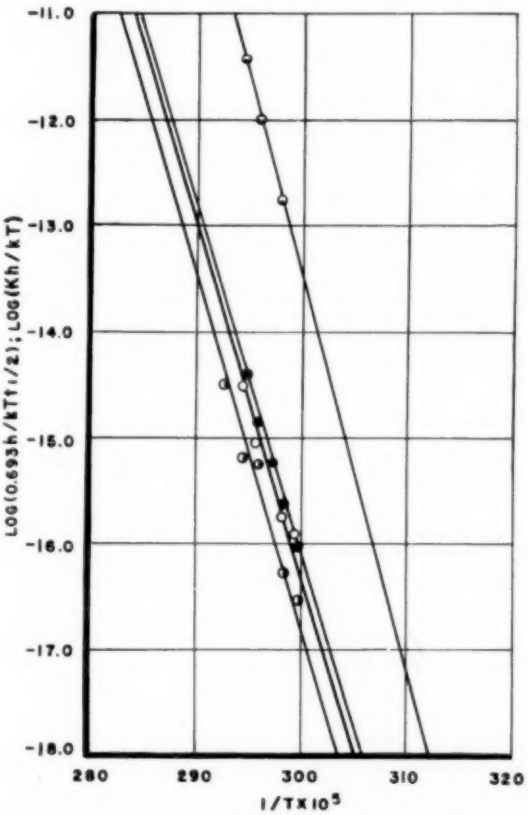

FIGURE 6. *Application of absolute reaction rate theory to data.*

◒, 14.4 g, K values; ●, 3.6 g, $t_{1/2}$ values; ○, 14.4 g, $t_{1/2}$ values; ◑, 10.2 g, $t_{1/2}$ values.

of $t_{1/2}$ values may be considered to be good approximations to the absolute values of ΔS and ΔF.

It will be noted that the transmission coefficient, κ, would appear in an added logarithm term in eq 10 and 11, and unless κ differs appreciably from unity, would have little effect on ΔS.

The results obtained under three different tensions are shown in figure 6, graphed in accordance with eq 9, log $0.6932h/kTt_{1/2}$ being plotted as ordinate and $1/T$ as abscissa. In addition, the reaction velocity constants of the measurements with the 14.4-g weight were obtained graphically and are plotted in accordance with eq 7. In the latter graph only three points are obtained, since no linearity and no velocity constant were obtained at the lowest temperature. The results for ΔH and ΔS shown in table 1 were obtained by application of least squares to the data shown in figure 6 and are considered to be in fair agreement. In practice it was observed that use of the largest stress greatly reduces the temperature range in which linearity may be found in a first-order application. Consequently, it is believed that the apparent deviation from the first-order reaction is in some manner related to initial stresses existing in the tendon from internal and external forces as well as to the method of measuring the course of the reaction through the change in length.

TABLE 1. *Effect of tension on activation constants*

Load	Data used for calculation	Heat of activation, ΔH	Entropy of activation, ΔS	Free energy of activation at 60° C, ΔF_{60}
g		*kcal/mole*	*cal/mole deg*	*kcal/mole*
3.6	$t_{1/2}$	136	330	26.2
14.4	$t_{1/2}$	136	334	24.8
14.4	K	113	277	20.8
40.2	$t_{1/2}$	154	385	25.8

The results of figure 6 indicate a trend toward higher temperatures under larger tension. The increase in shrinkage temperature under tension has been reported by Wohlisch [15], but the experimental variation is such that the differences noted in figure 6 may be due to sampling.

5. Heat, Entropy, and Free Energy of Activation of Untreated Tendons

The results of measurements of thermodynamic activation constants of various batches of tendons in distilled water (pH 6 to 7) are shown in table 2. Values of ΔH and ΔS were obtained by application of the least squares to data consisting of $t_{1/2}$ and $1/T$ values. Values of ΔF_{60} were obtained by use of results for ΔH and ΔS and application of eq 3 and are calculated at 60° C. This temperature was chosen since rapid shrinkage of tendons occurs at 60° C. All measurements were made using the 14.4-g weight.

TABLE 2. *Activation constants of tendon collagen*

Heat of activation, ΔH	Entropy of activation, ΔS	Free energy of activation at 60° C, ΔF_{60}
kcal/mole	*cal/mole deg*	*kcal/mole*
136	334	25.0
136	330	25.2
145	361	25.1
168	431	24.7
152	383	24.8
141	348	24.9
120	292	23.2
128	313	24.4
Average.....141	349	24.7
Standard deviation ..15	43	0.6

It is found that, although ΔH varies between 120 to 170 kcal/mole and ΔS between 290 to 430 cal/mole deg., the values of ΔF_{60} remain substantially constant at approximately 25 kcal/mole. The size of the values of ΔH and ΔS are indicative of chemical reactions involving large molecules and agree in magnitude with similar values previously obtained for denaturation of soluble proteins [21]. The heat of activation is probably identified with rupture of bonds during activation. The entropy change is probably associated with a marked disorientation occurring in the process of activation. The variation observed in these values may be due to varying stress caused by different cross-sectional areas, as indicated by figure 6, to varying degrees of crystallinity or bonding in different specimens, or to experimental errors inherent in determination of quantities of such magnitude.

The process of shrinkage may be assumed to be represented by the following reactions:

$$\underset{\text{(inactive)}}{\text{Collagen A}} \rightleftharpoons \underset{\text{(activated) (complex)}}{\text{Collagen B}} \rightarrow \underset{\text{(shrunk)}}{\text{Collagen C.}}$$

The heat, entropy, and free energies obtained relate to the equilibrium process on the left. A measure of the position of this equilibrium is given

by ΔF, as shown by eq 5, which relates ΔF and the equilibrium constant of this process. The value of ΔF is then considered to be a measure of the temperature interval of shrinkage, as the concentration of collagen B will be determined by the value of ΔF in conformity with eq 5.

6. Measurement of Shrinkage Temperatures

The foregoing results show that a true shrinkage temperature does not exist, since the process involved is a rate phenomenon. The high heat of activation, however, is probably responsible for the fact that shrinkage has heretofore not been recognized as a rate process and to a large extent minimizes errors in measurements of shrinkage temperatures. However, interpretation of shrinkage as a process occurring at a fixed temperature is subject to all errors inherent in interpreting a rate phenomenon as a fixed temperature process, plus an additional serious error related to the fact that the rate of shrinkage initially accelerates from zero.

By defining the end of the acceleration period as that time at which adherence to the first-order equation begins, it has been ascertained that it has a temperature coefficient approximately equal to that of the shrinkage reaction, that is, $\Delta H \approx 130$ kcal/mole. This means that the initial process is actually a portion of the shrinkage, and it will invariably cause a shrinkage temperature measurement to yield too high a temperature, that is, a positive error.

Specimens contained in a water bath heated at the rate of 2 deg C/min will necessarily remain at a temperature lower than that of the water. This consideration also leads to a positive error.

Dry specimens, when immersed in the bath require much longer periods of time before initial shrinkage than specimens that are soaked prior to test. A shrinkage test specimen placed in a bath and tested immediately may give a high result.

All experimental results indicate positive errors in measurements of shrinkage temperatures, and the results obtained from these measurements are doubtless too high [16]. For ordinary test purposes, it is believed that the present method [3] is adequate, since it is very doubtful if the error can exceed 5 deg C. For precise work, however, the method leaves much to be desired. In such instances it should be possible to define shrinkage temperature in either one of two ways: (1) prescribe a permissible change in surface area of a specimen of known area subjected to a fixed temperature for a specified length of time, (2) define the shrinkage temperature as that temperature causing half-shrinkage in 1 min. The first method of definition would require no apparatus other than that normally found in any laboratory. The latter, however, would necessitate rate measurements and is less preferable experimentally, although more desirable thermodynamically since it, in effect, specifies ΔF and therefore K' (eq 5).

IV. Results of Measurements on Treated Tendon

1. Effect of pH of Equilibrium Solution

Initial attempts to evaluate thermodynamic activation constants of tanned tendons led to erratic and inexplicable results. As tanning involved occasional use of extreme pH values, it was decided to ascertain the effect of pH on the activation. In these experiments, the low pH values were obtained with sulfuric acid and the high pH values with sodium hydroxide. All specimens were allowed to equilibrate in the solution of desired pH for 24 hr prior to test, and the measurements were made by using the equilibrium solution as the confining liquid. A large excess of liquid was used in every test. Extreme acid and alkaline pH values caused enormous swelling of the tendons, and early results showed the advisability of subjecting such specimens to refrigeration at all times prior to testing. Results of these tests are shown in table 3 and figure 7. Table 3 shows that heat, entropy, and free energy of activation decrease in acid and alkaline solutions. Attention is called to the two latter values of the table. These values represent results obtained on tendons that had been subjected to the extreme pH values and then leached with water until all acid or alkali was removed. It is observed that substantial recovery of the initial state has been obtained. This result is important since it justifies the use of acid or alkali in the tanning process, provided thorough washing is effected.

The nature of the shrinkage of highly swollen tendons differs from that of normal tendons in that the acceleration period is negligible and possibly entirely missing. There is considerable

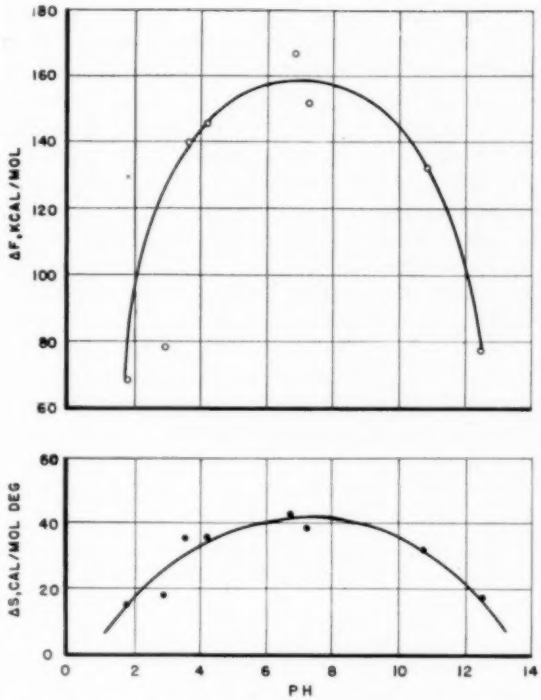

FIGURE 7. *Effect of* pH *on heat and entropy of activation.* ○, ΔF; ●, ΔS.

deviation from linearity under these conditions in the graph of log $0.6932h/kTt_{½}$ versus $1/T$ in the lower temperature ranges. It appears probable that linearity is the limiting condition occurring at high temperatures. In figure 8 the linear plots are shown from which the data of table 3 were obtained.

TABLE 3. *Effect of* pH *on activation constants of tendon collagen*

pH	Heat of activation, ΔH	Entropy of activation, ΔS	Free energy of activation at 60° C, ΔF_{60}
	kcal/mole	*cal/mole deg*	*kcal/mole*
1.8	67	150	17.4
3.0	79	175	20.6
3.6	141	363	19.8
4.2	145	368	22.5
6.8	168	431	24.7
7.2	152	383	24.8
10.8	132	327	23.5
12.5	77	177	18.4
1.8 leached with water to 7.2	142	358	23.3
12.5 leached with water to 7.3	125	305	23.0

Figure 8 shows indirectly that as the pH varies, the range of temperatures in which measurements

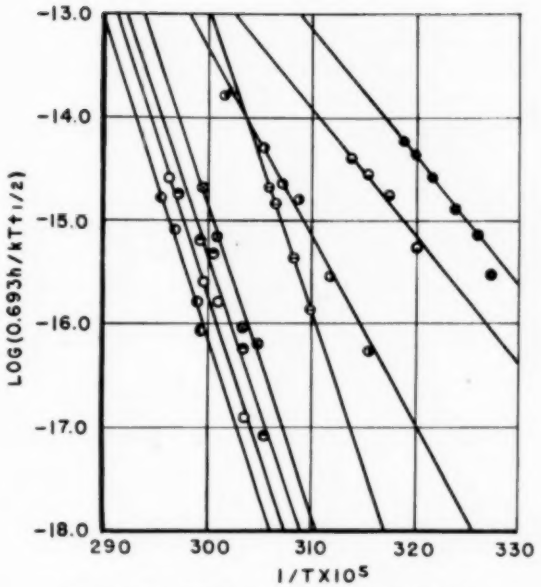

FIGURE 8. *Effect of* pH *on rate of shrinkage.* ●, pH 1.8; ◑, pH 3.0; ⊖, pH 3.6; ⊗, pH 4.2; ○, pH 6.8; ◐, pH 7.2; ◓, pH 10.8; ◒, pH 12.5

can be made, that is, the shrinkage "temperature" hereafter denoted as T_s and defined as that temperature causing half-shrinkage in 1 minute, varies in direct proportion to ΔF_{60}. The variation of T_s with pH is shown by the shift of the linear plots parallel to the $1/T$ axis. This finding is in agreement with observations made by Theis [6].

The dependence of the activation constants on pH implies that activation involves reaction with or loss of hydrogen ions [20]. The neglect of the role of H^+, implicit in application of the absolute reaction rate theory without considering the reaction of H^+, is equivalent to choice of variable standard states as regards hydrogen-ion concentration. Further measurements on the effect of pH on activation may be expected to yield valuable information concerning the nature of the activation process.

2. Effect of Sodium Chloride

Since salt is widely used in the tanning process as a swelling deterrent, it is of interest to ascertain the effect of salt on the activation constants. In these tests the pH was maintained at approximately 6.2, adjustments being made with dilute sulfuric acid when necessary. Solutions were made by weighing the desired quantity of chemically pure sodium chloride (NaCl). Tendons

were soaked in the solutions for 24 hr prior to test and tested with the equilibrium solution as the confining liquid. Results of these tests are shown in table 4 and figure 9.

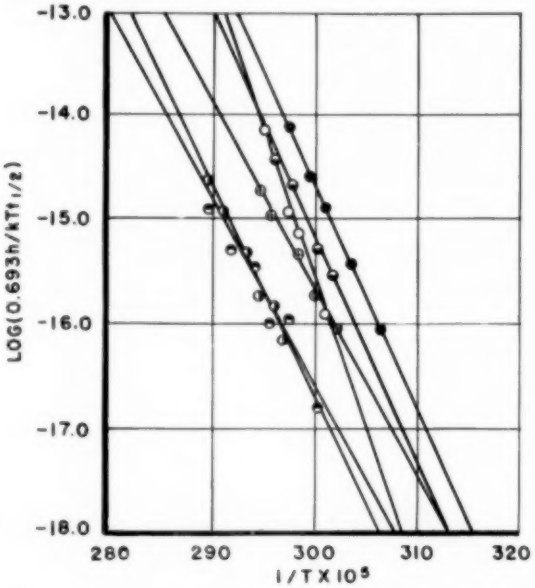

FIGURE 9. *Effect of sodium chloride on rate of shrinkage, pH 6.3.*

○, 0.05 *M*; ◒, 0.1 *M*; ●, 1.0 *M*; ⊕, 2.0 *M*; ◑, 4.0 *M*; ◓, saturated.

TABLE 4. *Effect of sodium chloride on activation of tendon collagen*

Concentration of sodium chloride	Acidity, pH	Heat of activation, ΔH	Entropy of activation, ΔS	Free energy of activation at 60° C, ΔF_{60}
mole/liter		*kcal/mole*	*cal/mole deg*	*kcal/mole*
0.00	6.0	141	349	24.7
.05	6.3	119	285	23.8
.1	6.2	95	217	23.2
1.0	6.3	93	213	22.4
2.0	6.2	83	176	24.1
4.0	6.1	87	185	25.8
Saturated	6.0	75	149	25.3

It is observed in table 4 that ΔH and ΔS decrease with increased concentration of sodium chloride with one exception, that is, 4 *M* sodium chloride. This exception, however, lies well within the limits of variation noted for untreated tendon. The value of ΔF_{60} remains substantially constant but appears to proceed through a minimum in the region of 1 *M* sodium chloride. The variation of ΔF_{60} is beyond the experimental variation and is probably real. In figure 9 it is noted that T_s likewise reaches a minimum in this region of concentration of sodium chloride. This result corroborates findings by Theis [6].

3. Effect of Pickling

The effect of a combination of acid and sodium chloride was determined in a similar manner. One concentration of acid was used, and the salt content was varied. Sulfuric acid of pH 1.8 was used because of the low activation constants observed at this pH and the fact that maximum swelling of collagen occurs in this region of pH, as shown by Highberger [22]. Tendons were soaked in the solutions for 24 hr and tested using the equilibrium solution as the confining liquid. Desired concentrations of sodium chloride were obtained by weighing chemically pure NaCl. The results of these tests are given in table 5 and figure 10.

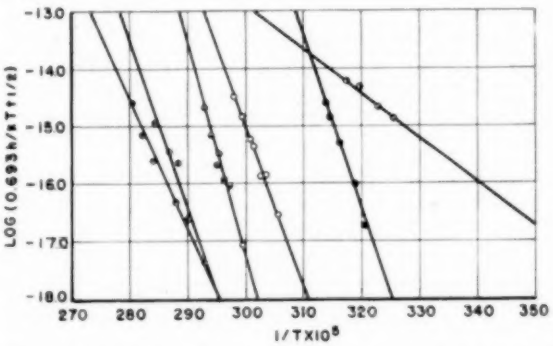

FIGURE 10. *Effect of sodium chloride on rate of shrinkage, pH 1.8.*

◑, 0.1 *M*; ●, 0.5 *M*; ○, 1.0 *M*; ◒, 2.0 *M*; ◐, 4.0 *M*; ◓, saturated.

TABLE 5. *Effect of acid and salt on activation constants of tendon collagen*

Concentration of sodium chloride	Acidity pH	Heat of activation, ΔH	Entropy of activation, ΔS	Free energy of activation at 60°C, ΔF_{60}
Mole/liter		*kcal/mole*	*cal/mole deg*	*kcal/mole*
0.0	1.8	67.0	150	17.4
.1	1.8	31.2	56.2	12.4
.5	1.8	139	359	16.3
1.0	1.8	126	310	23.3
2.0	1.7	161	405	26.2
4.0	1.8	138	324	29.9
Saturated	1.8	109	212	29.1

It is of interest to compare these values with the results previously obtained with sulfuric acid and sodium chloride individually. Bearing in mind the experimental variation previously obtained with

untreated tendons, the general trends with increasing concentration of sodium chloride appear to be as follows: (1) ΔH increases, passes through a maximum, and then decreases, (2) ΔS follows a similar behavior, (3) ΔF_{60} appears to increase monotonically. Comparing these results with those obtained previously, it is seen that the behavior of the combination of sodium chloride plus sulfuric acid toward collagen is not a simple additive property of the individual effects. The results indicate that pickling is complex in nature and possibly involves two competitive reactions involving collagen, sulfuric acid, and sodium chloride.

It is known that acid and salt individually cause swelling of collagen [22, 23]. It was observed that the swelling caused by 0.1 *M* sodium chloride in sulfuric acid of pH 1.8 was far greater than that resulting from sulfuric acid of pH 1.8 alone. This is probably the cause of the low constants found for the 0.1 *M* sodium chloride solution of pH 1.8.

4. Effect of Tanning

Tanning of the tendons has presented difficulties, particularly in view of the fact that extraneous masking salts are undesirable because they may introduce unknown effects. Tanning was effected in most instances by immersing the specimens in a solution of the tanning agent and adjusting the pH to the optimum value. Following tannage, specimens were thoroughly washed and tested by using distilled water as the confining liquid. Some specimens were reserved for analysis, consisting in most instances of an ash determination. Tannage with iron and aluminum was found to necessitate masking salts and, to date, no satisfactory vegetable-tanned tendons have been prepared. This does not imply that vegetable tannage does not occur, but for purposes of test a uniform tannage must be obtained, and the uniformity presents difficulties.

Tannages were secured by the following methods: formaldehyde: 15-percent solution of formaldehyde, pH 6 to 7 [24]. Vanadium: saturated solution of sodium vanadate, pH 3 [25]. Iron: solution of ferric sulfate and citric acid, pH 5 [26]. Aluminum: solution of aluminum sulfate and sodium citrate, pH 5 [27]. Uranium: solution of sodium uranate (complex carbonate formed), pH 5 [28]. Zirconium: solution of zirconyl sulfate, pH 2 [29]. Chromium: two-bath process consisting of immersion in a solution of potassium dichromate followed by reduction with a solution of sodium bisulfite [1]. Bating: trypsin treatment in saturated solution of calcium carbonate at 35° C for 24 hr.

The results of tests of tendons subjected to these tannages and treatments are given in table 6.

TABLE 6. *Effect of tanning and pretannage treatments on activation constants of tendon collagen*

Tannage or treatment	Ash (dry basis)	Heat of activation, ΔH	Entropy of activation, ΔS	Free energy of activation at 60° C, ΔF_{60}
	Percent	*kcal/mole*	*cal/mole deg*	*kcal/mole*
Bated		161	408	24.8
Thiosulfate		131	318	24.6
Bisulfite		164	421	23.7
Dichromate		129	286	23.7
Formaldehyde		113	232	29.0
Zirconium	27.0	137	307	35.1
Iron	5.3	119	282	25.4
Vanadium	12.3	118	281	25.2
Aluminum	1.5	82.1	172	24.8
Uranium	3.0	102	231	25.3
Chromium	0.06 (Cr_2O_3)	160	404	26.5
Do	.13 (Cr_2O_3)	203	522	28.5
Do	.57 (Cr_2O_3)	323	862	36.1
Do	1.02 (Cr_2O_3)	390	1,041	44.1
Do	1.98 (Cr_2O_3)	325	841	45.2

Three important conclusions are to be drawn from the results of table 6 as follows: (1) Chrome tanning alone drastically increases ΔH, ΔS, and ΔF_{60}. Further, the amount of chrome required to produce this effect is small, that is, about 0.6 percent of chromium oxide (Cr_2O_3). (Chromium contents were determined by perchloric acid and by colorimetric methods [3, 30]). (2) Tanning with zirconium and treating with sodium dichromate, sodium bisulfite, sodium thiosulfate, and trypsin have no appreciable effect on ΔH, and, of these, zirconium alone increases ΔF_{60}, an increase resulting by decrease of ΔS. (3) Tanning with formaldehyde, vanadium, iron, aluminum, and uranium appears to decrease ΔH but, except for formaldehyde, does not affect ΔF_{60} appreciably. In some instances the decrease in ΔH is doubtful since it is small.

Tanning with most metallic tanning agents increased the ash content only slightly, and in most instances probably mediocre tannage was obtained. However, in view of the extraordinary changes caused by 0.6 percent of Cr_2O_3, it is seen that other metallic tans differ from chromium.

The graphical results from which ΔH and ΔS

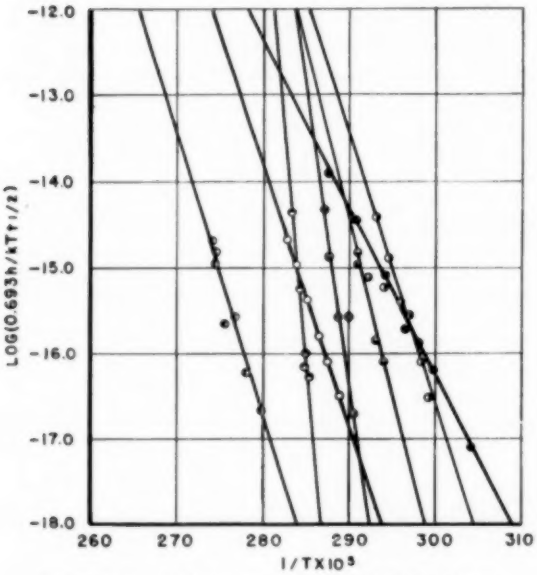

FIGURE 11. *Effect of tannage on rate of shrinkage.*

●, Alum tanned; ◑, iron tanned; ◐, zirconium tanned; ○, formaldehyde tanned; ◒, chrome tanned, 0.13 percent CR_2O_3; ⊕, chrome tanned, 0.57 percent CR_2O_3; ◓, chrome tanned, 1.03 percent CR_2O_3.

were determined are shown for some tannages in figure 11.

V. Discussion

1. Hydrothermal Stability of Leather and Collagen

Shrinkage is a rate process and, as such, presumably proceeds at all temperatures at a rate governed by the temperature, previous treatment, and environment as shown by the foregoing results. To obtain an idea of the behavior at room temperature a graph was made in which the logarithm of the time of half shrinkage in minutes, log $t_{1/2}$, is plotted as ordinate and the reciprocal of the absolute temperature, $1/T$, as abscissa. The measurements are limited to a short temperature interval by virtue of the large value of ΔH but, assuming the linearity is valid beyond this range, it is possible to extrapolate to room temperature and obtain the time of half shrinkage at such temperature. The graphs are shown in figure 12. Because of the nature of the slopes and intercepts, it is not possible to show all extrapolated curves on the same graph, but the extrapolations of all results shown in figure 12 yield the approximate values of $t_{1/2}$ at 25° C shown in table 7.

The results of table 7 must be considered approximations if only because of the length of the

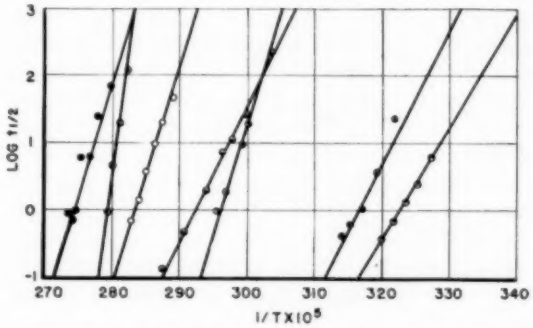

FIGURE 12. *Effect of tannage on half-shrinkage time.*

●, Zirconium tanned; ○, formaldehyde tanned; ◐, chrome tanned; ◒, alum tanned; ◑, untreated, pH 7.2; ⊕, sulfuric acid, pH 1.8; ◓, sodium hydroxide, pH 12.4.

necessary extrapolation, but, even as approximations, interesting conclusions result. It is noted that extreme pH values cause fairly rapid shrinkage, that is, small time of half-shrinkage. It is for this reason that specimens in alkaline and acid solutions were cooled as previously described. Tanning, with the exception of alum-tanning, drastically increases the time of half-shrinkage at room temperature. This increase is due to two factors: (1) A shift of the line to lower values of $1/T$, that is, increased T_s, and (2) an increase in the slope of the line, that is, increase in ΔH. This latter behavior is noted only in the case of chrome-tanned tendon. A comparison of the relative efficiency of these two processes in increasing $t_{1/2}$ is afforded by comparing the values of $t_{1/2}$ for chrome and zirconium tannages. The zirconium tannage caused the largest shift in T_s, whereas the chrome tannage increased ΔH. It is noted from table 7 that the latter effect is many fold more effective in increasing $t_{1/2}$. To date, however, no treatment other than chrome tanning has been observed to produce an increase in ΔH.

TABLE 7. *Time of half-shrinkage at 25° C*

Treatment	Time of half-shrinkage, $t_{1/2}$
	min
Chrome-tanned	2×10^{40}
Formaldehyde-tanned	3×10^{17}
Zirconium-tanned	5×10^{30}
Alum-tanned	8×10^{9}
Untanned, pH 7.2	5×10^{12}
Untanned, pH 1.8	1.5×10^{3}
Untanned, pH 12.4	8×10^{3}

Recent results obtained in this laboratory by Kanagy [31] indicate that shrinkage at slightly

elevated temperatures and high relative humidity may be an important factor in the deterioration of leather. From this point of view, it would appear that the most stable material would result from chrome-tanned leather having the highest possible shrinkage temperature.

The results of table 7 show that the time of half-shrinkage is drastically reduced when tendons are subjected to extreme values of pH. Assuming that hide behaves in a similar manner, it is concluded that exposure of untanned skins to extreme values of pH may cause irreparable damage to the finished leather, unless a swelling deterrent such as salt is present.

2. Interpretation of Heat, Entropy, and Free Energy of Activation

(a) General Considerations

Theories of the structure of collagen and the tanning process have been published by many authors. An excellent bibliography is given by McLaughlin and Theis [1]. Essentially, the present picture of collagen assumes three types of forces: (1) valence forces along the peptide chains, (2) salt bonds (ionic linkages) between carboxyl and amino groups occurring in side chains of acidic and basic amino acids, and (3) hydrogen bonds between carbonyl groups and neighboring amino or imino groups. The particular theory of tanning of interest here is the "bridging" theory, the origin of which is in controversy [32]. This theory depicts tanning as a reaction in which a tannin molecule reacts with portions of two adjacent peptide chains to form a "bridge." The resultant increase in shrinkage temperature is conceived as due to the increased thermostability conferred by the cross-linking tannin molecules. Shrinkage is then postulated as due to rupture of cross-linkages by thermal agitation and a subsequent collapse of the polypeptide gridwork [1]. The evidence for the rupture of linkages during shrinkage has been given by Gustavson [33] and Theis [34].

Gelatinization involves rupture of few peptide linkages [35], whereas the shrunken collagen possesses a larger number of active groups than the original material [33, 34]. Therefore it is probable that the activation process consists of rupture of key cross-linkages in the collagen molecule. On the assumption that the same cross-linkages must be broken irrespective of the initial configuration, that is, the structure of the activated complex is essentially the same, regardless of tannage, environment, etc., it is possible to obtain interesting information from the foregoing results.

Superficially, the results show that the activation reaction (eq 12) involves absorption of a tremendous quantity of heat. The total heat absorbed in the transformation of collagen A into collagen C has been measured calorimetrically and is of the order of 12.5 cal/g [36]. On the assumption that no heat is involved in the irreversible process (collagen B→collagen C), this figure combined with the value of heat of activation 141 kcal/mole gives a molecular weight of 11,300 for collagen, a figure of the order of magnitude expected for a protein. However, the assumption involved in the calculation is most probably not valid. It appears that no further progress along these lines is possible without extensive calorimetric investigations.

The size of the heat of activation is not disturbing, since large molecules are involved in this reaction. As shown above, an assumption of a molecular weight of 11,300 yields the correct value for the heat of shrinkage. Inasmuch as the molecule may be much larger, the values of heat and entropy involved are not excessive.

(b) Heat of Activation

The linkages ruptured in activation are probably either salt or hydrogen bonds. Consider the following facts about ΔH: (1) ΔH decreases with increasing concentration of sulfuric acid (to pH 1.8); (2) ΔH decreases with increasing concentration of sodium chloride, even in concentrated solutions; (3) ΔH decreases with increasing concentration of sodium hydroxide (to pH 12.5).

Since electrolytes may be expected to act primarily at ionic linkages and ΔH appears to decrease in acid, base, and salt solutions, the effect may be attributed to a salt-type interaction. From this consideration plus the fact that a large number of hydrogen bonds must be postulated to account for the magnitude of the ΔH value observed, it is believed that ΔH measures for the most part the strength of the salt linkages in the collagen molecule.

The results obtained may all be explained by interaction of solutes at salt bonds combined with swelling of the protein structure. However, the effects of electrolytes on hydrogen bonding might conceivably cause similar effects. In the light of

the results obtained with sodium chloride, it is believed preferable to conclude that salt bonds rather than hydrogen bonds are primarily responsible for the variations observed in ΔH, and further that salt bonds contribute at least 70 kcal to the total 140 kcal observed for ΔH.

If the bridging theory of tanning is correct, it is to be expected that ΔH will increase on tanning. Chromium is the only material investigated that causes such increase in ΔH. Other tanning materials, such as iron, uranium, vanadium, and formaldehyde, appear to decrease ΔH, although the variation is so small as to be doubtful in view of the experimental spread found previously. Aluminum decreases ΔH and, therefore, behaves as a salt interacting with the salt bond.

Chromium drastically increases ΔH, and the increase may be pictured as due to either strengthening existing cross-linkages or formation of new linkages.

Therefore it is believed, on the basis of the present experimental evidence, that ΔH measures the salt-bond cohesion energy and that chromium alone, of the materials studied, can form any cross-links between polypeptide chains. Highberger has presented evidence of a mechanical nature that formaldehyde does not form cross-linkages [37].

Inspection of results obtained with chrome-tanned tendons shows that about 1.0 percent of chromium oxide is sufficient to produce the apparent maximum cross-linking and that further increase in chrome content produces small effect. This amount of chromium is far less than the amount required to react with the excess acidic and basic groups present in collagen [35]. Therefore, it is necessary to conclude that only a fraction of these groups present possess the required spatial orientation to either form salt-bonds, which are strengthened by chromium, or react with chromium itself to form new cross-linkages. The amount of chromium combined in excess of 1 percent probably combines with other groups of the collagen in the same manner as the other tanning materials studied, that is, affects ΔS.

(c) Entropy of Activation

The entropy of activation is identified with the degree of disorganization or disorientation occurring in the activation process. This term will, in effect, measure the crystallinity of the collagen, prior to activation, assuming similar final states as regards collagen B. Thus the addition of 1 percent of chromium produces more orientation, a result in agreement with the bridging theory. Acids, bases, and salts, as well as all tanning materials, aside from chromium, in general appear to decrease the ΔS factor. This means that less orientation results under these conditions and implies reaction of collagen with these materials in a more or less random manner that may involve rupture of salt bonds, that is, decreased ΔH. The results obtained with aluminum are interpreted to mean a rupture of salt bonds and a corresponding disorientation sufficient in magnitude to offset the energy lost by rupture. The free energy in this case remains unchanged. Zirconium, on the other hand, tends to react in such a manner that few salt bonds are broken (normal ΔH). However, a loss in orientation is found to occur since ΔS is smaller than for untreated tendon, as shown by the increased value of ΔF_{60}. In chrome tanning, a marked increase in ΔH occurs, but the increase in ΔS is correspondingly less, since ΔF_{60} increases. A portion of the chrome, that is, possibly the whole amount $>$ 1 percent of Cr_2O_3 and a portion of the initial 1 percent, can be considered to add nothing to the orientation. This means some loss of organization due to chrome tanning as well as to other types of tanning. These conclusions are borne out by observations that tanning reduces crystallinity, as shown by X-ray diffraction studies [38].

(d) Free Energy of Activation

The free energy of activation is a measure of the position of equilibrium in the activation reaction. Since shrinkage will ensue rapidly, provided sufficient numbers of activated molecules are formed, ΔF_{60} will then be a measure of the shrinkage "temperature," T_s. ΔF_T will vary with temperatures by virtue of its dependence on the factor $T\Delta S$. It is found that rapid shrinkage occurs at temperatures at which $\Delta F_T \approx 25$ kcal/mole, that is, rapid shrinkage may take place only if the activation equilibrium has been displaced sufficiently to provide required numbers of activated molecules.

The foregoing conclusion implies that treatments that reduce ΔS or increase ΔH will increase ΔF_{60} and consequently the shrinkage "temperature." Chromium tans principally by the latter

method, that is, increases ΔH up to 1 percent of Cr_2O_3 and by the former in amounts exceeding this percentage. All other tannages tested appear to tan by reduction of ΔS. This reduction in ΔS may be pictured as resulting in an increased T_s by steric hindrance phenomena. The amount of steric hindrance may be assumed to be proportional to the tannin content—percentage of Cr_2O_3 in chrome tanning, pH in acid solutions, etc.

Since T_s is determined by ΔF_T, graphs were made using ΔF_{60} as the ordinate and logarithm of the percentage chrome as the abscissa. It was found that a linear relationship resulted. If the logarithm of the concentration of solute, [NaCl], or the pH is used as the abscissa, straight lines are also obtained. Figure 13 shows typical results obtained for such graphs.

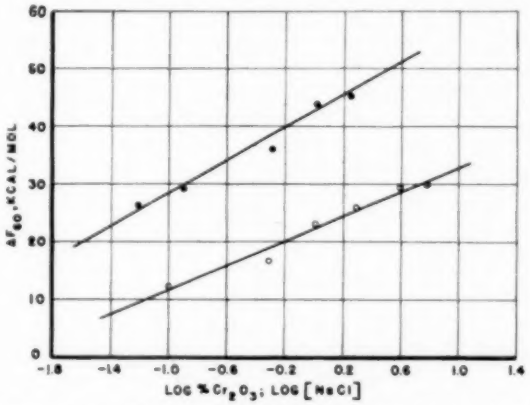

FIGURE 13. *Effect of chromium oxide content and sodium chloride on free energy.*

●, Chrome tanned; ○, pickled.

ΔF_T is related to the equilibrium constant of the activation process, K', by the equation,

$$\Delta F_T = -RT \ln K'. \quad (13)$$

The results shown in figure 13 imply that the logarithm of the equilibrium constant is linearly related to the logarithm of the chromium content, concentration of solute, etc.

Proceeding by speculation, assume $K' = C[Cr_2O_3]^n$, where C and n are constants. Then substituting in eq 3, the following equation is obtained:

$$\Delta F_T = -RT \ln C[Cr_2O_3]^n. \quad (14)$$

In the case of rapid shrinkage it has been ascertained that ΔF_T is nominally constant and approximately equal to 25 kcal/mole at that temperature considered to be the shrinkage "temperature." Substituting this value for ΔF_T and rearranging,

$$\log [Cr_2O_3] = -\frac{25 \times 10^3}{2.303\ RnT} + \frac{\log C}{n}. \quad (15)$$

The concentration of Cr_2O_3 is not known, but it will be assumed proportional to the percentage of Cr_2O_3. On this basis if the logarithm of the percentage chrome is plotted against the reciprocal of the absolute temperature of shrinkage, a straight line is expected. The data presented by Bowes, et al. [5] have been tested in this manner, and a straight-line results. Bowes showed that a straight line was obtained by using the temperature instead of the reciprocal of the absolute temperature but found it necessary to mention possible negative shrinkage temperatures, which might arise. The graph, according to eq 5, eliminates the difficulties of negative shrinkage temperatures and at the same times yields a satisfactory linear plot. Inasmuch as t is proportional to $1/T$ over the limited temperature range involved, the linearity using either t or $1/T$ is not unexpected. No conclusions are possible concerning the slope of the line obtained, since the unknown factor n is involved. By using the experimental value given by Bowes, it is found that the value of n is approximately 1.

No conclusions concerning the mechanism of shrinkage may be made from the present results at this time. It is believed, as a result of observations during shrinkage, that the shrinkage reaction involves water either as a reactant or a catalyst. Experiments are in progress to ascertain the role of water in the shrinkage.

The experimental results obtained in this investigation are in substantial qualitative and quantitative agreement with results of studies made on soluble proteins. Excellent summaries of these researches are given by Eyring and Stearn [39] and Neurath, et al. [21].

The author is indebted to A. A. Maryott for valuable suggestions concerning the treatment of the data and the manuscript.

815197—49——3

VI. References

[1] G. D. McLaughlin and E. R. Theis, The chemistry of leather manufacture (Reinhold Publishing Corp., New York, N. Y., 1945).

[2] R. B. Hobbs, J. Am. Leather Chem. Assoc. **35,** 272 (1940).

[3] Federal Specification for Leather and Leather Products; General Specifications, KK–L–311 (U. S. Government Printing Office, Washington 25, D. C., 1945).

[4] E. R. Theis and E. J. Schaffer, J. Am. Leather Chem. Assoc. **31,** 515 (1936).

[5] J. H. Bowes, H. M. Davies, T. A. Pressley, and C. Robinson, J. Intern. Soc. Leather Trades Chem. **31,** 236 (1947).

[6] E. R. Theis and R. G. Steinhardt, Jr., J. Am. Leather Chem. Assoc. **37,** 433 (1942).

[7] E. R. Theis, J. Am. Leather Chem. Assoc. **37,** 499 (1942).

[8] E. R. Theis and W. A. Blum, J. Am. Leather Chem. Assoc. **37,** 553 (1942).

[9] W. J. Chater, J. Intern. Soc. Leather Trades Chem. **13,** 24, 427 (1929).

[10] W. J. Chater, J. Intern. Soc. Leather Trades Chem. **14,** 28, 133 (1930).

[11] W. J. Chater, J. Intern. Soc. Leather Trades Chem. **22,** 432 (1938).

[12] J. W. Harnly and W. M. Parker, J. Am. Leather Chem. Assoc. **40,** 164 (1945).

[13] E. W. Merry, J. Intern. Soc. Leather Trades Chem. **29,** 223 (1945).

[14] W. J. Chater and J. Draper, J. Intern. Soc. Leather Trades Chem. **23,** 132 (1939).

[15] E. Wohlisch, Biochem. Z. **247,** 329 (1932).

[16] C. E. Weir, J. Research NBS **41,** 279 (1948) RP 1924.

[17] F. O. Schmitt, J. Am. Leather Chem. Assoc. **39,** 430 (1944).

[18] G. C. Nutting and R. Borasky, J. Am. Leather Chem. Assoc. **43,** 96 (1948).

[19] F. H. Getman and F. Daniels, Outlines of theoretical chemistry, 5th ed. (John Wiley & Sons, Inc., New York, N. Y., 1931).

[20] S. Glasstone, K. Laidler, and H. Eyring, The theory of rate processes (McGraw-Hill Book Co., New York, N. Y., 1941).

[21] H. Neurath, J. P. Greenstein, F. W. Putnam, and J. O. Erickson, Chem. Revs. **34,** 157 (1944).

[22] J. H. Highberger, J. Am. Leather Chem. Assoc. **31,** 345 (1936).

[23] D. Jordan-Lloyd and W. B. Pleass, Biochem. J. **21,** 1352 (1927); **22,** 1007 (1928).

[24] J. H. Highberger and F. O'Flaherty, J. Intern. Soc. Leather Trades Chem. **23,** 549 (1939).

[25] A. Kuntzel and H. Erdmann, Collegium **824,** 630, 639 (1938).

[26] J. R. Kanagy and R. A. Kronstadt, J. Am. Leather Chem. Assoc. **38,** 459 (1943).

[27] E. R. Theis. Unpublished results.

[28] C. E. Weir. Unpublished results.

[29] I. C. Somerville, J. Am. Leather Chem. Assoc. **37,** 381, 391 (1942).

[30] R. M. Lollar, J. Am. Leather Chem. Assoc. **42,** 180 (1947).

[31] J. R. Kanagy. Unpublished results.

[32] K. H. Gustavson, J. Intern. Soc. Leather Trades Chem. **31,** 176 (1947).

[33] K. H. Gustavson, J. Am. Leather Chem. Assoc. **41,** 47 (1946); K. H. Gustavson, Biochem. Z. **311,** 347 (1942).

[34] E. R. Theis, J. Biol. Chem. **157,** 7 (1945).

[35] J. R. Kanagy, Chemistry of collagen, NBS Circular 458 (1947).

[36] A. Kuntzel and K. Doehner, Angew. Chem. **52,** 175 (1939).

[37] J. H. Highberger, J. Am. Leather Chem. Assoc. **42,** 493 (1947).

[38] J. H. Highberger and H. J. Kersten, J. Am. Leather Chem. Assoc. **33,** 16, 289 (1938).

[39] H. Eyring and A. F. Stearn, Chem. Revs. **24,** 253 (1939).

WASHINGTON, September 20, 1948.

U. S. Department of Commerce
National Bureau of Standards

Research Paper RP1948
Volume 42, January 1949

Part of the Journal of Research of the National Bureau of Standards

Kinetic Study of the Reaction of Carbon Adsorbents with Oxygen[1]

By William V. Loebenstein,[2] Leland F. Gleysteen,[3] and Victor R. Deitz

A study was made of the kinetics of oxidation of bone char and other carbon adsorbents. The measurements were limited to temperatures between 250° and 390° C. The results were expressed in terms of the fraction of carbon burned per hour at known values of oxygen concentration, temperature, and total rate of flow for activated carbons and bone chars. The rate of oxidation could be expressed either in terms of simple first-order or retarded first-order relationships. A nomograph was used to obtain a rapid estimate of the total fraction of carbon burned at any time for a given rate constant and degree of retardation. The relationship between the reaction-rate constant and the oxygen concentration was linear for a given adsorbent under the same conditions of temperature and flow. Effect of variation in temperature on the rate of oxidation of a new bone char disclosed deviations from the Arrhenius equation even over a 100-deg interval. The influence of time, of oxygen concentration, and of temperature on decarbonization is discussed in relation to the conditions necessary in industrial operations for attaining the optimum uniformity in the carbon content of bone char.

I. Introduction

A study of the reaction of oxygen with carbon discloses many fundamental problems. Two combustion products, CO_2 and CO, are always found simultaneously but in varying relative amounts, depending upon the experimental conditions employed. Heats of adsorption of oxygen on carbon are known to be very high initially but decrease rapidly as the amount of oxygen adsorbed increases. This phenomenon was observed as early as 1924 by Beebe and Taylor [1][4] and by Garner and Blench [2]. The large range of activation energies (20 to 70 kcal/mole), which have been reported in the literature, may be ascribed to the complex reaction mechanism rather than to particular details in the experimental investigations.

Aside from the theoretical interests in the reaction of oxygen with carbon adsorbents, there is an important practical application. The regeneration of carbon adsorbents, which have been used for the purification of solutions, is accomplished by heating in the presence of a limited amount of oxygen or oxygen-containing gases at elevated temperatures. The heating is intended to remove the adsorbed organic matter by oxidation to volatile compounds and restore as completely as possible the adsorptive properties of the surface.

After the exhaustion of the decolorizing power of carbon adsorbents in the refining of sugars, it has been demonstrated that it is technically possible to regenerate almost all kinds of carbon adsorbents. However, there are large differences in the loss of weight realized during regeneration of adsorbents of different origin. This has an important bearing on the economic feasibility of the regeneration. The results given in this paper indicate a striking difference in the magnitude of the rates of oxidation of bone chars and of the activated carbons.

[1] This investigation resulted from a joint research project undertaken by the United States Cane Sugar Refiners & Bone Char Manufacturers, a greater part of the refining industry of the British Commonwealth, and the National Bureau of Standards.

[2] Research Associate at the National Bureau of Standards, representing the cooperating manufacturers.

[3] Present address, Owens Illinois Glass Co., Toledo, Ohio.

[4] Figures in brackets indicate the literature references at the end of this paper.

The raw materials from which carbon adsorbents are prepared vary considerably. The final products may be viewed as carbonaceous residues of varying stability resulting from a destructive distillation of the raw material followed by a limited oxidation under variously controlled conditions. The physical and chemical properties of these residues vary and, consequently, the exact specification of such residues is extremely difficult. The reproducibility of a particular product derived from a given raw material is not too easily maintained even when the requirements of a commercial application are considered. It is necessary, therefore, in order to meet the exact requirements of fundamental research, that the desired experiments be made with aliquot parts of a well-mixed sample. The materials used in obtaining the results reported in this paper have been so prepared. Data on activated carbons and new bone char are reported in this paper. The results for spectroscopically pure graphite and spent bone char are also given for comparison purposes.

In the experiments described in this paper the reaction is studied under conditions that maintain a large excess of oxygen in the gaseous phase compared to that consumed in the oxidation. By studying the reaction with respect to the carbon consumed it is possible to focus attention on the regeneration process.

II. Experimental Procedure

The sample for reaction with oxygen was supported in a vertical tube with inlet for the gas mixtures at the top and the outlet at the bottom. This tube was 15 mm in diameter and 40 mm high and held samples varying in amounts from 0.5 to 5.0 g. It was constructed of fused silica for the graphite experiments and of Pyrex glass for the carbon adsorbents. In order to insure uniform conduction of heat the reaction tube was fitted snugly into a cylindrical brass block 150 mm tall and 75 mm in diameter. This whole assembly was contained in a vertically mounted cylindrical furnace with a control thermocouple placed close to the windings of the furnace. A second thermocouple was fitted into the center of the brass block through a hole situated so that the junction lay as close as possible to the outside wall of the reaction tube in the vicinity of the sample.

The reacting gas mixtures contained in gas cylinders consisted of known percentages of oxygen in nitrogen. The compositions had been determined by the Gas Chemistry Section of this Bureau. Purified nitrogen was passed through the reaction tube during the preliminary heating interval. The flow of nitrogen was discontinued by the employment of a three-way stopcock ahead of the reaction tube at the same instant that the oxygen mixture was introduced. Intervals of time were measured from this moment. The gas mixture was metered into the system at 91 ml/min by means of a flowmeter and maintained at this rate throughout the entire run.

Preliminary tests showed that the water vapor contained in the exit gases, in comparison with the carbon dioxide and carbon monoxide, was so small that it could be neglected entirely. U-tubes of Ascarite-Anhydrone were used in the absorption train to determine carbon dioxide. At the end of each predetermined time interval, one tube was removed from the train and a second tube of the same dimensions immediately inserted. The side arms of the U-tube were bent downward so as to fit into mercury-seal couplings and thus maintain airtight connections. The replacement of the tared U-tubes required but a few seconds. By alternating the twin U-tubes in this manner, it was possible to follow the course of the combustion by gravimetric determination without interrupting the conditions of flow and yet have a quantitative cumulative measurement. The remaining gases, which contained residual oxygen and carbon monoxide along with nitrogen, were next passed through a hopcalite catalyst, which converted the carbon monoxide quantitatively to carbon dioxide. This, in turn, was determined gravimetrically by means of a pair of U-tubes of Ascarite-Anhydrone in exactly the same manner as for the carbon dioxide.

Each sample, prior to its controlled combustion, was heated to constant weight at 110° C in an atmosphere consisting either of helium or purified nitrogen [3].

The constancy of temperature during a combustion was maintained manually for periods of 8 hours or less and by automatic means for longer periods of time. In the latter case, an indicating potentiometer controller was employed. Manually, it was possible to hold a desired temperature

to within less than ±1 deg C. A temperature control of about ±3 deg C was readily attainable by automatic means.

The total weight of carbon burned was computed from the yields of carbon dioxide and carbon monoxide. The rate of reaction was expressed as that fraction, f, of the initial carbon present in the sample which burned per hour. No attempt is made in this present treatment to interpret individually the amounts of carbon dioxide and carbon monoxide produced.

The rate of flow during the experiments was chosen so that the oxygen concentration was not significantly decreased by its consumption. Furthermore, the residual oxygen concentration was sufficient for the quantitative oxidation of the carbon monoxide to carbon dioxide. This is a necessary requirement in the analysis of the gaseous reaction products. Moreover, it was thought that by keeping the oxygen in excess, the interpretation of the reaction mechanism might be simplified. The oxygen concentration in the exit gases was verified later with a specially calibrated Pauling oxygen meter.

III. Kinetics of the Reactions

The rate of combustion is expressed throughout this paper with respect to carbon. The control of the carbon content of bone char during the revivification process is of vital importance in char house operations of sugar refineries. Hence, the study of the combustion with respect to carbon lends itself most readily to practical interpretations.

If the over-all combustion is of the first order with respect to carbon, the rate at which carbon burned should be proportional to the fraction of the carbon remaining, thus

$$\frac{df}{dt}=k(1-f), \tag{1}$$

where f is the fraction of initial carbon burned in t hours and k is the constant of proportionality (reaction rate constant). Upon integration, eq 1 becomes

$$2.303 \log_{10} \frac{1}{1-f}=kt, \tag{2}$$

with the constant of integration vanishing upon substitution of the initial conditions that f is zero when t is zero. It will be seen from figures 1 and 2 that a linear plot of $\log 1/(1-f)$ against t applies to graphite and the activated carbons, but not to any of the bone chars investigated.

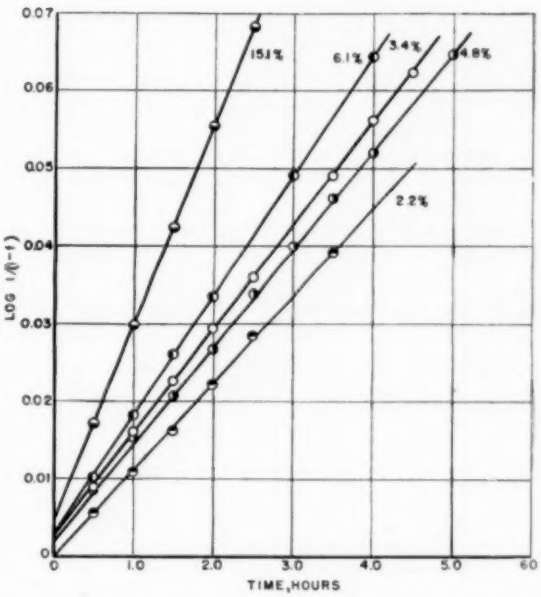

FIGURE 1. *Reaction of activated carbon 6 with varying oxygen concentrations.*

The ordinate is $\log_{10} 1/(1-f)$, where f is the fraction of carbon oxidized. The abscissa is the time in hours. The rate of flow is 91 ml/min. and the temperature is 390° C.

The combustion of bone chars will be shown to obey a retarded first-order relationship identical in form with that proposed by C. N. Hinshelwood [4] for the kinetics of the catalytic decomposition of nitrous oxide, in which it was assumed that the reaction was retarded by the oxygen produced. This does not necessarily imply that the retardation in the combustion of bone chars can be attributed to a similar mechanism.

In the present treatment, the differential equation for combustion of bone chars may be written as follows:

$$\frac{df}{dt}=\frac{k(1-f)}{1+bf}, \tag{3}$$

where the constant b is a measure of the degree of retardation during a given combustion. This is also similar to an equation suggested by J. D. Lambert [5] for the oxidation of charcoal where the reaction was investigated with respect to oxygen consumed. It can be seen from eq 3 that if no

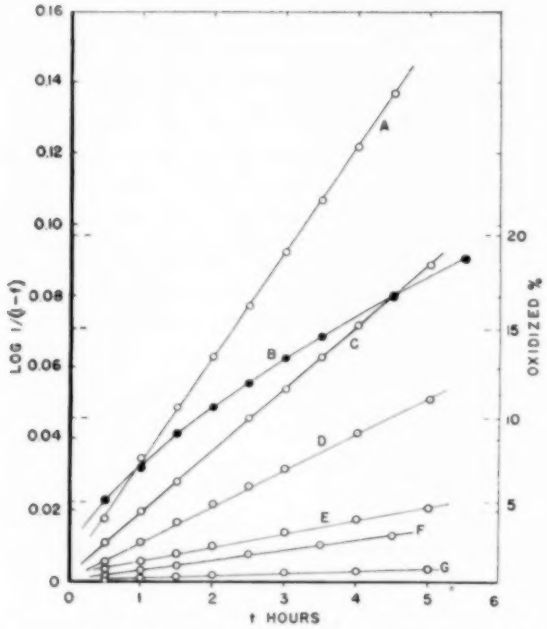

FIGURE 2. *Oxidation of carbon adsorbents and graphite in 6.1 percent of oxygen and a rate of flow of 91 ml/min.*

The left ordinate scale is $\log_{10} 1/(1-f)$, where f is the fraction of carbon oxidized, and the right ordinate scale is percentage oxidized (100f). A, Carbon 5 (390° C); B, bone char 2 (280° C); C, carbon 6 (390° C); D, graphite (711° C); E, carbon 4 (390° C); F, graphite (600° C); G, carbon 4 (320° C).

retardation exists, b becomes zero and the expression reverts to the special case of eq 1. It is also apparent, even with a finite value of b other than zero, that the limiting value of eq 3 as f approaches zero is the same as eq 1. Equation 3, upon integration, yields

$$\frac{1}{t}\ln\frac{1}{1-f}=\frac{b}{1+b}\frac{f}{t}+\frac{k}{1+b}, \qquad (4)$$

which may be used by plotting $1/t \ln [1/(1-f)]$ against f/t to determine both k and b. Equation 4 may be rearranged, however, into the form

$$\frac{1}{t}\ln\frac{1}{1-f}=k-b\frac{1}{t}\left[\left(\ln\frac{1}{1-f}\right)-f\right], \qquad (5)$$

which lends itself more readily to a direct evaluation of b and k, since these two quantities emerge immediately from the slope and intercept, respectively.

IV. Application of Simple First-Order Kinetics to Carbon Adsorbents Other Than Bone Char

Table 1 lists the values of f computed at the periods of time indicated during the course of five experiments with different samples of the same activated carbon 6. Each of the five experiments was conducted with a different percentage of oxygen in nitrogen, as listed in the first column. All five combustions were performed at the same temperature, 390° C, and at the same rate of flow of reactant gases, 91 ml/min. The data from table 1 are plotted in figure 1. The corresponding values of k computed from the slopes of these lines are recorded in the last column of table 1. Additional curves are presented in figure 2 for activated carbons 4, 5, and 6. Some results are also included for samples of spectroscopically pure graphite at 600° and 711° C.

TABLE 1. *Combustion of an activated carbon*

[Reaction of activated carbon 6 with different oxygen-nitrogen mixtures at 390° C and 91 ml/min flow showing the variations in the fraction of carbon burned, f, with time]

Oxygen	Fraction burned at (hours)—										Rate constant, k (calculated)
	0.5	1.0	1.5	2.0	2.5	3.0	3.5	4.0	4.5	5.0	
Percent											
2.2	0.0129	0.0246	0.0367	0.0496	0.0630	.....	0.0863	.....	0.113	.....	0.026
3.4	.0203	.0363	.0511	.0656	.0796	.....	.107	0.120	.134	.....	.031
4.8	.0197	.0347	.0468	.0596	.0749	0.0878	.101	.113	.....	0.139	.029
6.1	.0231	.0413	.0583	.0745	.....	.107	.....	.138	.....	.....	.036
15.1	.0388	.0665	.0930	.120	.146	.....	.....	.....	.....	.....	.060

V. Application of Retarded First-Order Kinetics to Bone Char

When values of $\log 1/(1-f)$ were plotted against t for bone chars, the resulting graphs were never linear, but invariably showed a marked curvature, which was concave to the time axis. Such a curve for a typical bone char (char 2 at 280° C) is shown in figure 2 (filled-in circles) as compared to other activated carbons and graphite (open circles). Even in some of the latter cases a slight deviation from linearity is apparent, although the effect is not nearly as marked. The percentage of the original carbon oxidized at any time, t, for each of the experiments plotted on figure 2 can be estimated by reference to the vertical axis at the right.

Before attempting to apply the concepts of retarded first-order kinetics (eq 4 and 5) to the experimental data, it is necessary that zero time be known with more precision. One reason for this is that the time variable occurs in both coordinates of the proposed graphs for testing eq 4 and 5. Although this complication did not exist in the simple first-order test as given in eq 2, a close examination of figures 1 and 2 will disclose that even in this case most of the lines do not pass through the origin. The displacement of these lines to the left of the origin in figure 1 may be due to the presence of chemisorbed oxygen in the samples. This remains despite the preliminary heating in pure nitrogen prior to the introduction of gaseous oxygen. There is also a tendency to displace the lines to the right of the origin. This is due to the dilution of the reaction mixture with the pure nitrogen and the time lag involved in sweeping out the dead space. The actual displacement observed suggests the dominating effect of chemisorbed oxygen.

It is possible to avoid these errors by computing a steady-state zero time from the original data for each experiment with bone char. The beginning of the steady-state condition was made to agree with a time at which the Ascarite-Anhydrone tubes were changed early in the experiment.

Figure 3 is a typical plot of data obtained for the controlled combustion of a sample of new bone char 2 according to eq 4 after corrections [5] had been made for steady-state conditions. A similar illustration for a spent bone char (char 15) is given in figure 4.

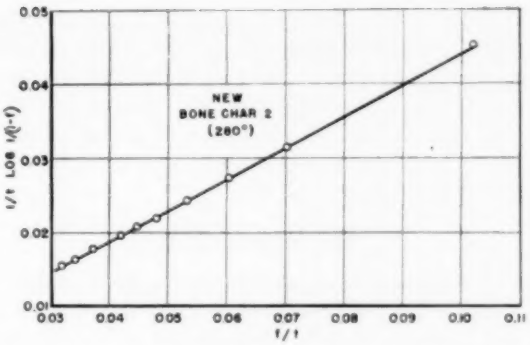

FIGURE 3. *Oxidation of new bone char 2 in 6.1 percent of oxygen and at 91 ml/min.*

The abscissa is f/t and the ordinate $1/t \log [1/(1-f)]$, where f is the fraction of carbon oxidized, and t is the time in hours.

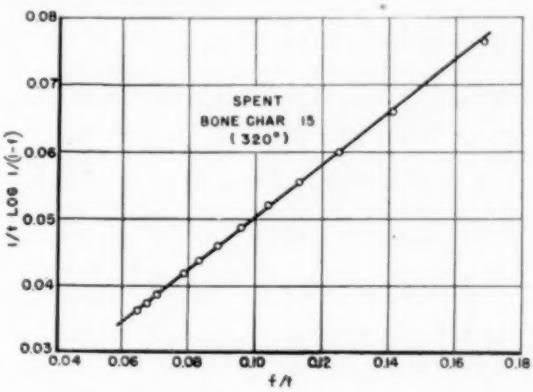

FIGURE 4. *Oxidation of spent bone char 15 in 6.1 percent of oxygen and at 91 ml/min.*

The plot is similar to that in figure 3.

[5] The weight of carbon, Δw, burned up to this time was subtracted from the original weight of the sample and also subtracted from the original weight of carbon, W, present in the sample. In the same manner, Δw was subtracted from the accumulative weights of carbon burned, w, subsequent to this time in order to get the corresponding accumulative steady-state values. The steady-state fraction f, can then be expressed by the relationship $(w-\Delta w)/(W-\Delta w)$.

TABLE 2. *Combustion of a bone char*

[Reaction of new bone char 2 with different oxygen-nitrogen mixtures at 280° C and 91 ml/min flow showing the variations in the fraction of carbon burned with time. The data are referred to steady-state conditions for each combustion.]

Oxygen	Fraction burned at (hours)—														Retardation factor, b	Rate constant, k
	0.5	1.0	1.5	2.0	2.5	3.0	3.5	4.0	4.5	5.0	5.5	6.0	6.5	7.0		
Percent																
2.2			0.0672	0.0829	0.0985		0.124		0.149		0.172		0.191		7.3	0.057
3.4	0.0280	0.0527	.0720	.0906		0.123		0.150		0.173		0.197		0.218	7.1	.063
4.8	.0315	.0559	.0768	.0978	.116	.130	.145	.161		.187				.231	6.9	.069
5.6	.0365	.0661	.0905		.132	.151	.167	.184	.203		.232		.259		6.7	.083
7.0	.0449	.0817	.110		.159	.181	.202	.223		.260		.295		.326	3.2	.087
9.1	.0423	.0756	.103	.127		.169									6.5	.097
15.1	.0551	.0957		.160		.212									5.8	.129

Table 2 lists the steady-state values of f for new bone char 2 at 280° C and 91 ml/min of flow at various oxygen concentrations of the reactant gas mixtures. In the last two columns of the table are the calculated values of b and k computed graphically when the data were plotted according to eq 5.

VI. Nomograph

If it is desired to estimate the fraction of carbon f that is burned at any time, t, assuming both b and k to be known, the solution of eq 4 or 5 becomes rather laborious. By the use of a nomograph, however, this may be accomplished in a matter of seconds. Such a nomograph has been constructed, figure 5, which may be utilized for any first-order combustion described in this paper regardless of the temperature, oxygen concentration, rate of flow, or degree of retardation. A straight edge is laid across the sheet connecting the particular value of b located on the vertical axis at the right with a value of kt located on the scale at the left. Where this straight edge crosses the curved line the corresponding value of f is obtained. For example, consider first the combustion of activated carbon 6 in 2.2 percent of oxygen at 390° C and 91 ml/min flow, as shown in the top row of table 1. In this case $k=0.026$ and $b=0$. Since it is desired to estimate the fraction of carbon burned after 4.5 hr, $kt=4.5\times0.026=0.117$. The nomograph gives directly an f-value of 0.11. This compares quite well with the 4.5-hr value of f (table 1), which is 0.113.

As a second example, consider the combustion of new bone char 2 in 3.4 percent of oxygen at 280° C and 91 ml/min flow. These data are found in the second row of table 2. In this case b and k were calculated to be 7.1 and 0.063, respectively. It may be of interest to estimate the fraction of carbon which would be expected to burn in 1 hr under this particular set of conditions. For $t=1$, $kt=0.063$, and the nomograph gives an f-value of 0.052. The corresponding value of f in table 2 is 0.0527. It is thus seen that the nomograph has an exceedingly wide range of applicability. It is possible to extend either or both of the vertical axes in order to accommodate still larger values of b and k, since each of these two axes is marked off in a linear scale.

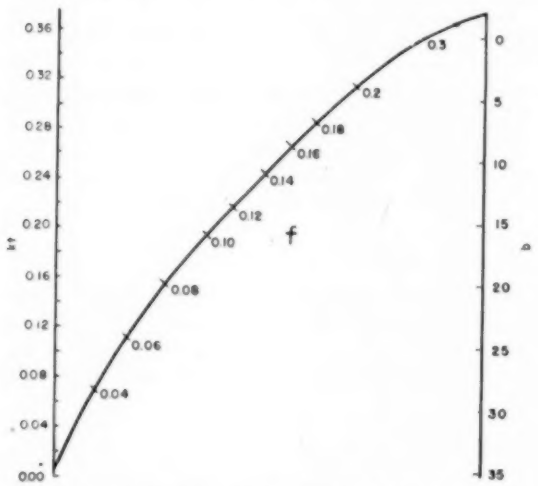

FIGURE 5. *Nomograph for the rapid solution of equation 4 or 5.*

The left vertical scale is expressed in units of $k\,t$, where k is the reaction rate constant (initial fraction of carbon burned per hour), and t is the time in hours. The right vertical scale is given in terms of b, the degree of retardation. The intermediate scale is in units of f, the fraction of carbon burned.

VII. Influence of Oxygen Concentration and Temperature on the Oxidation of Some Carbon Adsorbents

When the specific reaction rate constant k was plotted against the corresponding oxygen percentage in the reaction mixture under the same conditions of temperature and rate of flow, the resulting points were again best correlated by a linear relationship. Curve A in figure 6 shows the dependency of k upon oxygen percentage in the

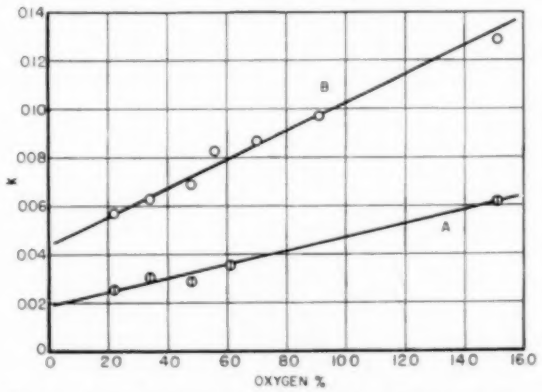

FIGURE 6. *Rate constant k as a function of oxygen concentration.*

The line A is for the oxidation of activated carbon 6 at 91 ml/min flow and 390° C (see table 1). Line B is for the oxidation of new bone char 2 at 91 ml/min flow and 280° C (see table 2). The ordinate is the rate constant k, and the abscissa is the oxygen percentage.

TABLE 3. *Combustion of a new bone char in 6.1 percent of oxygen in nitrogen at a total velocity of 91 ml/min. The data are referred to steady-state conditions for each combustion.*

Temperature, ° C	Fraction burned at (hours)—													Retardation factor, b	Rate constant, k
	0.5	1.0	1.5	2.0	2.5	3.0	3.5	4.0	4.5	5.0	5.5	6.0	6.5		
250	0.0106	0.0199	0.0274	.....	0.0416	.....	0.0564	.....	0.0664	.....	0.0772	.....	0.0861	13.5	0.0224
280	.....	.0417	.0580	0.0727	.0874	0.100	.....	0.123	.....	0.144	.....	0.164	.....	7.9	.0495
320	.0843	.144	.190	.228	.260	.....	.....	.....	.....	.....	.....	.....	.....	6.0	.221
325	.0860	.151	.200	.....	.277	.310	.....	.364	.....	.....	.....	.....	.....	5.3	.231

reaction mixture for the combustion of activated carbon 6. The data used for this graph were obtained from the first and last columns of table 1. Curve B was constructed in the same manner by using the data for new bone char 2 as given in table 2. The fact that neither of these lines appears to intersect the origin of coordinates is quite striking. The magnitude of this deviation is greater than can apparently be accounted for on the basis of experimental error.

The reaction rate constant for the combustion of a new bone char was determined at four temperatures within the range of 250° to 325° C. In each case the reactant gas consisted of 6.1 percent of oxygen in nitrogen flowing at a total velocity of 91 ml/min. It was not practical under the conditions employed to exceed this range of temperatures. When this was attempted, the combustion proceeded either too rapidly to obtain reliable measurements or too slowly to insure constancy of conditions over the period of time required to obtain measurable differences in weight. The steady-state values of the fraction of carbon burned at each interval of time are recorded in table 3. Corresponding values of k and b computed from eq 5 are also tabulated for each of these temperatures.

The dependence of k on temperature is usually expressed by the well-known Arrhenius equation

$$\ln k = -E/RT + \ln k_0, \qquad (6)$$

where E is the activation energy (or free energy of activation), R the gas constant, and k_0 is a constant. Figure 7 shows that the logarithm of k when plotted against the reciprocal of the absolute temperature, gave a smooth curve, which was slightly convex to the $1/T$ axis. An over-all activation energy (or free energy) computed from the slope of this curve would seem to vary between 15 and 35 kcal under the conditions of these

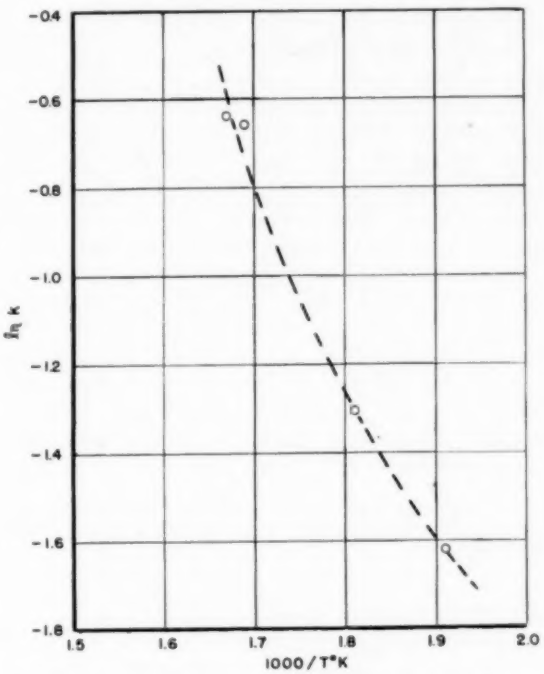

FIGURE 7. *A plot of* ln k *against* $1/T$ *for new bone char 2, where* T *is the absolute temperature.*

experiments. However, the deviation from linearity definitely points to the need for further investigation before any reliable interpretations are to be made concerning this apparent anomaly. Also, the physical significance of the parameter b along with its dependency upon the other variables present is beyond the scope of this paper. However, there is no doubt that the reaction rate does depend more or less exponentially upon $1/T$.

Other combustion experiments in which only the rate of flow of reactant gas mixture was varied by a twofold factor or more seemed to have very little effect upon the reaction rate constant. Furthermore, the weight of the sample was varied under

815197—49——4

otherwise identical conditions from one combustion experiment to another, yet the total fraction of carbon burned at each of the similar time intervals remained constant. These results, together with the linear effect of oxygen concentration upon the combustion rate, form a fairly complete picture as to the various effects of each factor.

VIII. Decarbonization of Bone Char as Influenced by Time, Oxygen Concentration, and Temperature

Uniform decarbonization of service bone char is an important factor in industrial installations in sugar refining [6]. In practice, methods to control decarbonization have entailed deliberate variations in time, oxygen concentration, or temperature that were involved in the burning process. The relative effects of changes in each of these variables are illustrated in figure 8. It may be seen in figure 8, a, that the rate of oxidation diminishes. Figure 8, b, on the other hand, illustrates that the changes in the fraction of carbon burned are always directly proportional to increases in the oxygen concentration. In contrast, the effect of temperature as shown in figure 8, c, is considerable. The fraction

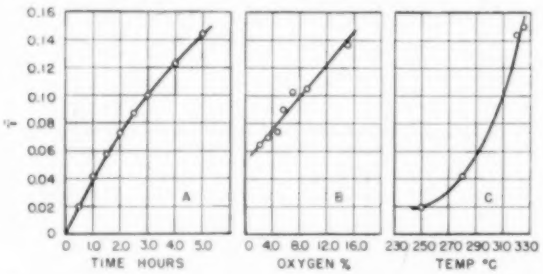

FIGURE 8. *Influence of time, oxygen concentration, and temperature on decarbonization of a bone char.*

The ordinate scale common to the three curves is given in terms of f. The abscissa of curve A is in hours (6.1 % of O_2, 280° C, 91 ml/min); that of curve B is in percentage of O_2 (1.5 hr, 280° C, 91 ml/min); that of curve C is the temperature °C (1.0 hr, 6.1% of O_2, 91 ml/min).

of carbon burned becomes progressively more and more sensitive to changes in temperature as the latter increases.

It is thus seen that temperature is by far the most important single factor in influencing the extent of decarbonization. The temperature range investigated in the laboratory is appreciably lower than the peak temperatures (400° to 500° C) realized in industrial operations. At these high temperatures it was impossible to measure the exceedingly high rates of combustion with the apparatus described. An extrapolation from the data in the temperature range 250° to 325° to 400° C or higher may be seen not to be feasible from either figure 7 or 8, c.

Some quantitative comparisons regarding the conditions affecting the variation in the fraction of carbon burned are evident in the contents of table 4. There are two ranges of f-values, which have immediate application to refinery practice. In a single cycle of regeneration with the conventional kiln, less carbon is to be removed than in a single passage through a decarbonizer. In the first case the order of magnitude of the change in f is 0.02 to 0.03; in the second case it may be as high as 0.13 to 0.14. In order to realize the desired carbon removal by adjustment in temperature alone (1.0 hr, 6.1% of oxygen, and 91 ml/min), it is necessary to maintain a temperature of 260° and 320° C, respectively. While a fluctuation of ± 10.5 deg can be permitted at the low temperature for the desired carbon removal, a no greater variation than ±1.0 deg is allowed at 320° C. Correspondingly, to obtain the desired decarbonization by adjustment of oxygen concentration alone (1.5 hr, 280° C, and 91 ml/min), it is necessary to hold the concentration within the range of ±0.85 percent in either case. Finally, to obtain the decarbonization by adjustment of the time factor alone (6.1% of oxygen, 280° C, and 91 ml/min), it is necessary to heat the char for 0.6 and 4.5 hr, respectively. A fluctuation of only ±7 min is permitted at the lower time, while as much as ±15 min may be tolerated at the higher time.

These results definitely point to the following criteria for uniform decarbonization: (1) long reaction times, (2) low temperatures, and (3) whatever concentrations of oxygen are required to give the desired decarbonization. A rough visual indication of such uniformity is evidenced by the

absence of the familiar black and white appearance of decarbonized char which is observed in most refinery operations. A more precise estimate of uniformity requires numerous laboratory analyses. There is an additional advantage in low-temperature operation based on considerations of the liberation of the heat of combustion. Temperature control is dependent upon an adequate dissipation of this heat which, in turn, depends upon the heat transfer away from the char. Because of the poor heat conductivity of char, the necessary heat transfer is obtained only at the low temperatures, where the heat of combustion per unit time can be kept at a minimum.

TABLE 4. *Conditions affecting fluctuations in f*

Assumed range of f	Permissable deviation of any one variable			
	Time	Oxygen concentration	Temperature	
	hr	*Percent*	*°C*	*°F*
0.02 to 0.03	±0.125	.....	±10.5	±18.9
.13 to .14	±.250	±0.85	±1.0	±1.8

IX. References

[1] R. A. Beebe and H. S. Taylor, J. Am. Chem. Soc. **46,** 43 (1924).

[2] W. E. Garner and E. A. Blench, J. Chem. Soc. (London) **125,** 1288 (1924).

[3] V. R. Deitz and L. F. Gleysteen, J. Research NBS **28,** 795 (1942) RP1479.

[4] C. N. Hinshelwood, Kinetics of chemical change, p. 192 (Oxford Univ. Press, Oxford, Eng., 1947).

[5] J. D. Lambert, Trans. Faraday Soc. **32,** 1584 (1936).

[6] V. R. Deitz, Preliminary survey of bone char revivification and filtration, Bone char research project at National Bureau of Standards, Special Report (1947).

WASHINGTON, August 27, 1948.

U. S. Department of Commerce
National Bureau of Standards

Research Paper RP1949
Volume 42, January 1949

Part of the Journal of Research of the National Bureau of Standards

Weather Resistance of Porcelain Enamels Exposed for Seven Years

By William N. Harrison and Dwight G. Moore

A study of the weather resistance of porcelain-enameled architectural panels was begun at the National Bureau of Standards in 1939. The study involves 864 1-foot-square panels and a like number of 4- by 6-inch laboratory specimens. A previous report (1942) gave the results after 1 year of exposure. The present paper describes the condition of the panels after 7 years of weathering at Washington, D. C., St. Louis, Mo., Lakeland, Fla., and Atlantic City, N. J.

The results of the 7-year inspection showed a good correlation between the acid resistance of enamels and their resistance to weathering. Where initial coverage was complete and no mechanical damage had occurred, protection of the metal by the enamel for all specimens was unimpaired after 7 years.

Fading of colored enamels occurred only on those panels with very poor acid resistance.

I. Introduction

During the past 2 decades, the increased use of porcelain enamel as an architectural material, including its recent application in the low-cost housing field [1, 2],[1] has accentuated the need for adequate data on the weather resistance of various types of enamel and also for laboratory tests to indicate weather resistance.

An investigation designed to obtain such data was begun by the Enameled Metals Section of the National Bureau of Standards in 1939 and was planned with the assistance of an advisory committee from the industry. Through the cooperation of 16 manufacturers, 864 1-ft-sq. panels and an equal number of 4- by 6-in. laboratory specimens were prepared. Most of the enamels furnished were regular commercial products, but they were not, in all cases, enamels that had been proved suitable for architectural purposes. On the contrary some were not expected to have good resistance to weathering. The exposure sites selected were Washington, D. C.; St. Louis, Mo.; Lakeland, Fla.; and Atlantic City, N. J.

The present paper, which describes the test panels after 7 yr of exposure, is the second progress report of this investigation. The first report, describing the results obtained for 1 year of exposure, was published in 1942 [3]. The lapse of 6 years between the first and second progress reports was due to the impracticability of carrying out a regular inspection program during the war years.

II. Conditions Prevailing at Locations of Exposure

Table 1 lists the exposure locations, and table 2 gives pertinent data on weather conditions during the 7-yr period of exposure at each site. At all four locations the racks face south, the panels being exposed at 45° from the horizontal.

[1] Figures in brackets indicate the literature references at the end of this paper.

TABLE 1. *Exposure test locations*

City	Exposure site	Exposure conditions represented
Washington, D. C.	Roof, Industrial Building, National Bureau of Standards.	Temperate, residential.
St. Louis, Mo.	Roof, Union Electric Co. warehouse.	Temperate, industrial.
Lakeland, Fla.	Ground, Municipal Airport.	Semitropical, residential.
Atlantic City, N. J.	Ground, U. S. Coast Guard Station.	Temperate, "salt air."

TABLE 2. *General weather data for the first 7 years of exposure (from U. S. Weather Bureau records)*

City	Exposure period	Annual rainfall [1]	Annual sunshine [1]	Average temperature [1]
		in.	*hr*	*° F*
Washington, D. C.	Dec. 1939 through Nov. 1946.	39.6	2,597	57.0
St. Louis, Mo.	April 1940 through May 1947.	39.7	2,770	57.3
Lakeland, Fla.	July 1940 through March 1947.	47.7	[2] 2,945	72.3
Atlantic City, N. J.	Aug. 1940 through April 1947.	40.0	2,751	53.7

[1] Average computed from data for actual period of exposure.
[2] Taken from Tampa, Fla., records. Total sunshine for Lakeland not available.

III. General Description of Panels

The 14 types of enamel included in the study are indicated in table 3. For a more complete description of the specimens and their fabrication, reference is made to the first report [3].

The supporting racks were constructed of angle iron and, after priming, were painted with aluminum paint. Seven racks were required for each location. Figure 1 shows a part of the installation at St. Louis.

Figure 2 is a view of the reverse side of one of the panels. The two clips at one side (*C*) and the flange extension at the opposite side (*F*) both fitted into galvanized channels on the exposure rack. The spaces between the panels were not caulked but were left open to facilitate removal of the panels for inspection.

At the 7-yr inspection, notes were taken as to the general condition of both panels and racks. The following remarks summarize their condition at each location.

1. Panels at Washington, D. C.

All panels and racks were in comparatively good condition. Periodic painting of the steel racks had been possible during the war years, and no serious corrosion had taken place. The panels were substantially free from dirt and grime and the natural washing by rain was apparently all that was required at this location to keep surface deposits from accumulating.

On one panel (V–71) the surface had been accidentally fractured in April of 1941, resulting in a local exposure of the metal. It was estimated that during the interventing 6 yr, corrosion had progressed into the metal to a depth of 0.003 in., but there was apparently no appreciable penetration of the corrosion under the adjacent enamel. The size of the fracture had not increased from its original ½-in. diameter.

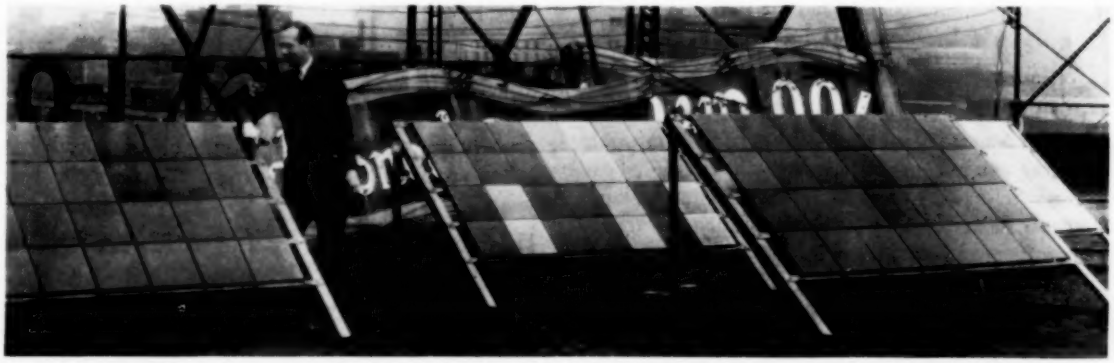

FIGURE 1. *Partial view of exposure-test installation on roof of Union Electric Co. warehouse in St. Louis, Mo., near the railway terminal.*

Photograph taken in 1941 before heavy deposit of combustion products had formed on panel surfaces (see page 48).

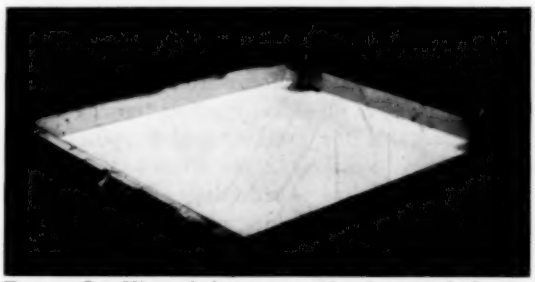

FIGURE 2. *View of the reverse side of a panel showing attachment of clips (C) and lower flange extension (F) used for fastening panels to racks.*

TABLE 3. *Percentage of initial specular gloss retained by 14 enamels for 7 years at four exposure locations and results of acid-resistance tests on same compositions*

Specimen identification [1]	Fabricator	Average 45° initial specular gloss	Average percentage of initial specular gloss retained at—[2]					Acid resistance PEI test [4]
			Washington	St. Louis [3]	Atlantic City	Lakeland	Average for three locations	
WHITE, GLOSSY, ACID-RESISTANT ENAMEL								
		Percent						
A-1 to 8	a	5.70	81.4	99.6	64.5	77.5	74.5	AA
A-11 to 18	b	5.74	83.2		63.6	87.2	73.7	AA
A-21 to 28	a	6.04	79.8		76.5	85.7	80.7	AA
A-31 to 38	b	6.01	74.8		60.4	95.4	76.9	AA
A-41 to 48	a	5.85	84.1		81.8	77.8	81.2	AA
A-51 to 58	b	5.81	77.5		66.6	64.6	69.6	AA
A-61 to 68	a	6.20	74.6		74.8	83.7	77.7	AA
A-71 to 78	b	6.01	70.5	92.9	61.2	90.7	74.1	AA
Avg			78.2		68.7	81.2	76.1	
WHITE, GLOSSY, NONACID-RESISTANT ENAMEL								
B-1 to 8	b	5.26	28.9		44.4	37.7	37.0	C
B-21 to 28	b	5.41	34.8		36.4	26.4	32.5	C
B-41 to 48	b	5.16	26.5	48.2	37.7	26.4	30.2	D
B-61 to 68	b	5.32	34.8		43.4	37.7	38.6	C
Avg			31.2		40.5	32.0	34.6	
WHITE, SEMIMAT, ACID-RESISTANT ENAMEL								
C-11 to 18	c	4.06	51.8	>100.0	50.2	45.0	49.0	C
C-31 to 38	c	5.24	61.5		42.0	64.8	56.1	A
C-51 to 58	c	5.16	76.8		58.1	80.5	71.8	A
C-71 to 78	c	5.32	73.1		60.2	70.3	67.9	A
Avg			65.8		52.6	65.1	61.2	
WHITE, SEMIMAT, NONACID-RESISTANT ENAMEL								
D-1 to 8	c	[5]						D
D-21 to 28	c	5.69	43.2		46.0	41.8	43.7	D
D-41 to 48	c	5.51	38.0		31.9	36.6	35.5	D
D-61 to 68	c	[5]						D
Avg			40.6		38.9	39.2	39.6	
BUFF, GLOSSY, ACID-RESISTANT ENAMEL								
E-11 to 18	d	5.09	68.2		42.0	57.8	56.0	B
E-31 to 38	d	5.43	64.2		51.2	79.6	65.0	AA
E-51 to 58	d	5.44	74.0	70.4	80.8	75.6	76.8	AA
E-71 to 78	d	5.35	77.7		71.0	51.1	66.6	AA
Avg			71.0		61.2	66.0	66.1	
BUFF, GLOSSY, NONACID-RESISTANT ENAMEL								
F-1 to 8	d	5.15	43.0		33.5	21.9	32.8	D
F-11 to 18	e	4.87	61.2		44.0	24.7	43.3	D
F-21 to 28	d	5.02	52.9	76.0	50.1	35.7	46.2	C
F-31 to 38	e	5.56	48.8		48.4	31.8	43.0	D
F-41 to 48	d	4.31	37.3		44.6	40.1	40.7	D
F-51 to 58	e	5.66	33.7		39.7	44.6	39.3	D
F-61 to 68	d	4.64	22.5		42.1	36.8	33.8	D
F-71 to 78	e	5.26	28.0		46.7	25.3	33.3	D
Avg			40.9		43.6	32.6	39.1	

See footnotes at end of table.

TABLE 3. *Percentage of initial specular gloss retained by 14 enamels for 7 years at four exposure locations and results of acid-resistance tests on same compositions*—Continued

Specimen identification [1]	Fabricator	Average 45° initial specular gloss	Average percentage of initial specular gloss retained at—[2]					Acid resistance FEI test [4]
			Washington	St. Louis [3]	Atlantic City	Lakeland	Average for three locations	
BUFF, SEMIMAT, ACID-RESISTANT ENAMEL								
		Percent						
H-1 to 8	e	3.96	60.7		62.5	55.2	59.5	A
H-11 to 18	f	4.81	57.6		70.6	57.0	61.7	A
H-21 to 28	e	5.65	70.7			63.1	66.9	A
H-31 to 38	f	5.45	71.2		40.1	70.5	60.6	A
H-41 to 48	e	4.74	75.7	>100.0	80.6	81.9	79.4	AA
H-51 to 58	f	4.85	72.5		69.6	74.5	72.2	AA
H-61 to 68	e	5.51	74.4	>100.0	56.6	88.0	73.0	AA
H-71 to 78	f	5.54	76.4		60.2	81.4	72.7	AA
Avg			69.9		62.9	71.5	68.3	
BUFF, SEMIMAT, NONACID-RESISTANT ENAMEL								
K-1 to 8	f	[5]						D
K-11 to 18	g	[5]						D
K-21 to 28	f	5.41	49.0	75.3	47.3	38.8	45.0	D
K-31 to 38	g	5.37	36.4		48.2	27.6	37.4	D
K-41 to 48	f	5.20	63.5	73.8	49.5	46.7	53.2	D
K-51 to 58	g	5.35	36.5		42.4	29.4	36.1	D
K-61 to 68	f	[5]						D
K-71 to 78	g	[5]						D
Avg			46.4		46.9	35.6	42.9	
RED, GLOSSY, ACID-RESISTANT ENAMEL								
L-1 to 8	g	5.58	76.4	97.1	77.7	59.2	84.4	AA
L-11 to 18	h	5.61	74.7		88.6	96.5	86.6	AA
L-21 to 28	g	5.42	78.1		57.4	86.7	74.1	B
L-31 to 38	h	5.64	79.7		49.6	92.8	74.0	A
L-41 to 48	g	5.58	75.7		78.7	94.1	82.8	AA
L-51 to 58	h	5.23	67.6		79.7	86.6	78.0	A
L-61 to 68	g	5.30	73.2		76.3	91.0	80.2	A
L-71 to 78	h	4.18	74.0		82.7	78.1	78.3	AA
Avg			74.9		73.8	90.6	79.8	
RED, GLOSSY, NONACID-RESISTANT ENAMEL								
N-1 to 8	h	5.17	70.0		62.3	40.2	57.5	C
N-11 to 18	k	5.05	60.9		55.0	39.9	51.9	C
N-21 to 28	h	5.12	74.3		48.4	46.1	56.3	D
N-31 to 38	k	4.55	70.4		59.2	53.6	61.1	D
N-41 to 48	h	5.17	65.0		62.4	35.0	54.1	C
N-51 to 58	k	4.68	61.4		52.8	52.8	55.7	C
N-61 to 68	h	4.71	43.0		57.4	32.9	44.4	D
N-71 to 78	k	5.44	36.4	38.4	52.9	44.8	54.4	D
Avg			60.2		56.3	43.2	54.4	

See footnotes at end of table.

TABLE 3. *Percentage of initial specular gloss retained by 14 enamels for 7 years at four exposure locations and results of acid-resistance tests on same compositions*—Continued

Specimen identification [1]	Fabricator	Average 45° initial specular gloss	Average percentage of initial specular gloss retained at—[3]					Acid resistance PEI test [4]
			Washington	St. Louis [2]	Atlantic City	Lakeland	Average for three locations	
RED, SEMIMAT, ACID-RESISTANT ENAMEL								
		Percent						
P-1 to 8	k	5.54	70.3		77.1	81.0	76.1	AA
P-11 to 18	l	[5]						AA
P-21 to 28	k	1.41	62.6	69.9	49.1	65.4	59.0	C
P-31 to 38	l	3.99	64.4		58.7	42.9	55.3	C
P-41 to 48	k	4.95	69.2		66.7	75.4	70.4	A
P-51 to 58	l	3.34	73.8		73.4	84.1	77.1	A
P-61 to 68	k	4.97	76.2		66.4	92.9	78.5	AA
P-71 to 78	l	5.54	81.0		81.3	97.2	86.5	AA
Avg			71.1		67.5	77.0	71.1	
RED, SEMIMAT, NONACID-RESISTANT ENAMEL								
S-1 to 8	l	[5]						D
S-11 to 18	m	[5]						D
S-21 to 28	l	4.51	65.8		51.1	48.1	55.0	B
S-31 to 38	m	4.51	57.6		47.2	45.1	50.0	C
S-41 to 48	l	3.50	58.0		49.8	32.0	46.6	A
S-51 to 58	m	3.95	84.1		75.8	44.4	68.1	A
S-61 to 68	l	4.50	35.2		47.9	30.4	37.8	C
S-71 to 78	m	3.57	70.3		53.3	40.2	54.6	C
Avg			61.8		54.2	40.0	52.0	
BLACK, GLOSSY, ACID-RESISTANT ENAMEL								
T-1 to 8	m	7.30	56.1		47.8	56.3	53.4	AA
T-11 to 18	n	6.60	64.2	90.7	62.2	70.6	68.7	AA
T-21 to 28	m	5.38	80.6		75.7	96.3	84.2	AA
T-31 to 38	n	5.55	70.0		79.4	93.9	81.1	AA
T-41 to 48	m	6.09	70.7		65.6	88.4	74.9	AA
T-51 to 58	n	5.90	68.9		66.9	82.5	72.8	A
T-61 to 68	m	6.55	59.8		53.9	61.8	58.5	AA
T-71 to 78	n	6.56	54.9	77.6	63.1	68.3	70.5	AA
Avg			65.6		64.3	78.4	69.4	
BLACK, GLOSSY, NONACID-RESISTANT ENAMEL								
V-1 to 8	n	5.52	63.6		59.8	36.8	53.4	C
V-11 to 18	a	5.62	57.0		51.8	43.9	50.6	C
V-21 to 28	n	5.76	58.8		61.8	41.2	53.9	C
V-31 to 38	a	5.60	40.1		40.5	43.3	41.3	C
V-41 to 48	n	5.30	59.7	77.4	67.2	43.8	56.9	C
V-51 to 58	a	5.49	58.0		65.5	40.4	54.6	C
V-61 to 68	n	4.67	75.9		58.9	67.0	67.3	C
V-71 to 78	a	5.45	73.9		70.1	65.8	69.9	C
Avg			60.9		59.4	47.8	56.0	

[1] Groups of 8 panels exposed, 2 at each location. Ninth panel kept in storage.

[2] Cleaned by nonstandard procedure of prolonged scrubbing with commercial scouring powder.

[3] Values are average of 2 panels with 2 readings on each panel.

[4] Test made on storage panel according to Porcelain Enamel Institute standard acid-resistant spot test for flatware issued April, 1940.

[5] Full-mat enamels, initial gloss too low for measurement.

2. Panels at St. Louis, Mo.

The 192 panels at the St. Louis location (on a roof near a railway terminal) were found to have a dark gray deposit over the entire surface, which was sufficiently heavy to make all panels have approximately the same appearance, regardless of their original color or gloss. An examination showed this deposit to consist of fly ash, soot, and a tar-like substance. A small sample scraped from the surface of one panel of high acid resistance showed an ignition loss of 31 percent, indicating that the greater part of the deposit (69 percent) consisted of the noncombustible fly ash. The deposit originated from soft-coal combustion products that were present in high concentration in the exposure area.

The standardized cleaning procedure of washing with 1-percent trisodium-phosphate solution did not remove this deposit, and vigorous scrubbing with a scouring powder was the only method found to give satisfactory cleaning. Unfortunately, this scrubbing had a polishing action that affected the gloss measurements and vitiated their reliability as a criterion of the degree of weathering.

The aluminum paint on the steel supporting racks had deteriorated badly at the St. Louis location, but corrosion of the steel was not as yet pronounced. The previously mentioned deposit was also present on the steel racks and may have had a protective influence in decreasing the corrosion rate.

3. Panels at Lakeland, Fla.

Tiny patches of an organic growth were attached to all panels at the Lakeland exposure site. The patches were largest and most numerous on the white enamels, but the black panels also showed some evidence of the growth. The patches adhered tightly to the enamel surface but could be removed by vigorous washing with a wet rag. When dry, the patches were gray but when thoroughly wetted they became green or, in some cases, brown.

An examination of these patches was made at the Florida Agricultural Experiment Station at Lake Wales. Under the microscope the patches appeared as clusters of oval-shaped fungus spores with occasional algae growth present, especially on the white panels.

On many of the nonacid resistant enamels, there were areas having much higher gloss than the remainder of the surface. Examination showed these areas to be substantially free of the growth, indicating that these organisms produced an acid reaction that accelerated the deterioration of the enamel surface. None of the panels with acid resistance of class B or better showed this localized etching

Jones [4], in explaining the behavior of optical glass elements used in the tropics, states that fungi produce organic acids that etch glasses subject to acid attack.

Corrosion of the steel racks was only moderate at the Lakeland location. The aluminum paint had deteriorated but rusting was not serious.

4. Panels at Atlantic City, N. J.

At Atlantic City, damage to the installation was considerable and was caused by a combination of factors including the following: (1) The 1944 hurricane that struck the site with full intensity, (2) moving of the racks to make room for wartime expansion at the Coast Guard Station, (3) the location in 1943 of a Navy athletic field immediately adjacent to the exposure site, and (4) the corrosive action of salt air on the steel. Nine of the panels were missing, and seven others had become detached from the mounting and were on the ground. Many of the panels had been damaged by impact, probably caused by stones thrown from the adjacent athletic field. Nevertheless, surface measurements were possible on practically all of the panels.

Observations at this site indicated that both the paint and galvanizing failed rapidly under the salt-air conditions. Corrosion had seriously damaged the painted steel racks and the galvanized channels were, in many cases, so rusted that replacement was necessary.

The top attachment clips (*C* in fig. 2) had become detached on some of the panels. These clips had been spot-welded to the panels prior to enameling, and, in some cases, this joint was protected only by a thin ground coat application. On many of the clips this thin coat was insufficient to give complete coverage where the clip joined the panel, and the severely corrosive conditions had caused failure.

This severe corrosion of the metal at Atlantic City was also responsible for a somewhat unexpected type of damage to the enamel surface resulting from poor enamel coverage of the backs

of panels. On those panels that had been covered on the reverse side with only a ground coat and then fired in a box furnace while resting on alloy points, poor coverage of the steel occurred at the contact points. Corrosion had started at these areas and had, in some cases, progressed completely through the 16-gage steel to the under surface of the enamel on the face side. Fracture of the enamel on the face immediately above these areas occurred as the corrosion approached the enamel-metal interface. The resulting fractures resembled very large fish scales and were believed to have been caused by hydrogen generated during the corrosion process. That hydrogen diffusing through steel may literally explode the enamel from the opposite surface had been demonstrated previously by Zapffe and Sims [5]. The fact that a number of "fish-scale" type fractures were noted on the faces of panels over localized corrosion areas while some metal still remained beneath indicates that the fractures could not have been caused by the forcing off of the enamel by corrosion products, nor could they be caused by buckling of the enamel due to the release of compressive strains resulting from a small area of the underlying metal being removed by corrosion.

Figure 3 shows the face of a panel that was damaged by corrosion originating from firing marks on the reverse side. Several holes and also a number of the previously described fractures are apparent on this specimen. It should be pointed out, however, that these defects did not occur on the panels that had been given a thin second coat of enamel on the reverse side, nor had corrosion progressed to this extent at any location except Atlantic City.

Another type of surface defect, noted only at Atlantic City, was a type of staining that invariably appeared on the enamel surface adjacent to any damaged area that exposed the metal. These stains appeared as iridescent films and were believed to be analogous to the iron stain on glass containers described previously by Marboe and Weyl [6]. These investigators found that staining of wet glass in contact with iron results from the interreaction of positively charged ferrous ions with the glass surface, thus leading through oxidation to the formation of an insoluble, colored ferric hydrosilicate. In this study, gloss measurements on areas showing these stains gave exceptionally high readings.

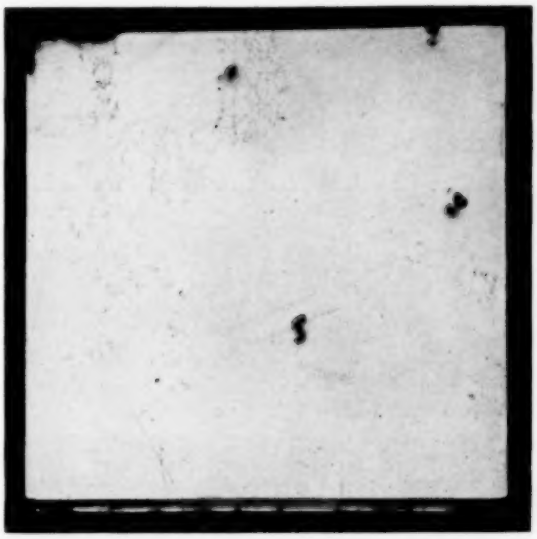

FIGURE 3. *Panel A-58 after 7 yr of exposure in the salt air at Atlantic City, N. J.*

Surface defects, including hole at right center, were caused by rusting through from areas of incomplete coverage on the back of panel. Specimens with a thin second coat of enamel on the reverse side were not affected in this way.

Numerous tiny localized areas of iron staining were also noted on many of the Atlantic City panels. Close examination of these patches showed tiny pin holes at the centers, which were allowing corrosion of the metal.

IV. Surface Changes Resulting From 7 Years of Weathering

Reference has been made in the preceding section to corrosion of the steel where it was not adequately covered by enamel. This part of the report pertains to changes that occurred as a result of weathering on the enamel surfaces where coverage was complete.

1. Microstructure

As shown in figures 4 and 5, photomicrographs taken with a metallographic microscope indicated practically no change from the original surface microstructure of the enamels with high acid resistance after 1 and 7 yr of weathering. Enamels of poor acid resistance, on the other hand, showed considerable progressive deterioration. The "pits" on most of these enamels (illustrated by several photomicrographs in the first report [3]) were no longer a characteristic feature of the microstruc-

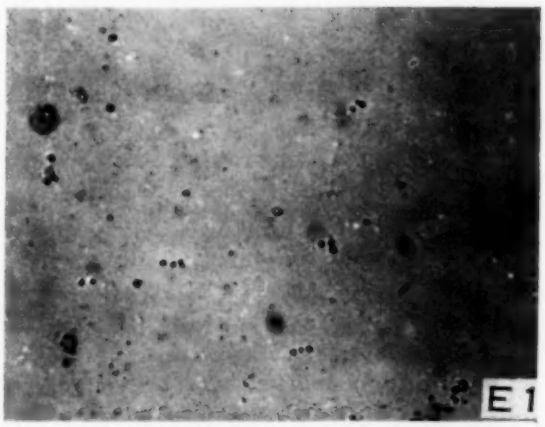

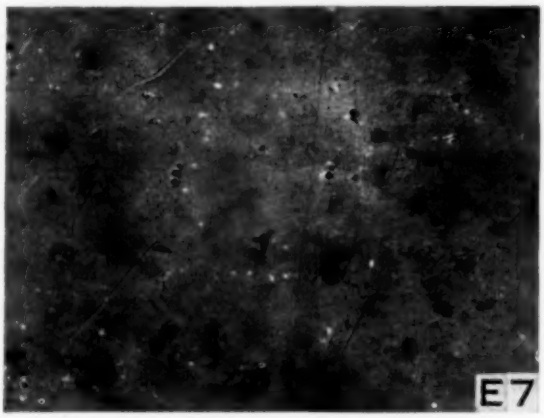

FIGURE 4. *Photomicrograph (×600) of typical black, glossy, acid-resisting enamel showing no fundamental change in microstructure with progressive weathering.*

S is storage panel, T-69. E-1 and E-7 show areas on a duplicate panel, *T*-61, after exposure for 1 and 7 yr, respectively, in Washington, D. C. Specks are probably mill additions.

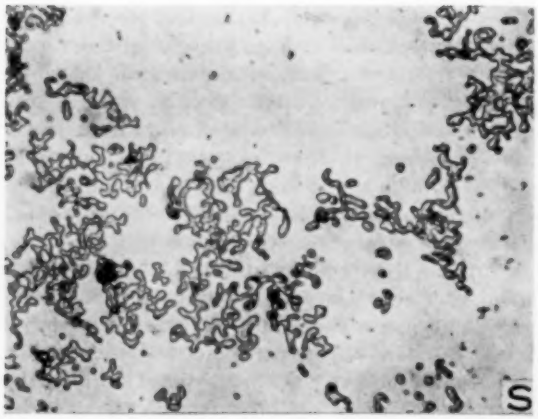

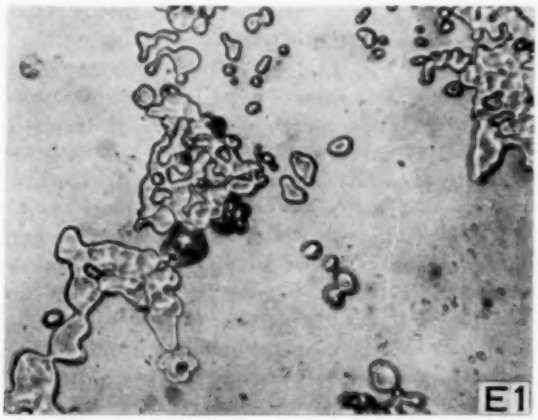

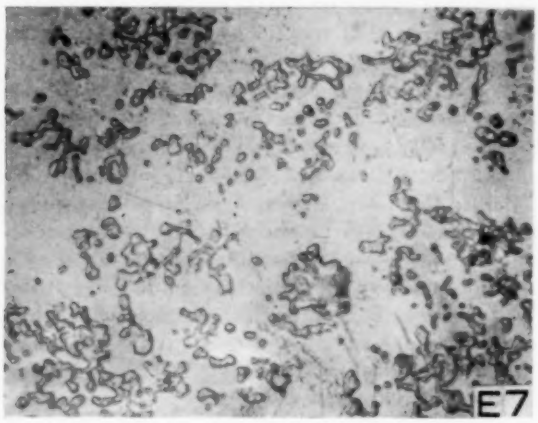

FIGURE 5. *Photomicrograph (×600) of a red, semimat enamel of good acid resistance, showing no appreciable change in surface microstructure from weathering during a 7-yr period.*

S, storage panel, P-49. E-1 and E-7 show areas on a duplicate panels *P*-41, exposed for 1 and 7 yr, respectively, in Washington, D. C. Particles exposed at surface are undissolved material added to give a mat finish. The difference in size of the exposed particles is not considered significant.

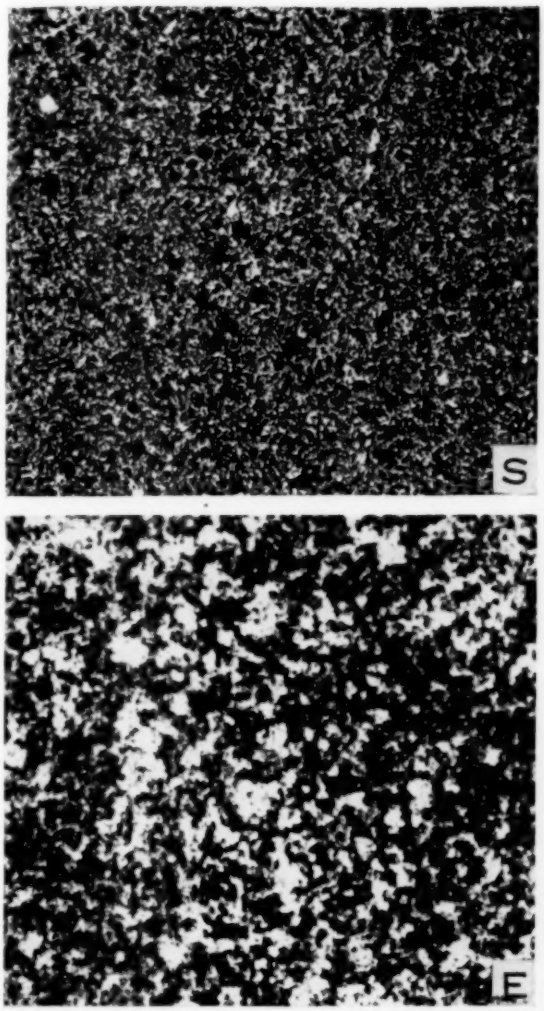

FIGURE 6. *Photomicrograph (×20) of a black, nonacid resisting enamel showing large surface change after 7 y of weathering.*

S is storage panel, V-19. E is duplicate panel, V-11, exposed 7 yr in Washington, D. C. Large light areas in E are alteration products resulting from a chemical change in the surface layer.

ture, and deterioration of the surface had progressed considerably beyond the pitting stage. Two examples of these enamels are illustrated in figures 6 and 7.

The photomicrographs in figure 6 provide a comparison between the storage panel (V–19) and the duplicate panel (V–11) after 7 yrs of weathering. The surface in the photomicrograph of V–11 is that of a relatively heavy gel layer, which formed during the 7-yr exposure. This gel is apparently a hydrated layer, rich in silica, resulting from the leaching of soluble constituents from the enamel surface. The layer was much softer than the underlying enamel and could be scraped from the surface with a sharp blade.

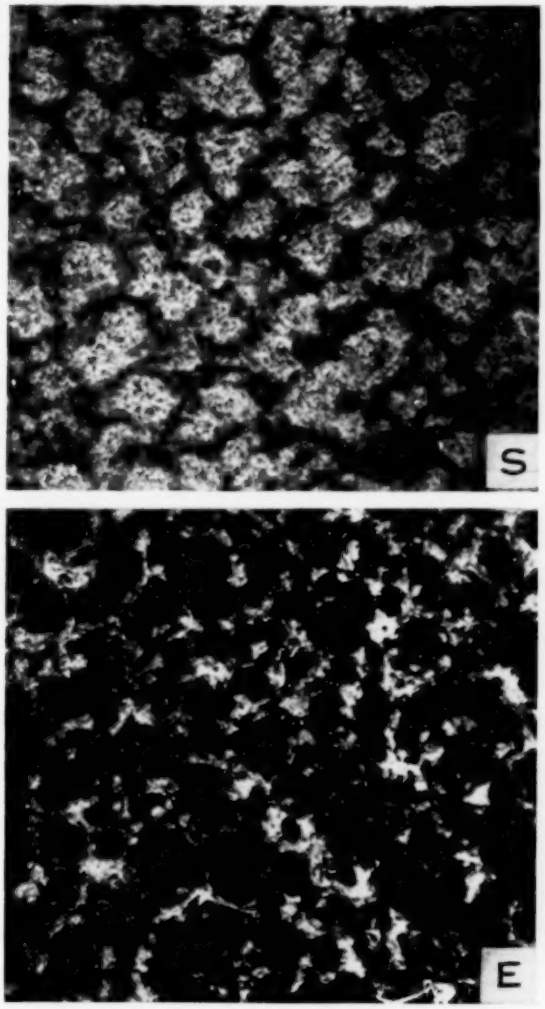

FIGURE 7. *Photomicrograph (×20) of a red, nonacid-resistant, semimat enamel prepared with a two-frit combination showing a grain boundary type of disintegration after weathering.*

S is storage panel P-29. E is duplicate panel P-22 after exposure for 7 yr at Washington, D. C. Dark gray material surrounding lighter colored grains in S is made up of the more fusible of the two enamel frits. This more fusible frit shows greater weathering effects and appears as a light material bounding darker grains in E. This light material appears under the microscope to be shattered.

Thickness measurements, as made with a magnetic thickness gage, before and after scraping, indicated a gel layer of 0.0008 in. on the Washington panel, V–11, and 0.0012 in. on the St. Louis panel, V–15. The surface film on all V–11 to V–18 panels had a vitreous texture and still retained an average of 50.6 percent of the initial gloss. Fading was pronounced on these panels at all locations, the color changing from black when first installed to a light gray after 7 yrs.

A portion of the gel-like layer was scraped from the St. Louis panel, V–15, after cleaning. The ignition loss of the scrapings upon heating to 1,650° F was 23.4 percent. The material after heating was a brown, partially sintered powder having no resemblance to a porcelain enamel. The loss in weight of the heated material was believed to be due almost entirely to loss of water.

The photomicrograph of panel *P*–22 (fig. 7) shows a peculiar type of surface break-down. The original enamel was a glossy red of class C acid resistance.[2] According to the frit manufacturer, the enamel represented by panels P–21 to P–28 was prepared from a two-frit combination. From the results obtained it is apparent that one of the frits was much more resistant to weathering than the other, and the two frits did not blend during firing into a homogeneous glass. The frit of poor weather resistance is shown by the light areas in figure 7, E, which appear in figure 7, S, as dark boundaries to the relatively large grains. Another enamel (panels P–31 to P–38) prepared from the same frits, but applied by a different fabricator, did not show this effect. In this case the enamel may have been more finely ground and fired for a longer time.

2. Fading

Observations of color difference made on all panels during the 7-yr inspection indicated that:

1. No colored enamel of class AA or A by the Porcelain Enamel Institute acid-resistance test (see footnote 2) showed any noticeable change in color.

2. No colored enamel of class B acid resistance showed any objectionable fading.

3. Practically all deeply colored enamels of classes C and D acid resistance showed color change, and in most cases this fading was sufficiently pronounced to be considered objectionable.

4. The colored full-mat enamels that showed pronounced fading at the end of the first year did not change much in appearance during the next 6 yrs.

5. Fading of the colored enamels of poor acid resistance was almost equally pronounced at all four exposure locations, even beneath the surface deposit that formed at St. Louis.

Reflectance measurements for color difference were not attempted at the 7-yr inspection. Determinations of this type are currently under study, and it was believed that color difference data taken at the time of the inspection would be of questionable value. A standard method of measuring color difference is expected to be established in time for the 10-yr inspection in 1950, at which time quantitative comparisons of stored panels and exposed panels may be made.

3. Specular Gloss

Specular-gloss measurements were made on each panel at the exposure site, by using the Hunter Multipurpose Reflectometer [7] adjusted for a 45° angle of incidence. Measurements were made at two fixed locations near the center of the panel immediately after the cleaning operation, which consisted of (a) washing with a warm 1-percent solution of trisodium phosphate, (b) thoroughly rinsing with tap water, and (c) drying in air. The initial gloss measurements were standardized against a liquid film [8]. The 7-yr data were obtained with the same multipurpose reflectometer and with the same liquid-film standards.

The changes in 45° specular gloss that had occurred at the end of 7 yr of weathering are summarized in table 3. The values as given for Washington, Lakeland, and Atlantic City are for the most part complete, but only a few representative values are reported for St. Louis. The St. Louis measurements were all made on surfaces

[2] Test for Acid Resistance of Porcelain Enamels; Part I—Flatware. Issued by the Porcelain Enamel Institute, 1010 Vermont Ave., NW., Washington, D. C. In the commercial test, which separates enamel according to classes, a small pool of 10-percent citric acid is placed on the specimen for 15 min at 80° F. The degree of attack is then evaluated by visual methods by using such characteristics as visual strain, blurring of image, and ease of removal of a pencil mark. Class AA shows no visible effect from the treatment and is the most resistant, with class A, class B, class C, and class D following in that order. Enamels falling in the latter two classes are not considered as acid resistant.

A research test for acid resistance is included in the same pamphlet. The research test is quantitative in that the loss of 45° specular gloss is measured for each specimen after a 15-min immersion in the 10-percent citric acid at 80° F.

that had been cleaned by the nonstandard procedure of a vigorous and prolonged scouring, which in effect constituted a polishing action that affected the gloss and thus invalidated the gloss measurements on these specimens.

In general, it was noted that the 45° surface gloss changed at a faster rate in the earlier stages of exposure than later. Figure 8 illustrates this effect for three Washington panels that were chosen as being representative. In all three panels there was considerably more change during the first 3 years than during the next 4, and in the case of panel F–11, there was more change during the first year than during the next 6.

The relation between acid resistance and weather resistance, as measured by the percentage of initial specular gloss retained, is given in table 4. It will be noted that there is a direct correlation between the class of acid resistance by the PEI commercial test (see footnote 2) and the average percentage of gloss retained.

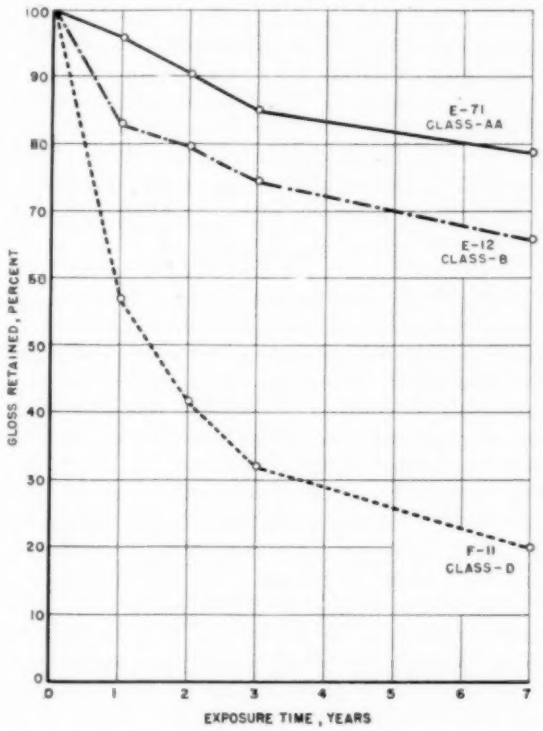

FIGURE 8. *Curves showing decrease in percentage of gloss retained with increasing exposure time for three typical panels exposed at Washington, D. C.*

TABLE 4. *Summary of gloss data showing the average percentage of specular gloss retained after 7 years of weathering for various classes of acid resistance*

Number of enamels averaged [1]	Acid resistance class [2]	Average percent of initial specular gloss retained [3] at—			
		Washington	Lakeland	Atlantic City	Average at three locations
29	AA	73.3	81.6	69.6	74.8
15	A	69.7	70.0	62.3	67.3
3	B	70.7	64.2	50.2	61.7
24	C	54.9	43.1	52.8	50.3
16	D	44.4	36.0	46.3	42.2

[1] Each enamel represented by 2 panels at each location.

[2] From spot tests made on 12- by 12-in. storage panels, using the porcelain Enamel Institute standard acid-resistance spot test for flatware.

[3] Percentage of gloss retained for St. Louis panels not included because tightly adhering surface deposits made gloss measurements unreliable.

The results at Lakeland showed the same excellent correlation between the class of acid resistance and gloss retention that was shown by the average. At Washington and Atlantic City there was a reversal of two values, involving class B enamels in both instances. Only three class B enamels were included in the investigation. If more enamels of this class had been included a better average value would have been obtained and these reversals might not have occurred.

Table 4 shows only moderate differences in the perentage gloss retained at the three locations after 7 yr of exposure. The class AA and class A enamels were somewhat more affected by the conditions existing at Atlantic City than at Washington and Lakeland. On the other hand, the semitropical conditions at Lakeland and the accompanying fungus growth appear to have produced more surface deterioration on class C and class D enamels.

V. Effectiveness of Scouring in Restoring Gloss

The effectiveness of scouring with a commercial cleanser [3] in restoring gloss to two weathered panels was investigated during the Lakeland inspection. A red, nonacid resistant panel (N-54) was found to increase from 52.8-percent gloss

[3] Examination showed the cleansing powder to consist of finely ground feldspar with a soap admixture.

retained after trisodium phosphate cleaning to 60.4 percent after 5 min of scouring with the powder. A red, acid-resistant composition (panel L–13) on the other hand, decreased from 96.5 to 88.3 percent. Indications were that a more prolonged rubbing with the commercial scouring powder did not materially change these values. The continued, severe scouring required to clean the surface deposit from the St. Louis panels, on the other hand, showed a polishing action that raised the gloss readings of some of the enamels of better acid resistance to even higher than their initial values (see table 3).

VI. Accelerated Weathering Tests

In the earlier report [3] reference was made to a carbon dioxide test that produced a type of surface breakdown of the finish coat closely related to the deterioration that occurred with the poorer enamels during the first year of weathering. Gloss measurements made before and after the carbon dioxide treatment gave gloss-retention values that correlated well with the percentage of gloss retained by the exposed panels.

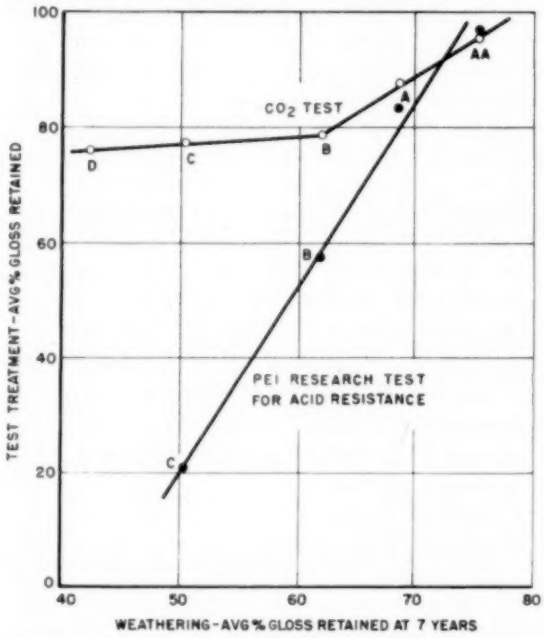

FIGURE 9. *Curves showing relationship between the average percentage of gloss retained after weathering and the percentage of gloss retained after treatment of duplicate specimens by both the* CO_2 *test and the PEI research test for acid resistance.*

Letters on curves show class of acid resistance by PEI spot test. The gloss values for class D enamels were too low for measurement after the PEI research test treatment.

It was hoped that this correlation might continue with a more prolonged exposure of the panels, but the results of the 7-yr inspection indicated that the carbon dioxide test is not a sensitive criterion for predicting the durability of an enamel exposed to weather. As presently constituted, the test does not sufficiently differentiate between the best and the poorest enamels. This is brought out in figure 9, which shows the relationship between the average percentage of gloss retained by the weathered panels after 7 yr and the average percentage of gloss retained after treating the duplicate laboratory specimens in accordance with the carbon dioxide test and with the Porcelain Enamel Institute research test for acid resistance. It will be noted from these curves that the 7-yr resistance to weathering has a considerably better correlation with the PEI research test for acid resistance (see footnote 2) than with the carbon dioxide test.

As pointed out earlier in section IV, 3, the PEI commercial test for acid resistance (see footnote 2) also correlates well with the average percentage of gloss retained after 7 yr of weathering and can undoubtedly continue to function satisfactorily as an acceptance test until such time as more complete data are available.

VII. Discussion

In the first report of this investigation [3] there was considerable discussion regarding the mechanism by which porcelain enamel surfaces are affected by weathering. The inspection after 7 yr has not appreciably altered these concepts except perhaps with regard to pitting. The pitting that was previously illustrated by a number of photomicrographs is now recognized as being only an early manifestation of surface deterioration. On longer exposure, these same surfaces show an advanced stage of attack, an extreme case of which is illustrated by panels V–11 to V–18 (see fig. 6). The entire surface of the enamel on these panels has been altered by chemical change.

It should be strongly emphasized that the type of surface breakdown referred to in the preceding paragraph occurs only on those enamels of extremely poor weather resistance, which can be

eliminated from use by the criterion of acid resistance. All enamels of class B acid resistance or better were still in excellent condition at the latest inspection.

At the end of the first year of exposure, it was noted that weathering effects were more pronounced at St. Louis and Washington than at Atlantic City and Lakeland, and this was ascribed to differences in combustion gases in the respective atmospheres. At 7 yr, these differences in severity were no longer in the same order. After the longer exposure time, conditions at Atlantic City seemed the most severe on the acid-resistant enamels, whereas Lakeland conditions were most severe on the nonacid resistant compositions. The deposit that formed on the St. Louis panels made a reliable comparison with the other exposure sites impossible. Any future tests in such areas should include arrangements for at least semiannual cleaning of the specimens.

The cause of the gradual decrease in gloss of the enamel surfaces with weathering, as illustrated in figure 8, is believed to be a slow leaching of slightly soluble constituents from the enamel surface, leaving a gel-like layer rich in silica. The rate at which this alteration occurs is a function of the composition of the enamel and the conditions to which the surface is exposed. After 7 yr, the thickness of the altered layer may be comparatively heavy (up to 0.0012 in. thick), as is the case with enamel V–11 to V–18, or it may be very thin on the enamels of high acid resistance.

This same type of surface deterioration also occurs with glass. According to Jones [4], when glasses containing less than 60 percent of silica are subjected to weathering, the divalent ions from the glass surface go into solution and are replaced by hydrogen ions from weakly acid water, thus resulting in a hydrated-silica surface layer. That glasses of higher silica content also may show this same gel formation on longer exposure is shown by Laubengayer [9] in his study of a soda-lime-silica glass (66.5 percent of silicon dioxide) that was entombed in a burial vault in Cyprus for approximately 1,800 yr. Laubengayer found that this glass was incrusted with a white flaky material that consisted mainly of hydrated silica. Also, other investigators [10] have found indications of the presence of a gel layer on old window glass and old glass tubing.

Fading of the colored enamels with poor acid resistance is also probably caused by the leaching and subsequent hydration of the surface layer. The resulting hydrated film on colored enamels usually assumes a lighter color than the original surface and gives a faded appearance to the panels. The degree of color change depends on the thickness and composition of the film and on the original color of the enamel. Unlike the panels studied by Sweo [11], in this investigation enamels having the deeper colors, rather than the pastel shades, showed the maximum color change. The etching at the bottom edges of the panels, as reported by Sweo, was noted on a few panels at Lakeland. The method of mounting the panels was such as to prevent water from collecting in pockets, but the heavy rainfall at Lakeland (see table 2), together with the resulting high humidity, probably allowed water to remain along the bottom edge for prolonged periods during humid weather.

Protection of the surface of nonacid-resistant colored enamels by a very thin application of a clear overglaze enamel has proved only moderately successful. In the earlier report [3] this method of protecting the surface appeared to show marked promise, but after 7 yr, surface pits had begun to appear in several of these overglazed surfaces. Heavier applications of the overglaze would undoubtedly overcome this weakness.

One of the more important observations made during the 7-yr inspection was the great importance of good enamel coverage when panels are exposed to salt air. The salt air conditions at the exposure site at Atlantic City are probably more severe than at most seacoast installations, and in commercial practice the reverse sides of the panels, where corrosion began, would not be exposed as they were in this investigation. It is the authors' recommendations that on all seacoast installations, special care be taken to insure complete enamel coverage of the backs of panels and attachment lugs. The same precaution should probably also be followed on tropical or subtropical units, and as an engineering safety factor the practice could well be universal.

A discussion of the mechanism of weathering naturally results in bringing to the fore the enamels of relatively poor weather resistance. The important fact is, however, that enamels of good acid resistance, applied to obtain good coverage, were still in very good condition in all locations after 7 yr. Hudson and Banfield [12] working in Eng-

land, also found acid-resistant enamels to be in excellent condition after 5 yr in industrial or nonindustrial atmospheres, or after 2 yr submerged in sea water.

On the basis of both the 1-yr and the 7-yr data, the authors feel that the recommendations as made in the earlier report continue to be valid. These recommendations were:

1. Where appearance is an important factor, full-mat enamels of the type included in this investigation should not be used for outside installations, as they tend to accumulate and retain a dingy film and to fade.

2. Enamels of acid resistance less than class B (PEI test) should not be used in any architectural installation where general appearance and absence of fading are important. An acid resistance of class A or class AA is to be preferred.

VIII. Summary

A second inspection of the 784 1-ft.-sq. porcelain enameled panels of varying types exposed at Washington, D. C., St. Louis, Mo., Lakeland, Fla., and Atlantic City, N. J. was completed during 1947. The observations made during this inspection, which represents 7 yr of exposure, may be summarized as follows:

1. Good correlation existed between acid resistance and the percentage of initial gloss retained, the enamels of best acid resistance retaining the highest percentage of their original gloss.

2. No noticeable fading of enamels of class AA or class A acid resistance occurred, nor was there objectionable fading of class B enamels. Practically all class C and class D colored enamels, however, showed very noticeable color change.

3. In contrast to the results of the first-year inspection, which showed greatest weathering effects at St. Louis and Washington, the 7-yr data indicate that the conditions at Atlantic City were slightly more severe than elsewhere on the acid-resistant enamels, whereas Lakeland conditions were most severe on the nonacid-resistant compositions.

4. The salt-air conditions at Atlantic City caused considerable corrosion of those parts of the panels that were incompletely covered by enamel. This corrosion caused failure of attachment lugs and in some cases failure of enamel on the face by rusting through to near the enamel-metal interface from areas of poor coverage on the back. Specimens with a thin second coat of enamel on the back were not affected in this way.

5. Where the initial coverage was complete on all parts of the panel and where no mechanical damage had occurred during exposure, protection of the metal against corrosion was unimpaired on all specimens after 7 yr of weathering.

This study was made possible by the cooperation of the following companies in supplying the necessary enamel frits and specimens for the study:

Baltimore Enamel & Novelty Co.	Ingram-Richardson Mfg. Co.
W. A. Barrows Porcelain Enamel Co.	Pemco Corporation.
Chicago Vitreous Enamel Product Co.	Porcelain Metals Corp.
Davidson Enamel Products Co.	Porcelain Products Co
Erie Enameling Co.	Seaporcel Corp.
Ferro Enamel Corporation.	J. M. Seasholtz & Sons.
General Porcelain Enameling & Mfg. Co.	Texlite, Inc.
	Toledo Porcelain Enamel Products Co.
	Wolverine Porcelain Enameling Co.

Acknowledgment is made also to the Porcelain Enamel Institute, whose financial contribution to the installation and inspection of the specimens has been most helpful in carrying the work toward completion.

The advisory committee, which offered much valuable assistance in selecting the types of enamel for study and planning the investigation, consisted of P. H. Bates, E. C. Greenstreet, J. I. Irwin, P. B. McBride, Paul Seasholtz, J. D. Tetrick, and H. G. Wolfram.

IX. References

[1] C. G. Straundlund, E. Olsen, and E. E. Howe, Finish **5,** L1 (1948).
[2] C. T. Post, Iron Age **157,** 110 (1946).
[3] W. N. Harrison and D. G. Moore, J. Research NBS **28,** 735 (1942) RP1476.
[4] F. L. Jones, J. Am. Ceram. Soc. **28,** 32 (1945).
[5] C. A. Zapffe and C. E. Sims, J. Am. Ceram. Soc. **23,** 192 (1940).
[6] E. C. Marboe and W. A. Weyl, J. Am. Ceram. Soc. **30,** 320 (1947).
[7] R. S. Hunter, J. Research NBS **25,** 581 (1940) RP1345.
[8] D. G. Moore and R. S. Hunter, J. Am. Ceram. Soc. **24,** 167 (1941).
[9] A. W. Laubengayer, J. Am. Ceram. Soc. **14,** 833 (1931).
[10] J. W. Mellor, Trans. Eng. Ceram. Soc. **34,** 113 (1934).
[11] B. J. Sweo, The Enamelist **18,** 13 (1940).
[12] J. C. Hudson and T. A. Banfield, J. Iron Steel Inst. **158,** 99 (1948).

Washington, September 15, 1948.

U. S. Department of Commerce
National Bureau of Standards

Research Paper RP1950
Volume 42, January 1949

Part of the Journal of Research of the National Bureau of Standards

On the Precision of a Certain Procedure of Numerical Integration

By Harry D. Huskey
With an appendix by Douglas R. Hartree

An example of numerical integration is given that shows very systematic effects in the less significant digits. This lack of randomness gives rounding-off errors that exceed the predicted standard deviation by a factor of three.

The example considered in this paper shows that systematic rounding-off errors can occur in numerical integration, irrespective of the number of digits kept in the contributions to the integral. In the appendix this phenomenon is examined, and criteria are set up to detect the cases in which it may arise to a serious extent.

I. Introduction

The use of numerical methods has led to the study of the accumulation of errors in computations by various people.[1] In this paper we apply formulas developed by Rademacher to the errors involved in the integration of simultaneous linear differential equations. The system chosen for this application is

$$x'(t)=y(t),$$

$$y'(t)=-x(t).$$

The results of integrating these equations were easily checked by comparison with the sine and cosine tables published by the National Bureau of Standards.[2]

The errors involved in the numerical integration of these equations arise from two sources. One, called the truncation error, arises from replacing the differential equations by difference equations; the other, a round-off error, comes from the rounding-off procedure used in the computation. Formulas developed by Rademacher account for the truncation error. The rounding-off error can be estimated in a statistical manner, provided the dropped digits are randomly distributed. Rademacher suggests that this random property is satisfied provided the increments involved in the integration are not too small. We shall exhibit an integration where this assumption is satisfied, but the dropped digits vary from zero to four and back to zero over a range involving nearly three hundred steps in the integration. This causes the error to increase by a factor of twenty and to become almost three times the standard deviation as given by Rademacher's formulas.

In certain other runs the error exceeds the predicted standard deviation by a small factor. In two of these cases results were tabulated every five or ten steps in the integration and a frequency count of the digits taken. Standard statistical tests indicate that these numbers did not consist of randomly distributed digits.

These results show that one must be very careful in applying error estimates based on an assumption of randomness. To be safe it is best to use the estimates for the maximum rounding-off error.

1. Rademacher Theory

(a) Heun Method

We now indicate the method of solution studied by Rademacher and give the formulas developed by him. He starts with the system.

[1] F. Schlesinger, Astron. J. **30**, 183 (1917); D. Brouwer, Astron. J. **46**, 149 (1937); H. Rademacher, On the accumulation of errors in processes of integration on high-speed calculating machines, Proceedings of a Symposium on Large-Scale Digital Calculating Machinery (Harvard University Press, Cambridge, Mass., 1948).

[2] Tables of sines and cosines for radian arguments (National Bureau of Standards, 1940) MT4; Tables of Circular and Hyperbolic sines and cosines for radian arguments (National Bureau of Standards, 1939) MT3.

$$\left.\begin{aligned} x'(t) &= f(x,y) \\ y'(t) &= g(x,y) \end{aligned}\right\} \tag{1}$$

and the solution is to be found for an interval $t_0 \leq t \leq T$ by application of the Heun method. That is, having found x_{j-1} and y_{j-1} as approximations to the solutions at $t_{j-1} = t_0 + (j-1)(\Delta t)$, the following formulas give x_j and y_j.

$$\left.\begin{aligned} x_j^* &= x_{j-1} + \Delta t \cdot f(x_{j-1}, y_{j-1}) \\ y_j^* &= y_{j-1} + \Delta t \cdot g(x_{j-1}, y_{j-1}) \end{aligned}\right\}, \tag{2}$$

$$\left.\begin{aligned} x_j &= x_{j-1} + \frac{\Delta t}{2}[f(x_{j-1}, y_{j-1}) + f(x_j^*, y_j^*)] \\ y_j &= y_{j-1} + \frac{\Delta t}{2}[g(x_{j-1}, y_{j-1}) + g(x_j^*, y_j^*)] \end{aligned}\right\} \tag{3}$$

(b) Definitions

Let us make the following definitions:

(a) Let $x(t)$, $y(t)$ be solutions of eq 1 satisfying the condition that $x(t_o) = x_o$ and $y(t_o) = y_o$.

(b) Let x_j, y_j, $j = 1,2, \ldots, n$, be the numbers obtained by successive application of eq 2 and 3.

(c) Let $\lambda(t)$, $\mu(t)$ be generic notation for solutions of the system

$$\left.\begin{aligned} d\lambda/dt &= -(\partial f/\partial x)\lambda - (\partial g/\partial x)\mu, \\ d\mu/dt &= -(\partial f/\partial y)\lambda - (\partial g/\partial y)\mu \end{aligned}\right\} \tag{4}$$

(d) Let $u(t_j) = x(t_j) - x_j$ and $v(t_j) = y(t_j) - y_j$, $j = 1, \ldots, n$. The numbers $u(t_j)$ and $v(t_j)$ are a measure of the truncation error in each step of the integration.

(c) Truncation Error

Rademacher derived the following formulas for the truncation error:

$$\left.\begin{aligned} &\lambda(T)u(T) + \mu(T)v(T) \sim \\ &-\frac{1}{12}(\Delta t)^2[\lambda(t)x''(t) + \mu(t)y''(t)]\Big|_{t_0}^{T} \\ &-\frac{1}{6}(\Delta t)^2 \int_{t_0}^{T} [\lambda'(t)x''(t) + \mu'(t)y''(t)]dt \end{aligned}\right\} \tag{5}$$

The truncation errors $u(T)$ and $v(T)$ can be separately obtained from eq 5 by applying the proper terminal conditions to the solutions $\lambda(t)$ and $\mu(t)$ of eq 4. For example, $u(T)$ can be found by letting $\lambda(T) = 1$ and $\mu(T) = 0$.

(d) Rounding-Off Error

Thus far, it has been assumed that all computations are done exactly. In actual computing, this is not the case. The accumulators or registers of the computing machine accommodate only a limited number of digits. Thus eq 2 and 3 should be written as

$$\left.\begin{aligned} x_j^* &= x_{j-1} + \Delta t \cdot f(x_{j-1}, y_{j-1}) + \sum_m \epsilon_{jm} r_{jm}^{(1)} \\ y_j^* &= y_{j-1} + \Delta t \cdot g(x_{j-1}, y_{j-1}) + \sum_m \epsilon_{jm} r_{jm}^{(2)} \end{aligned}\right\} \tag{6}$$

$$\left.\begin{aligned} x_j &= x_{j-1} + \frac{\Delta t}{2}[f(x_j^*, y_j^*) + f(x_{j-1}, y_{j-1})] + \sum_m \epsilon_{jm} r_{jm}^{(3)} \\ y_j &= y_{j-1} + \frac{\Delta t}{2}[g(x_j^*, y_j^*) + g(x_{j-1}, y_{j-1})] + \sum_m \epsilon_{jm} r_{jm}^{(4)} \end{aligned}\right\} \tag{7}$$

The ϵ_{jm} satisfy $|\epsilon_{jm}| \leq 0.5$. The coefficients $r_{jm}^{(s)}$ depend not only upon the equations to be solved but upon the explicit procedure or order of operations in the process of solution. In the following discussion quantities with bars above them represent the actual numbers stored in the registers or accumulators of the computing machine. Although the analysis can be carried through using eq 6 and 7, Rademacher makes the simplifying assumption that

$$\overline{\Delta t\, f(\overline{x}_j, \overline{y}_j)} = \overline{\Delta t\, f(\overline{x}_j, \overline{y}_j)}.$$

This means that he assumes that $f(x_j, y_j)$ can be computed sufficiently accurately so that when multiplied by Δt any inaccuracies it may have are lost in the digits that are dropped. Thus, eq 7 can be replaced by

$$\left.\begin{aligned} \overline{x}_j &= \overline{x}_{j-1} + \frac{\Delta t}{2}[f(\overline{x}_j^*, \overline{y}_j^*) + f(\overline{x}_{j-1}, \overline{y}_{j-1})] + \epsilon_{j1} 10^{-k} \\ \overline{y}_j &= \overline{y}_{j-1} + \frac{\Delta t}{2}[g(\overline{x}_j^*, \overline{y}_j^*) + g(\overline{x}_{j-1}, \overline{y}_{j-1})] + \epsilon_{j2} 10^{-k}. \end{aligned}\right\} \tag{8}$$

Note that if the parentheses are removed in eq 8 so that there are four multiplications, then there are four rounding-off terms, say ϵ_{jm}^* $(s = 1,2;\ m = 1,2)$.

As in the case of the truncation error let us make the following definition: $\overline{u}_j = x_j - \overline{x}_j$ and $\overline{v}_j = y_j - \overline{y}_j$.

TABLE 1. *Sine-cosine rounding errors*

Δt		Angle, in radians							
		0.2	0.3	0.4	0.5	0.6	0.7	0.8	0.9
2×10^{-2}	S. D.	4.082	5.773	7.071	8.164	9.129	10.00	10.80	11.55
	Sin (A)	1	1	1	3	5	8	13	19
	Cos (A)	2	3	4	9	9	15	3	9
	Sin (B)	0	−1	5	7	5	7	10	11
	Cos (B)	1	2	1	0	1	−3	−3	−5
1×10^{-2}	S. D.	5.774	8.166	10.00	11.55	12.91	14.14	15.28	16.33
	Sin (A)	1	−1	−5	2	−1	0	−5	−4
	Cos (A)	−2	1	9	6	4	2	9	9
	Sin (B)	4	0	−6	−5	−7	−10	−7	−8
	Cos (B)	−1	−2	0	−2	−2	−4	−3	−2
5×10^{-3}	S. D.	8.161	11.54	14.14	16.32	18.25	19.99	21.60	23.08
	Sin (A)	1	10	11	12	14	25	20	14
	Cos (A)	2	5	3	3	6	5	−2	−2
	Sin (B)	1	3	0	−3	−12	−15	−12	−17
	Cos (B)	2	1	3	−2	−8	−7	−3	−5
2×10^{-3}	S. D.	12.91	18.25	22.36	25.82	28.86	31.62	34.15	36.51
	Sin (A)	5	−17	−11	24	50	77	104	134
	Cos (A)	26	55	85	84	90	99	92	105
	Sin (B)	−2	6	3	−13	−19	−14	−11	−6
	Cos (B)	−3	−2	−8	−4	−9	4	1	−2
1×10^{-3}	S. D.	18.26	25.82	31.62	36.51	40.83	44.72	48.31	51.64
	Sin (A)	1	−2	−48	−53	−95	−97	−116	−148
	Cos (A)	−17	−36	−21	−41	−32	−32	−45	−39
	Sin (B)	−7	−10	9	8	−5	−15	−20	−4
	Cos (B)	−7	−15	−9	−13	−7	−5	−7	−1
5×10^{-4}	S. D.	25.81	36.51	44.71	51.63	57.73	63.24	68.30	73.02
	Sin (A)	32	21	60	34	45	4	9	10
	Cos (A)	8	60	42	21	25	−1	1	−7
	Sin (B)	18	−2	−16	−4	−5	10	16	32
	Cos (B)	−1	−21	−10	−14	−24	−26	−20	−20
2×10^{-4}	S. D.	40.82	57.73	70.71	81.64	91.29	100.0	108.0	115.5
	Sin (A)	−17	23	−3	8	−190	−222	−254	−317
	Cos (A)	3	5	16	−18	21	57	49	86
	Sin (B)	14	34	32	30	50	61	68	7
	Cos (B)	2	6	−9	−16	−44	−40	−79	−94
1×10^{-4}	S. D.	57.74	81.66	100.0	115.5	129.1	141.4	152.8	163.3
	Sin (A)	−5	−26	−35	−62	−110	−91	−87	−71
	Cos (A)	4	12	40	63	84	65	84	122
	Sin (B)	−2	−17	−4	−4	14	16	6	17
	Cos (B)	−10	0	−11	−16	−28	−24	−49	−53
5×10^{-5}	S. D.	81.61	115.4	141.4	163.2	182.5	199.9	216.0	230.8
	Sin (A)	19	11	11	−27	−52	−68	−46	−39
	Cos (A)	4	10	−6	−8	−10	17	4	−4
	Sin (B)	−5	−4	20	28	39	51	37	50
	Cos (B)	−2	1	−7	4	32	53	56	45
2×10^{-5}	S. D.	129.1	182.5	223.6	258.2	288.6	316.2	341.5	365.1
	Sin (A)	37	30	52	34	27	32	40	24
	Cos (A)	20	5	13	16	0	8	8	−7

Letting $\overline{u}_n=\overline{u}(T)$ and $\overline{v}_n=\overline{v}(T)$, the expression for the rounding-off error is

$$\lambda(T)u(T)+\mu(T)v(T)=-10^{-k}\sum_{j=1}^{n}(\epsilon_{j1}\lambda_j+\epsilon_{j2}\mu_j). \quad (9)$$

From the inequalities $|\epsilon_{jm}|\leq 0.5$, $m=1,2$, the maximum possible value of the rounding-off error is

$$|\lambda(T)u(T)+\mu(T)v(T)|\leq 10^{-k}\sum_{j=1}^{n}(|\lambda_j|+|\mu_j|)$$
$$\sim\frac{10^{-k}}{\Delta t}\int_{t_0}^{T}[|\lambda(t)|+|\mu(t)|]dt. \quad (10)$$

However, if the ϵ_{jm}, $m=1,2$, are random variables then the standard deviation of the rounding-off error is

$$\sigma[\lambda(T)u(T)+\mu(T)v(T)]\sim$$
$$\frac{10^{-k}}{\sqrt{3}}(\Delta t)^{-1/2}\left[\int_{t_0}^{T}[\lambda^2(t)+\mu^2(t)]dt\right]^{1/2}. \quad (11)$$

II. Example

1. Sine-cosine Integrations

To check the theory developed by Rademacher the system

$$\left.\begin{aligned}x'(t)&=y(t)\\ y'(t)&=-x(t)\end{aligned}\right\} \quad (12)$$

was integrated on the Electronic Numerical Integrator and Computer.[3] The range $0.1\leq t\leq 0.9$ radians was chosen as the integration interval, since neither function was zero in that interval. (While the function is near zero the increment $\Delta t\, f(\overline{x},\overline{y})$ is small and might lead to a systematic effect in the rounding-off.) All computations were done to 10 decimal digits. About 10 values of Δt were used ranging from 2×10^{-3} to 2×10^{-6}. A run "A" was made with the parentheses appearing in eq 8 removed; this gives four round-offs per integration step. A run "B" was made with the parentheses in; this gives two round-offs per integration step. The results of these runs are tabulated in table 1.

The first entry in each rectangle in table 1 is the run A standard deviation for the respective angle and increment as given by eq 11. For run B this standard deviation should be divided by two. Underneath are the residual errors (after the truncation error is removed) for the various runs and functions. A typical entry (such as the residual error of 15 for the cosine in run A, angle equal to 0.7 radians, and increment of 2×10^{-3}) is found as follows:

Integration result =	0.76484 19311
Truncation error as given by eq 5 =	+0.00000 02577
	0.76484 21888
True value =	0.76484 21873
Residual error =	0.00000 00015

The most interesting feature in the table occurs in run A for the sine with an increment of 2×10^{-5}. For the angle changing from 0.5 to 0.6 radian the residual error jumps from +0.00000 00008 to −0.00000 000190. This integration was rerun, and results were printed more frequently. It was found that most of the disturbance occurred between 0.5211 and 0.5264 radian. Table 3 gives the results over this range with printings at every five integration steps, and table 2 exhibits a typical five steps between the values of table 3.

TABLE 2. *Sample step in the sine-cosine integration*

$\Delta t=0.00002$ $\quad 0.52250\leq t\leq 0.52260$

$x_i^*=x_{i-1}+\Delta t\, y_{i-1}$ $\quad x_i=x_{i-1}+\frac{\Delta t}{2}[y_i^*+y_{i-1}]$

$y_i^*=y_{i-1}-\Delta t\, x_{i-1}$ $\quad y_i=y_{i-1}-\frac{\Delta t}{2}[x_i^*+x_{i-1}]$

t	$\overset{x}{\sin t}$	x^*	$\overset{y}{\cos t}$	y^*
0.52250	0. 49904 81273	0. 49904 81273	0.86657 42703	0. 86657 42703
	86657 4	1 73314	−49904 8	−99810
	86656 4	. 49906 54587	−49906 5	. 86656 42893
.52252	. 49906 54586	. 49906 54586	. 86656 42891	. 86656 42891
	86656 4	1 73312	−49906 5	−99814
	86655 4	. 49908 27898	−49908 2	. 86655 43077
.52254	. 49908 27897	. 49908 27897	. 86655 43076	. 86655 43076
	86655 4	1 73310	−49908 2	−99816
	86654 4	. 49910 01207	−49910 0	. 86654 43260
.52256	. 49910 01206	. 49910 01206	. 86654 43258	. 86654 43258
	86654 4	1 73308	−49910 0	−99820
	86653 4	. 49911 74514	−49911 7	. 86653 43438
.52258	. 49911 74513	. 49911 74513	. 86653 43436	. 86653 43436
	86653 4	1 73306	−49911 7	−99824
	86652 4	. 49913 47819	−49913 4	. 86652 43612
.52260	. 49913 47818	. 49913 47818	. 86652 43611	. 86652 43611

[3] The "ENIAC" was built by the Moore School of Electrical Engineering of the University of Pennsylvania and is now located at the Ballistic Research Laboratories of Aberdeen Proving Ground.

TABLE 3. *Sine-cosine integration*

$\Delta t = 0.00002$

t	Sine	E	Cosine	t	Sine	E	Cosine
0.5100	0.48817 72474	−4	0.87274 45090	0.5240	0.50034 74198	102	0.86582 47235
.5110	.48904 97478	−8	.87225 58955	.5241	.50043 39993	107	.86577 46845
.5120	.48992 17591	−11	.87176 64098	.5242	.50052 05738	112	.86572 46368
.5130	.49079 32802	−2	.87127 60521	.5243	.50060 71433	117	.86567 45803
.5140	.49166 43102	−2	.87078 48234	.5244	.50069 37078	122	.86562 45153
.5150	.49253 48499	−9	.87029 27237	.5245	.50078 02673	127	.86557 44416
.5160	.49340 48968	−18	.86979 97538	.5246	.50086 68218	132	.86552 43593
.5170	.49427 44483	−3	.86930 59143	.5247	.50095 33713	137	.86547 42683
.5180	.49514 35083	−13	.86881 12054	.5248	.50103 99158	142	.86542 41686
.5190	.49601 20698	+2	.86831 56275	.5249	.50112 64553	147	.86537 40603
.5200	.49688 01398	−18	.86781 91812	.5250	.50121 29898	152	.86532 39433
.5201	.49696 69193	−23	.86776 94889	.5251	.50129 95193	157	.86527 38178
.5202	.49705 36938	−18	.86771 97879	.5252	.50138 60438	152	.86522 36835
.5203	.49704 04633	−23	.86767 00782	.5253	.50147 25633	157	.86517 35405
.5204	.49722 72278	−18	.86762 03597	.5254	.50155 90778	162	.86512 33890
.5205	.49731 39873	−23	.86757 06327	.5255	.50164 55873	167	.86507 32287
.5206	.49740 07418	−18	.86752 08970	.5256	.50173 20918	172	.86502 30599
.5207	.49748 74913	−23	.86747 11525	.5257	.50181 85913	177	.86497 28824
.5208	.49757 42358	−18	.86742 13995	.5258	.50190 50858	172	.86492 26961
.5209	.49766 09753	−13	.86737 16378	.5259	.50199 15753	177	.86487 25013
.5210	.49774 77098	−18	.86732 18673	.5260	.50207 80598	182	.86482 22978
.5211	.49783 44393	−13	.86727 20881	.5261	.50216 45393	187	.86477 20856
.5212	.49792 11638	−8	.86722 23004	.5262	.50225 10138	182	.86472 18649
.5213	.49800 78833	−3	.86717 25039	.5263	.50233 74833	187	.86467 16354
.5214	.49809 45978	−8	.86712 26987	.5264	.50242 39478	192	.86462 13974
.5215	.49818 13073	−3	.86707 28850	.5265	.50251 04073	187	.86457 11507
.5216	.49826 80118	+2	.86702 30625	.5266	.50259 68618	192	.86452 08954
.5217	.49835 47113	7	.86697 32313	.5267	.50268 33113	187	.86447 06314
.5218	.49844 14058	12	.86692 33916	.5268	.50276 97558	192	.86442 03587
.5219	.49852 80953	7	.86687 35431	.5269	.50285 61953	187	.86437 00774
.5220	.49861 47798	12	.86682 36859	.5270	.50294 26298	192	.86431 97874
.5221	.49870 14593	17	.86677 38202	.5271	.50302 90593	187	.86426 94889
.5222	.49878 81338	22	.86672 39457	.5272	.50311 54838	192	.86421 91816
.5223	.49887 48033	27	.86667 40625	.5273	.50320 19033	187	.86416 88658
.5224	.49896 14678	32	.86662 41708	.5274	.50328 83178	192	.86411 85413
.5225	.49904 81273	37	.86657 42703	.5275	.50337 47273	187	.86406 82081
.5226	.49913 47818	42	.86652 43611	.5276	.50346 11318	182	.86401 78664
.5227	.49922 14313	47	.86647 44434	.5277	.50354 75313	187	.86396 75159
.5228	.49930 80758	52	.86642 45169	.5278	.50363 39258	182	.86391 71569
.5229	.49939 47153	57	.86637 45817	.5279	.50372 03153	177	.86386 67892
.5230	.49948 13498	62	.86632 46380	.5280	.50380 66998	172	.86381 64129
.5231	.49956 79793	57	.86627 46855	.5281	.50389 30793	167	.86376 60279
.5232	.49965 46038	62	.86622 47243	.5282	.50397 94538	162	.86371 56344
.5233	.49974 12233	67	.86617 47546	.5283	.50406 58233	157	.86366 52321
.5234	.49982 78378	72	.86612 47761	.5284	.50415 21873	157	.86361 48213
.5235	.49991 44473	77	.86607 47889	.5285	.50423 85458	162	.86356 44018
.5236	.50000 10518	82	.86602 47932	.5286	.50432 48993	167	.86351 39736
.5237	.50008 76513	87	.86597 47887	.5287	.50441 12478	172	.86346 35369
.5238	.50017 42458	92	.86592 47757	.5288	.50449 75913	177	.86341 30914
.5239	.50026 08353	97	.86587 47540	.5289	.50458 39298	182	.86336 26374

Thus, most of the change in error occurs in an interval of about 0.0053 radian. This represents about 260 integration steps and over a thousand round-offs. In one half of the multiplications, the digit being dropped in the rounding-off process (see the sixth digit in the cosine values of table 3) changes gradually from zero up to four and back to zero again.

The errors in the sine values (see column headed E in table 3) may be wrong by up to plus or minus five units, since they were obtained by subtracting the integration results (listed in table 3) from nine digit values of the true results taken from Tables of Circular and Hyperbolic Sines and Cosines.[4]

It will be noted that the last digits of the sine values in table 3, generally speaking, are alternately 3's and 8's. This can be traced to the

[4] See footnote 2.

alternate 2's and 7's or 1's and 6's in the fifth digit of the cosine values. This is another warning against unconsidered assumption of randomness in the less significant digits of numbers involved in computations.

Rademacher asserts there will be statistical independence of the dropped digits in the rounding-off process provided $(\Delta t/2)\ f(\overline{x}_{j-1},\overline{y}_{j-1})$ and $(\Delta t/2)\ f(\overline{x}_j,\overline{y}_j)$ differ in the place 10^{-k}. The example given here shows that Rademacher's condition is not sufficient. In fact, inspection of table 2 shows that the increments $\Delta t/2\ f(x,y)$ may differ in the place 10^{-k} and yet be alike for a large number of integration steps in the place 10^{-k-1}.

There are other examples listed in table 1 leading to large residual errors. For example, consider in run A the sine and cosine values for $\Delta t=2\text{x}10^{-4}$ and the sine values for $\Delta t=1\times10^{-4}$. More frequent tabulation of results shows a steady increase of residual error with no such jumps as described above.

The author thanks various members of the staff of the Ballistics Research Laboratories and of the Moore School who assisted in running the problem, and extends his appreciation to L. S. Dederick of the Ballistics Research Laboratories, whose permission and cooperation made this paper possible.

III. Appendix

Note on Systematic Rounding-off Errors in Numerical Integration

By D. R. Hartree [5]

In this paper, which summarizes the results of a numerical study of truncation and rounding-off errors in the numerical solution of a differential equation by a step-by-step process, Huskey has exhibited a case in which rounding-off errors in a sequence of successive contributions to the solution are systematically of one sign and approximately equal in magnitude, although the leading digit rounded off is the sixth significant figure in each contribution. The result is that the rounding-off errors build up to a total substantially greater than would be estimated in the basis of a random distribution of rounding-off errors in the individual contributions. The purpose of this note is to examine this situation further and to establish criteria for identifying the conditions in which it is likely to occur, so that steps can be taken to deal with it, as for example by carrying an extra significant figure temporarily in the course of the solution.

Consider the numerical evaluation of $\int y dt$, k decimals being kept in the calculation.

[5] On the staff of the Institute for Numerical Analysis.

Systematic rounding-off errors occur when the leading digit rounded off remains the same in a number of successive contributions to the integral; that is, when for successive contributions, last integer digit of $10^{k+1}y\delta t$ is the same. When this occurs, [last integer digit of $\delta(10^{k+1}y\delta t)]=0$, or [last integer digit of $10^{k+1}\dot{y}(\delta t)^2]=0$; that is,

$$10n-0.5<10^{k+1}\dot{y}(\delta t)^2<10n+0.5, \tag{13}$$

for some integer n. This will usually occur for some value or other of t if

$$10^k \max|\dot{y}|(\delta t)^2>1; \tag{14}$$

it will also occur if

$$10^k \max|\dot{y}|(\delta t)^2<1/10. \tag{15}$$

The range $\Delta\dot{y}$ of $\dot{y}$ over which the inequalities (eq. 13) are satisfied is

$$\Delta\dot{y}=1/[10^{k+1}(\delta t)^2],$$

and the number N of intervals required to cover this range is given approximately by

$$N(\delta t)|\ddot{y}|=\Delta\dot{y},$$

so that

$$N=1/[10^{k+1}(\delta t)^3|\ddot{y}|]. \tag{16}$$

The accumulation of systematic errors is only serious if N is greater than 3 or 4, that is, if

$$4\cdot10^{k+1}(\delta t)^3|\ddot{y}|<1; \tag{17}$$

for this not to occur

$$(\delta t)^3>1/[4\cdot10^{k+1}|\ddot{y}|]. \tag{18}$$

The inequalities (eq. 13 and 17) together provide a criterion for identifying the situations in which accumulation of systematic rounding-off errors may be dangerous. Such a situation may arise in any numerical integration, not only in the solution of a differential equation, the context in which it was first found by Huskey. The inequality (eq. 17) shows how much more likely it is to arise with small values of the integration interval (δt) than with large values.

In the case considered particularly by Huskey, $y=\cos t$, $k=10$, $\delta t=2\cdot10^{-5}$, $\dot{y}=\sin t$, so that eq 13 becomes

$$10n-0.5<40\sin t<10n+0.5;$$

this is satisfied for a range of t in the neighborhood of $\sin t=\frac{1}{2}$, which is just the region in which the phenomenon does occur; and it happens to be particularly marked in this case, since the digit which is rounded off systematically happens to be a 4 over a considerable range. Also

$$10^{k+1}(\delta t)^3|\ddot{y}|\approx7\cdot10^{-4},$$

so that, from eq. 16, N is about 1,400, and the inequality (eq. 17) is very far from being satisfied; hence it is not surprising that the phenomenon arose in a marked form. The condition (eq. 18) suggests that with the value of $k=10$, the interval length should certainly be greater than $\delta t=10^{-4}$.

WASHINGTON,, July 17, 1948.

U. S. Department of Commerce
National Bureau of Standards

Research Paper RP1951
Volume 42, January 1949

Part of the Journal of Research of the National Bureau of Standards

Treatment of Leather with Synthetic Resins [1]

By Rene Oehler and Timothy J. Kilduff

Laboratory methods have been developed for treating leather with snythetic resins. The first method of treatment may be accomplished by immersing the leather specimens in monomer and subsequently polymerizing *in situ;* the second method consists of immersing the specimens in polymer solutions; and the third method involves immersion in a solution of partially polymerized liquid resin, which is further polymerized in the leather itself. The last method was developed in cooperation with the Thiokol Corporation, using Thiokol LP–2.

Abrasion resistance of vegetable-tanned crust leather treated with *n*-butyl methacrylate, polymerized *in situ*, is increased by approximately 75 percent, as measured on the National Bureau of Standards abrasion machine. Treatment with Thiokol LP–2 increased abrasion resistance by approximately 30 percent. However, treatment of vegetable-tanned crust leather with polybutyl methacrylate solution-polymer resulted in no improvement in abrasion resistance. One-half-hour water absorption data show a reduction of one-tenth to one-third that of untreated leather, depending upon the kind of treatment and leather.

By proper choice of monomers and polymerization conditions, stiffness may be controlled to meet the needs of different types of leather.

Water vapor permeability of shoe upper leather is reduced 60 percent, but is still considered ample for foot comfort.

I. Introduction

Preliminary research, conducted at the National Bureau of Standards in 1944, showed that certain acrylate monomers might be successfully polymerized in leather within leather. However, it was not possible to resume work on this project until 1946. Because of the excellent penetration of monomers into leather and the promise of successful polymerization *in situ*, to give resins of suitable molecular weights, it was hoped that the wear resistance of sole leather and the water resistance of sole upper leather could be improved.

This paper presents the first results of a systematic study of the general problem of impregnating leather with resins and plastics.

Earlier work has resulted in many well-known finishing agents or coating materials for different types of leather. However, very little is known concerning their use as impregnants for leather. The chief reason for this lack of information is that ordinary, commercial resins do not penetrate leather to any considerable extent. This lack of penetration is borne out in a paper by Niedercorn and Thayer [1],[2] who studied 25 different resins of several types. They found that the maximum resin content of treated sole leather was only 6.9 percent, which resulted in only a slight improvement in abrasion resistance. In fact, they found that an oil treatment resulted in a greater and more consistent improvement than did the resin treatments.

Chadwick [2] reviewed the whole field of plastics as applied to leather. He proposed, among other things, that since polyisobutylene is compatible with certain waxes and oils, it might advantageously replace part of the waxes and oils normally used in sole leather; he also suggested that certain thermosetting resins that were only partially

[1] This report is made as a part of the Leather Research Program sponsored by the Research and Development Branch, Military Planning Division, of the Office of the Quartermaster General, United States Army. This program is under the Advisory Direction of the National Research Council.

[2] Figures in brackets indicate the literature references at the end of this paper.

815197—49——5

polymerized might be further cured by heat after impregnation; he suggested, too, that properly plasticized thermoplastic resins, such as polyvinyl chloride, polyvinyl chloride-acetate copolymer, and polyvinylidene chloride should be especially useful for sole leather because of their outstanding abrasion resistance.

Virtue [3] has reported 50-percent improvement in wear resistance by impregnating finished taps with 8 to 12 percent of maleic anhydride modified alkyd, or modified phenolic resin.

The wide differences in type of resins used and suggested by the above authors present the problem of selecting suitable resins with which to work. The salient points considered in making selections are discussed in the next section.

II. Selection and Properties of Resins

The resins selected to begin this study were the acrylates and methacrylates, because of ready availability, rather wide range of properties within the series of esters and relative ease of polymerization. The resin selected should have properties which will improve the wear of leather without seriously detracting from the desirable characteristics of leather. For example, a resin to be used for sole leather should have a greater abrasion resistance and may be more viscous than a resin to be used for shoe upper leather. Specific characteristics to be considered in selecting a resin are: proper flexibility of the treated leather, toughness, high abrasion resistance, high extensibility, low water absorption, and low water penetration.

TABLE 1. *Properties of methacrylate ester polymers*

Properties	Methyl	Ethyl	Normal propyl	Normal butyl	Isobutyl
Density at 25°C	1.19	1.11	1.06	1.05	1.02
Hardness (Pfund) at 25°C	220	141	100	1	210
Thermal yield point, °C	125	65	38	30	70
Tensil strength, lb/in.²	9,000	5,000	4,000	1,000	3,400
Impact strength (Dynstat), kg-cm/cm.²	10.5	7.1	6.5	11.5	1.6
Refractive index	1.490	1.485	1.484	1.483	1.477
Extensibility, 5-mil films (percentage at break)	4	7	5	230	2
Toughness, area under load-elongation curve, expressed in arbitrary units	98	174	76	1,000	23

The principal properties of the common polymethacrylates have been reported, as shown in table 1, by Strain, et al. [4]. This table shows that polybutyl methacrylate should be the most satisfactory of the group for treating sole leather. Of course, no single resin or any other material can have all the desirable properties that may be enumerated. Consequently, compromises must be made to obtain the most desirable properties. These compromises can best be achieved by the addition of plasticizers or by polymerizing two or more monomers to form copolymers or interpolymers with properties intermediate between those of the separately polymerized monomers.

III. Methods of Treating Leathers

The three methods used for impregnating leather with resins are immersion of leather in monomer and subsequent polymerization *in situ*; immersion in polymer solutions followed by evaporation of the solvent; immersion in partially polymerized resin followed by varying degrees of cure, depending upon the desired results. These methods have been studied and will be discussed one at a time.

1. Immersion in Monomer Followed by Polymerization in situ

This method of impregnating leather with resins essentially consists in immersing the weighed leather specimens in a monomer containing benzoyl or lauroyl peroxide catalyst for 15 minutes, wiping off excess solution, reweighing, transferring to a suitable bomb or closed system, heating overnight at a given temperature, evaporating the excess monomer, and weighing again to determine the amount of resin. Several variations were tried in the type of leather treated, the kind and amount of catalyst used, the temperature and time of heating, the different monomers or combinations thereof, the use of oils or other solvents with monomers, the use of liquid monomer (without catalyst) in the polymerization chamber, the relative size of polymerization chamber, and different materials for polymerization chambers.

Preliminary experiments disclosed no consistent relationship between the amount of resin in the treated sole leather and different catalyst concentrations, different vegetable tannages, chrome-tanned specimens, and different oils used as diluents or plasticizers, or both. However, vegetable-tanned crust leather does have the advantage of large pore size and a large void space or capacity to absorb monomer. A temperature range of 70° to 80° C was regarded as about the maximum

polymerization temperature that could be used without damaging vegetable-tanned crust leather. Accordingly, most of the data presented are concerned with vegetable-tanned crust leather in which polymerization was carried out at 70° C.

Table 2 shows that the mean resin content obtained in the leather specimens decreased as the volume of the polymerization chamber increased from 19 to 54 ml. For chambers larger than 36 ml, the resulting resin content falls off rapidly, and all chambers larger than 54 ml are sufficiently large to give more or less uniformly low results. These low results may be due to the evaporation of monomer from the leather, or to the inhibiting action of oxygen, which has been reported by Barnes [5], Heuck [6], and Kolthoff [7]. These factors will, of course, be reduced if the ratio of specimen volume to total volume is nearly 1. Another way of reducing evaporation from the leather is to add liquid monomer to the polymerization chamber. Both ways of improvement will be presented.

Figure 1 clearly shows the effects of adding liquid monomer to the polymerization chamber. In both groups of data, the points scatter quite uniformly about their respective averages. It should be noted that both the average and the run-to-run variation are considerably higher in the case of added monomer. However, the variability within runs is quite uniform and the same for both sets of data; only two points fall outside reasonable range limits.

TABLE 2. *Results of in-situ polymerization of ethyl acrylate in vegetable-tanned crust leather heated at 70° C for 16 hours*

(Composition of impregnant: ethyl-acrylate-neatsfoot oil 50:50, with 5-percent benzoyl peroxide catalyst)

Polymerization chamber	Range of resin content	Mean resin content of specimens
	Percent	*Percent*
Test tube, 19 ml [a]	13.4 to 23.9	19.7
Test tube, 36 ml [a]	13.6 to 17.5	16.0
Test tube, 54 ml [a]	7.5 to 15.3	11.4
Jar, 75 ml [b]	3.8 to 7.7	6.0
Jar, 125 ml [b]	3.2 to 6.4	4.5
Pint jar [b]	2.5 to 4.0	3.2

[a] Single ½- by 3-in. specimens in each of three tubes.
[b] Three ½- by 3-in. specimens in each jar.

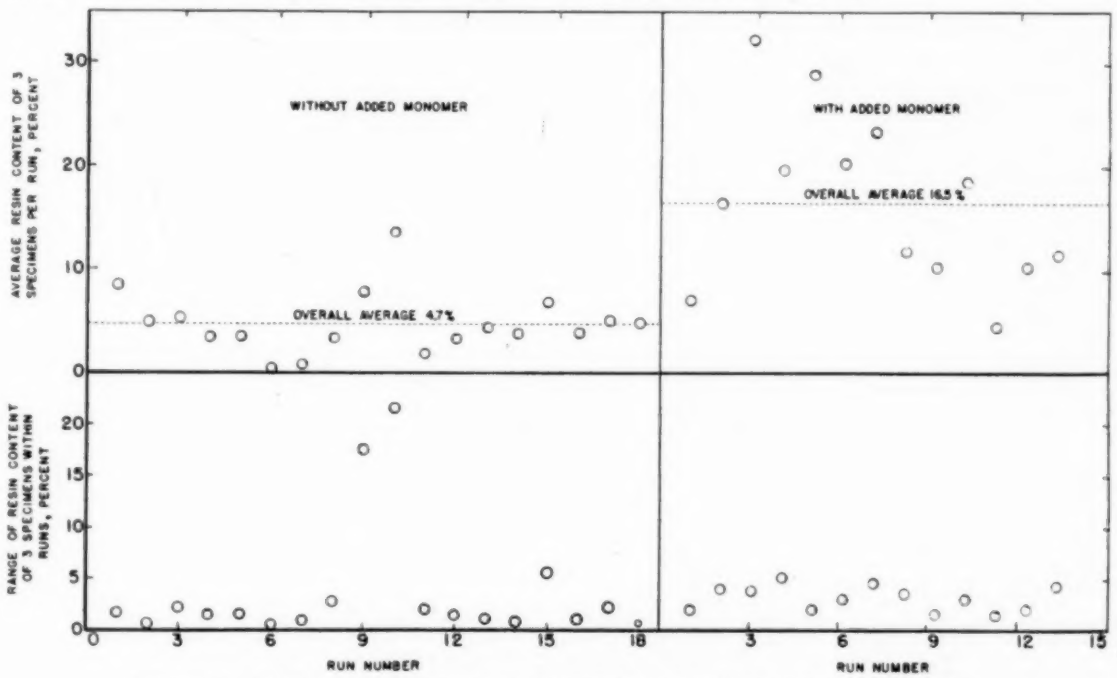
WITHOUT ADDED MONOMER
WITH ADDED MONOMER
OVERALL AVERAGE 4.7%
OVERALL AVERAGE 16.5%
AVERAGE RESIN CONTENT OF 3 SPECIMENS PER RUN, PERCENT
RANGE OF RESIN CONTENT OF 3 SPECIMENS WITHIN RUNS, PERCENT
RUN NUMBER
RUN NUMBER

FIGURE 1. *Effect of liquid monomer in polymerization chamber on in situ polymerization.*

Each point represents one run consisting of three specimens, 1 by 3 in., of vegetable-tanned crust leather impregnated with ethyl acrylate-neatsfoot oil, 50:50, and 5-percent benzoyl peroxide, heated in pint jars for 16 hours at 70° C.

Several attempts were made to reduce evaporation of monomer from the leather by using sand as a filler for the excess volume in the polymerization chambers. The amount of resin obtained in the leather specimens varied widely from run to run and from specimen to specimen within runs.

Table 3 shows the inconsistent results obtained when a large steel bomb is used to accommodate full-sized soles. These variations are typical and were repeated several more times than shown in the table. Sometimes nearly all the liquid monomer had polymerized, whereas hardly any polymerization occurred within the leather itself. At other times practically all the liquid monomer was recovered with almost no change in weight of the leather specimens during the heating period. The fact that liquid monomer remained in the polymerization chamber apparently precludes any possibility of a pressure phenomenon influencing the polymerization.

TABLE 3. *Results of in-situ polymerization of ethyl acrylate in vegetable-tanned crust leather heated at 70° C (except as noted) for 16 hr*

[Composition of impregnant, 50:50 ethyl acrylate and neatsfoot oil]

Polymerization chamber	Catalyst concentration	Specimens treated		Range of resin content	Mean resin content of specimens
		Number	Size		
	Percent		*in.*	*Percent*	*Percent*
Steel bomb (8 in. in diameter by 14 in. long).	5	3	2 by 6 taps.	3.2 to 16.4	12.0
		4			
	5	6	2 by 6 taps.	5.5 to 24.2	18.2
		7			
Steel bomb+30 ml monomer [a]	5	8	2 by 4	2.8 to 19.4	15.4
Steel bomb (preheated)+30 ml monomer.[a]	5	6	2 by 4	9.7 to 19.8	13.9
Steel bomb+30 ml monomer [b]	2	4	2 by 4	1.2 to 2.5	1.7
	4	4	2 by 4	3.8 to 11.8	7.0
	6	4	2 by 4	12.8 to 25.3	17.4
Steel bomb+30 ml monomer [b]	3	4	2 by 4	3.8 to 5.6	4.5
	6	4	2 by 4	0.8 to 5.3	4.6
	12	4	2 by 4	3.6 to 15.2	9.1

[a] Polymerized overnight at 100° C.
[b] All 12 specimens were in chamber simultaneously.

Table 4 illustrates the excellent results obtained when there is practically no excess volume in the polymerization chamber over that required for the leather. Not only is the mean resin content higher, but the run-to-run variation is very much reduced. A larger chamber to accommodate full soles with a minimum of excess volume is being built to investigate this avenue of approach further. Table 4 also indicates that a temperature of 50° C. is sufficient to secure consistent results of about half the resin content obtained at 70° C. These lower results are probably sufficient for sole leather, as will be pointed out below.

TABLE 4. *Polymerization in situ, using 2-in. disks of vegetable-tanned crust leather, 5-percent lauroyl peroxide catalyst, and 2-in. pipe fittings as the polymerization chamber*

Impregnant	Polymerized at 70° C.		Polymerized at 30° C.	
	Range of resin content of four specimens per run	Mean resin content of four specimens	Range of resin content of four specimens per run	Mean resin content of four specimens
	Percent	*Percent*	*Percent*	*Percent*
n-Butyl methacrylate	50.6 to 53.3 49.9 to 54.3 50.8 to 59.2	52.0 52.5 54.0	25.3 to 29.7	27.6
n - Butyl methacrylate - ethyl acrylate (90:10).	45.8 to 60.7 48.4 to 54.9 46.3 to 51.4	52.2 51.3 48.5	20.5 to 24.2	22.7
n - Butyl methacrylate - ethyl acrylate (75:25).	42.9 to 44.6 46.2 to 49.2 47.5 to 61.1	43.2 47.7 52.0	22.2 to 29.8	27.3
n - Butyl methacrylate - ethyl acrylate (50:50).	48.0 to 54.1 43.1 to 55.9 43.6 to 59.2	52.0 47.8 50.7	28.3 to 31.2	29.9

Additional data show that oils and diluents alone or together have varying effects on *in situ* polymerizations. Neatsfoot and castor oil do not appear to have an appreciable effect on the extent of polymerization, but they do act as plasticizers and diluents. Polyethyl acrylate by itself shrinks and distorts the leather specimens. However, when it is copolymerized with *n*-butyl methacrylate, or when used with about 10 percent of oil, no shrinkage or distortion results. Methyl ethyl ketone is satisfactory as a diluent, but Stoddard solvent, perchloroethylene, Marcol JX (a water-white mineral oil), carbon tetrachloride, dioxane, ethanol, and ethyl acetate inhibit practically all polymerization.

Test data on treated leather will follow in section IV, which compares other treatments, as well as this one, with untreated leather.

2. Immersion in Polymer Solutions

Leather may be impregnated with resins by means of certain polymer solutions. In order to use polymer solutions, the molecular weight of the resin and the viscosity of the solution must be

sufficiently low to obtain penetration into the leather. Impregnating solutions for this purpose may be obtained by making solution-polymers in a solvent, especially for use in leather, or by using solutions of resins, which are known to have low molecular weight.

(a) Specially Prepared Solution-Polymers

The preparation of special solution-polymers is quite easy, and by using different dilutions of the prepared resin, any desired resin content up to 50 percent has been obtained. Briefly, the method of preparing these solution-polymers consists in placing a solution of one or more monomers with lauroyl peroxide catalyst in a flask, and refluxing until the desired resin solids are obtained. The extent of penetration depends upon the nature of the monomer used, the molecular weight of the polymer, the viscosity, and the solids content of the resin solutions. For sole leather a resin is desired that will add materially to abrasion resistance (requires moderately high molecular weight) and yet penetration of the resin must be secured (requires low molecular weight or viscosity). Hence, a compromise between high and low molecular weight resins must be found. Variations were made in a number of factors that influence molecular weight, such as solvents, temperature, catalyst concentration, monomer concentration in solution, etc. The prepared resin solutions were used by immersing the leather specimens for ½ hour, wiping off the excess solution, and evaporating the solvent at 80° C for 4 to 6 hours.

Typical changes in polymerization conditions and resultant effects on the amount of resin obtained in treated vegetable-tanned crust leather are shown in table 5. The different reflux periods for run 1 show that resin solids or polymerization yield increases with prolonged heating. As the solids increase, the viscosity also increases. Consequently, run 1 shows that the mean resin contents of treated specimens corresponding to the different reflux periods are all approximately the same. The last column of table 5 lists the ratio of resin found in the treated leather to the resin calculated. The calculated resin is the product of the solution pick-up and resin solids in solution. Ratio values of 95 percent and higher indicate that the resins are sufficiently low in molecular weight and viscosity for rather complete absorption. Ratios in excess of 100 percent are probably due to the difficulty of removing the solvent from the resin in the interior of the treated leather. If one considers that the absorption is complete in all four parts of run 1, it would be expected that the resin content would increase with increasing solids, but the fact that the resin contents do not increase with increasing solids indicates that it is the increased viscosity that offsets the increased solids content.

TABLE 5. *Preparation of solution-polymers and impregnation results*

Run number	Monomer used with equal volume of toluene as solvent unless otherwise noted	Reflux time	Amount catalyst	Resin solids of solution-polymer	Mean resin content of three treated specimens	Mean ratio of resin found to resin calculated for three specimens
		Hours	*Percent*	*Percent*	*Percent*	*Percent*
1	n-Butyl methacrylate	1	2.0	37.5	18.6	100
		3		39.5	19.3	103
		20		44.9	20.5	101
		44		48.8	19.6	103
2	do	1	0.2	24.3	10.3	88.4
		20		43.8	4.2	55.1
3	do	1	.5	29.4	12.2	91.4
		20		46.1	11.0	86.1
4	do [a]	1	1.0	35.5	17.1	101
5	Ethylacrylate	1	0.5	46.0	15.1	83.2
6	do	1	1.0	46.3	22.8	95.1
7	do	1	2.0	50.0	23.1	93.4
8	Ethyl acrylate:					
	Unpressed specimens	1	0.2	41.2	16.2	74.4
	Pressed specimens	1	.2	41.2	7.4	58.4
9	Ethyl acrylate:					
	Unpressed specimens	1	.5	45.0	23.6	94.3
	Pressed specimens	1	.5	45.0	16.7	83.3
10	Ethyl acrylate:					
	Unpressed specimens	1	1.0	50.0	30.7	92.0
	Pressed specimens	1	1.0	50.0	21.3	86.2
11	Ethyl acrylate:					
	Unpressed specimens	1	2.0	50.0	28.0	95.3
	Pressed specimens	1	2.0	50.0	19.4	89.3
12	Ethyl acrylate, n-butyl methacrylate (50:50)	1	1.0	40.1	16.3	99.5
13	Ethyl acrylate, n-butyl methacrylate (20:80)	1	1.0	37.1 diluted 50:50	20.4 12.6	80.0 96.6
14	Ethyl acrylate, n-butyl methacrylate (25:75)	4	0.5	37.6	16.6	94.0
15	Ethyl acrylate, n-butyl methacrylate (25:75) [b]	4	.5	31.3	15.4	96.1

[a] Benzene solvent used.

[b] Ethyl acetate solvent used. Extra solvent necessary to keep resin dissolved.

Run 2 of table 5 shows that when using 0.2-percent catalyst instead of 2.0 percent as in run 1, the molecular weight and viscosity are considerably increased so that only about half as much

resin is absorbed, and the ratio of resin found to resin calculated is reduced from 100 to 88 percent.

Run 2 also illustrates the difference in results obtained by treating leather with a solution-polymer of different solids content. Both the resin content of leather and the ratio of resin found to resin calculated are lower when treated with a solution-polymer of higher solids content. The reduction of both values points to increased viscosity directly or indirectly as an explanation for the lower resin content. Since Strain found that prolonged heating of polymethyl methacrylate solution-polymers decreases rather than increases molecular weight, then the lower resin content of leather corresponding to the higher solids content cannot be attributed to an increase in molecular weight during the 20-hour reflux period. The ratio of resin found to resin calculated corresponding to the higher solids content is only 55 percent, or about 30 percent less than for the solution-polymer of lower solids content. This wide difference in ratios suggests some preferential absorption of the solvent for the solution-polymer of higher solids content.

Runs 8 through 11 appear to show the effect of decreasing molecular weights with increasing catalyst concentration in a different way. Comparisons were made between leather specimens pressed at 3,000 lb/in.^{2} and unpressed specimens. The pressed specimens had a smaller volume, smaller pore size, and consequently less room for absorbing resin solution. It would be expected, therefore, that the resin content of the pressed specimens would be less than that for the unpressed. More important, however, is the apparent relation between catalyst concentration or molecular weight and the ratios of resin found to resin calculated. In the case of 0.2-percent catalyst, this ratio for the unpressed specimens is about 20 percent less than that for the other three resin solutions of this series (runs 9 through 11). In other words, a larger proportion of the resin solution pick-up consisted of solvent for the resin prepared with 0.2-percent catalyst, which tends to show that the molecular size for viscosity of this resin solution was too large for absorption. The ratios for the remaining three resins of this series are all about the same, which also tends to show that 0.5-percent catalyst produces a molecular size that is sufficiently small to allow very good absorption by the unpressed leather. This one-step difference in ratios for unpressed leather further tends to show that a molecular size smaller than that obtained with 0.5-percent catalyst does not materially alter the ratios obtained.

The results obtained from specimens that were pressed at 3,000 lb/in.^{2} prior to treatment with the same solution-polymers suggest additional relations between the molecular size and viscosity, resin contents, and ratios of resin found to resin calculated. In the case of pressed specimens treated with resin prepared with 0.2-percent catalyst, only slightly more than half of the calculated resin was actually absorbed by the leather. As the catalyst concentration increases and the molecular weight of the resin decreases, the ratio differences between pressed and unpressed specimens exhibit two downward steps. These steps appear to indicate that as the molecular size and/or viscosity decreases, the large pore size of unpressed crust leather becomes less and less necessary for good absorption. It should also be pointed out that no substantial improvement in ratio differences was obtained for resins made with 2.0-percent catalyst as compared to 1.0 percent, as shown by the results of runs 10 and 11.

Run 13 illustrates the effect of diluting a somewhat viscous resin in order to obtain treated leather of different resin content. It will be noted that slightly more than half as much resin is obtained in leather when it is treated with a solution-polymer that has been diluted with an equal volume of solvent. This is explained on the basis of reduced viscosity. The solution-polymer was diluted with an equal volume of toluene. The resin content obtained, however, was slightly more than half that obtained for the undiluted solution-polymer. A suggested explanation for this deviation from proportionality is based on reduced viscosity, and a higher proportion of solution solids absorbed by leather treated with the diluted solutions, as shown by the values for the ratios of resin found to resin calculated. It is apparent, therefore, that the resin content of treated leather may be varied at will to any value lower than that obtained with undiluted solution-polymer, although the actual value of resin content obtained with the diluted solution may not be predicted precisely from the extent of dilution.

Similar relations and effects may be observed in

the remaining data of table 5, which have not been discussed in detail. It should be remembered, of course, that when prepared under corresponding conditions, polyethyl acrylate is softer and its solutions less viscous than polybutyl methacrylate. As would be expected, copolymers will have properties intermediate between those of the separately prepared polymers.

(b) Solutions of Resins of Known Molecular Weights

In order to have some definite reference points from which to judge the effects of molecular weight variations on resin impregnating solutions, polymethyl methacrylates of known molecular weights were used for treatment, as indicated in table 6. The impregnations were carried out in the same way as those described above for specially prepared solution-polymers. Viscosities of the solutions increased with molecular weight, as would be expected. A resin of corresponding molecular weight but softer and less viscous would probably be absorbed better than polymethyl methacrylate. However, these polymethyl methacrylate solutions do demonstrate the same relations between molecular weight and resin content of treated leather, as discussed under specially prepared solution-polymers. Table 6 shows that when polymethyl methacrylate is used, as described above, and has a molecular weight of 11,000 or 16,000, about 14 percent of resin is absorbed. However, for a polymer with a molecular weight of 43,000, only about one-tenth as much resin is absorbed. The use of methanol indicates that it is only slightly helpful in reducing viscosity and increasing resin content.

TABLE 6. *Impregnation with polymethyl methacrylate resins of known molecular weight*

Molecular weight of resin	Solvent	Resin solids	Mean resin content of three treated specimens	Ratio of resin found to resin calculated for three specimens
		Percent	*Percent*	*Percent*
11,000	Toluene	20	15.3	110
16,000	do	20	13.6	107
43,000	do	20	1.4	30
43,000	Toluene-methanol (3:1)	20	2.4	47

3. Immersion in Thiokol LP–2 Followed by Special Cures

Another type of resin solution that has promise for treating sole and shoe upper leathers is a polysulfide rubber dissolved in toluene. The Thiokol Corporation has made exploratory treatments of leather specimens with Thiokol LP–2. In considering the test data that follow, it should be recalled that these experiments are preliminary ones and do not represent any development work whatever. The processing appears to be simple and after the elimination of certain difficulties, should lend itself to easy commercial application.

Essentially, the method depends upon impregnating the leather specimens with a low molecular weight resin solution, by immersing, wiping off the excess solution, and curing or further polymerizing *in situ*. For shoe uppers and other soft leathers, a "chain-terminator" is used to maintain a relatively low molecular weight and soft resin, which does not materially reduce flexibility.

Treated vegetable-tanned crust leather contained 34-percent Thiokol LP–2; factory finished taps, 18 percent; and degreased Army retanned upper leather, 50 percent. Contrary to previous experience, treatment with Thiokol LP–2, as described, contributes practically no odor to the leather specimens.

IV. Properties of Treated Leathers

Comparative tests were made on different types of treated and untreated leathers. The tests included abrasion, water absorption, water-vapor permeability, and relative stiffness.

All tests were carried out in accordance with Federal Specification KK–L–311, Leather and Leather Products; General Specifications (Methods of Sampling, Inspection, and Tests).

1. Abrasion Resistance

Results of abrasion tests are shown in figures 2, 3, and 4. Figure 2 shows comparative results of vegetable-tanned crust leather that was treated with solutions containing equal amounts by volume of the monomers indicated and neatsfoot oil followed by polymerization *in situ*. The improvement shown by extrapolating the curve for polybutyl methacrylate to the line corresponding to 60-percent abrasion loss is about 75 percent,

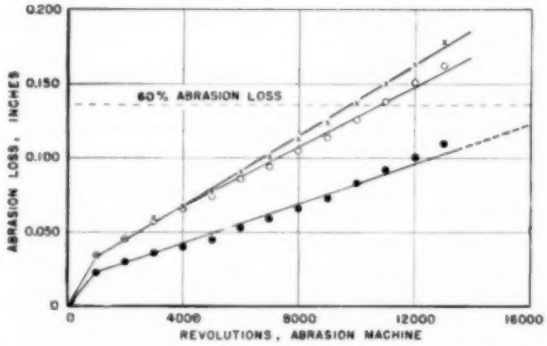

FIGURE 2. *Effect of polybutyl methacrylate and polyethyl acrylate (polymerized in situ) on abrasion resistance of vegetable-tanned crust leather.*

Mean values of four specimens for each treatment plotted. ●, *n*-Butyl methacrylate (20.10%); ○, ethyl acrylate (8.4%); ×, untreated.

and about 10-percent improvement for polyethyl acrylate. This wide difference in abrasion improvement is probably due to the fact that polyethyl acrylate is much softer than polybutyl methacrylate, and also because there was only 8 percent of the former resin in the treated leather compared to 20 percent for the latter resin. Figure 3 shows that the improvement found was not due to the neatsfoot oil. Figure 4 shows the improvement in abrasion resistance due to Thiokol treatment of factory-finished sole leather. The improvement of specimens treated with Thiokol LP–2 is about 30 percent. Attention is drawn to the fact that for all the curves the points are quite close to a straight line. Indirectly this linearity

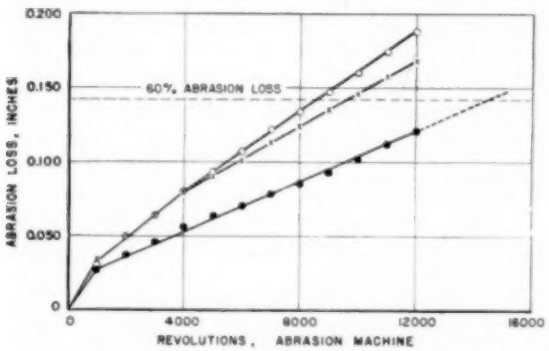

FIGURE 3. *Effect of polybutyl methacrylate (polymerized in situ) and neatsfoot oil on abrasion resistance of vegetable-tanned crust leather.*

Mean values of four specimens for each treatment plotted. ●, Butyl methacrylate (29.7%); ○, neatsfoot oil; ×, untreated.

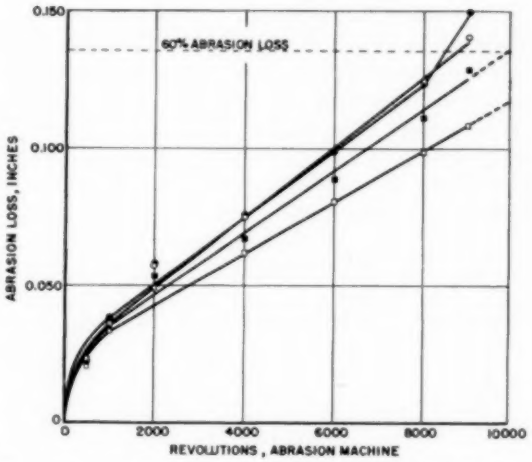

FIGURE 4. *Effect of treatment with Thiokol LP–2 on abrasion resistance of factory finished sole leather*

Mean values of three specimens for each treatment plotted. ●, Factory finished; ○, leached, factory finished; ■, Thiokol treated, factory finished; □, leached, Thiokol treated, factory-finished.

implies that penetration of the resins is more or less uniform throughout. Uniform penetration is to be expected for leather treated with monomer and subsequently polymerized, as the monomer has about the same viscosity as kerosine. The linear abrasion curves for soles treated with Thiokol LP–2 indicate uniform penetration, thereby showing that the molecular weight is suitable for adequate penetration.

Abrasion tests on leather treated with solution-polymers of specially prepared polyacrylates, polybutyl methacrylates, or copolymers thereof do not show any improvement in abrasion resistance over that of untreated leather. This difference from the improved abrasion resistance shown by the same polymerized monomers by the *in situ* method, suggests that in the latter process a higher degree of polymerization has occurred so as to impart greater abrasion resistance to treated leather.

2. Water Absorption

Curves for water absorption are shown in figures 5, 6, 7, and 8. The resins in the specimens shown in figure 5 were polymerized *in situ*. The curves for polybutyl methacrylate and copolymer of butyl methacrylate and ethyl acrylate practically coincide. The relative position of the curves for these two resin treatments of vegetable crust leather clearly establishes the superior

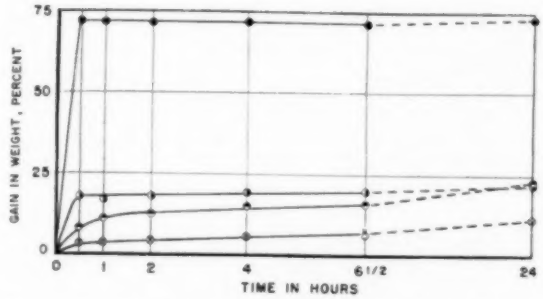

FIGURE 5. *Effect of resins (polymerized in situ) indicated on water absorption of vegetable-tanned crust leather*

Mean values of four specimens for each treatment plotted. ●, Controls; ◓, ethyl acrylate (40.6%); ×, butyl methacrylate (43.3%); ◑, ethyl acrylate-neatsfoot oil (21.0% R, 22.0% ○); ○, butyl methacrylate-ethyl acrylate (copolymer) (46.0%).

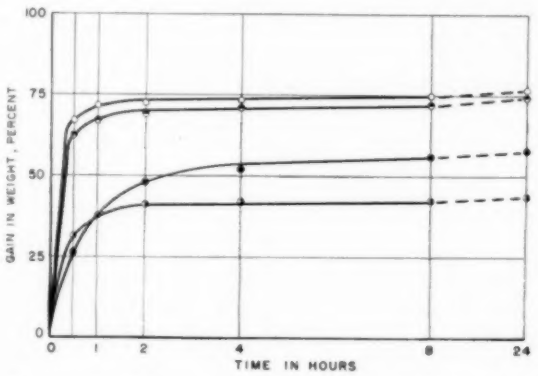

FIGURE 6. *Effect of solution-polymer resins on water absorption of vegetable-tanned crust leather.*

Mean values of four specimens for each treatment plotted. ○, Controls; ◓, polyethyl acrylate (6.8%); ◑, polyethyl acrylate (15.9%); ●, polybutyl methacrylate (8.3%).

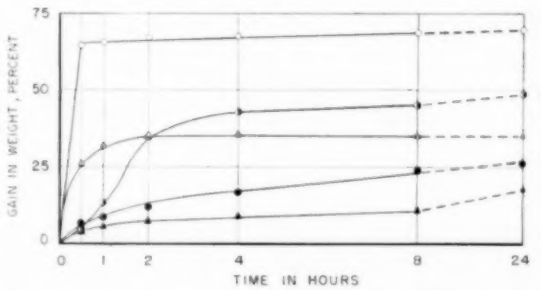

FIGURE 7. *Effect of different resins on water absorption of vegetable-tanned crust and factory finished sole leather.*

Mean values of two specimens for each treatment plotted. ○, Vegetable crust (controls); ◑, vegetable crust (copolymer, 10%); △, factory finish (controls); ●, vegetable crust (Thiokol, 34%); ▲, factory finish (Thiokol, 18%).

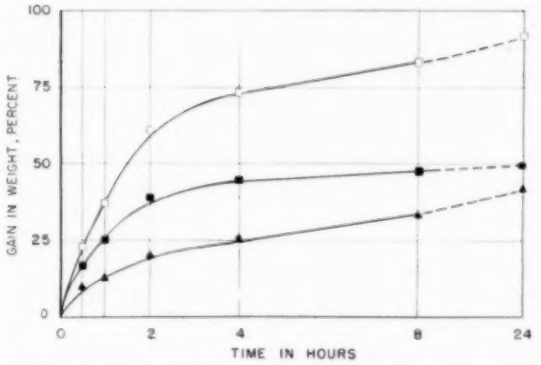

FIGURE 8. *Effect of different resins on water absorption of degreased chrome retan upper leather.*

Mean values of two specimens for each treatment plotted. □, Degreased chrome retan (controls), ■, degreased chrome retan (Thiokol, 50%); ▲ degreased chrome retan (polyethylacrylate, 50%).

resistance to water absorption by polybutyl methacrylate even when copolymerized with ethyl acrylate in equal amounts. The ethyl acrylate and ethyl acrylate-neatsfoot oil treatments have curves that are similar in general shape. However, the water absorption curve for ethyl acrylate is generally better than for the resin-oil treatment, and especially better for the ½-hour period.

Figure 6 illustrates the effect of treating vegetable-tanned crust leather with solution-polymers. It will be noted that polybutyl methacrylate is about five times as effective in decreasing resistance to water absorption as polyethyl acrylate for approximately the same resin contents. Compared to the curves in figure 4, it will be observed that the reductions in water absorption are much less, as are the amounts of resin in the treated specimens. The ½-hr absorption value for ethyl acrylate-neatsfoot oil (12 percent of resin and 22 percent of oil) in figure 4 is the highest of the treated specimens, and yet it is only about two-thirds the value of that obtained for 16 percent polyethyl acrylate solution-polymer. The more favorable results may be partially due to the neatsfoot oil or to a presumably higher degree of polymerization by the *in situ* process.

Figure 7 shows the effects of different solution-polymers and Thiokol LP–2 on vegetable-tanned crust leather and factory-finished sole leather. The ½-hr absorption values for vegetable-tanned crust leather treated with *n*-butyl methacrylate-ethyl acrylate solution-copolymer and Thiokol LP–2 are shown to be about the same. However,

as time increases to 24 hours, the specimens treated with Thiokol LP–2 absorbed only about half as much as those treated with the acrylate solution-copolymer. A substantial part of this difference in absorptions for longer periods may be due to the fact that there was 34 percent of Thiokol LP–2 in the leather but only 10 percent of the copolymer. From a service viewpoint, the ½-hr absorption values are probably more significant than the 24-hr values. Factory-finished sole leather treated with Thiokol LP–2 has the most favorable absorption curve.

Figure 8 shows the effect of different resin treatments on degreased chrome-retanned upper leather. The ½-hr absorption value for polyethyl acrylate is approximately two-thirds that of specimens treated with Thiokol LP–2. There was approximately 50 percent of resin in both sets of treated specimens, so that direct comparisons as to the effectiveness of the two treatments are valid.

3. Water-Vapor Permeability

Water-vapor permeability data on vegetable-tanned crust leather (table 7) show that 8.3 percent of polybutyl methacrylate and 15.6 percent of polyethyl acrylate both reduce the permeability from 567 to about 325 $(g/m^2)/24$ hr. Seven percent of polyethyl acrylate reduces permeability by an intermediate amount; i. e., 480 $(g/m^2)/24$ hr. The last three items of table 7 show degreased chrome retanned upper leather treated with polyethyl acrylate and Thiokol LP–2; both decrease water vapor permeability by about the same amount, i. e., to about 400 $(g/m^2)/24$ hr. This value is considered to be ample for shoe upper leather.

TABLE 7. *Physical tests on treated and untreated leathers*

Type of leather	Treatment	Mean resin content of four specimens	Mean water absorption of four specimens for—		Mean water vapor permeability of four specimens	Mean relative stiffness factor of four specimens
			½ hr	24 hr		
		Percent	*Percent*	*Percent*	*(g/m²)/24 hr*	*E*
Vegetable crust	Ethyl acrylate [a]	40.6	8.2	22.9	.....	.....
Do	Ethyl acrylate-Neatsfoot [a]	12.0	18.0	22.2	.....	.....
Do	Ethyl acrylate-Butyl methacrylate [a]	46.0	3.4	11.2	.....	.....
Do	Butyl methacrylate [a]	43.3	3.5	11.2	.....	.....
Do	None	0.0	71.7	72.8	.....	.....
Do	Ethyl acrylate solution-polymer	15.9	31.2	43.8	316	14.5
Do	do	6.8	62.5	74.3	480	20.1
Do	Butyl methacrylate solution-polymer	8.3	26.0	58.0	331	45.7
Do	None	0.0	67.1	76.6	567	18.1
Factory finished vegetable-tanned	do	.0	[b] 25.7	[b] 35.3	.....	.....
Do	Thiokol LP–2 solution	[b] 17.6	[b] 4.1	[b] 18.8	.....	.....
Vegetable crust	None	0.0	[b] 64.6	[b] 69.3	.....	[b] 7.5
Do	Thiokol LP–2 solution	[b] 34.1	[b] 6.6	[b] 26.4	.....	[b] 23.2
Do	Ethyl acrylate-Butyl methacrylate copolymer solution-polymer.	[b] 10.4	[b] 4.4	[b] 48.6	.....	.....
Degreased chrome retan upper	None	0.0	[b] 22.9	[b] 91.4	[b] 1,011	[b] 4.9
Do	Thiokol LP–2 solution	[b] 50.1	[b] 16.7	[b] 49.3	[b] 408	[b] 3.7
Do	Ethyl acrylate solution-polymer	[b] 49.5	[b] 9.5	[b] 42.1	[b] 394	[b] 3.3

[a] Polymerized *in situ*.
[b] Mean of two specimens.

4. Relative Stiffness

The relative stiffness factors of several leathers and treatments are shown in table 8. It will be noted that 16-percent polyethyl acrylate has practically no influence on stiffness of vegetable-tanned crust leather, whereas 8 percent of polybutyl methacrylate more than doubles the stiffness factor. Table 7 shows that treatment with Thiokol LP–2 triples the stiffness factor of vegetable-tanned crust leather. However, degreased chrome retan upper leather shows no appreciable change in stiffness when treated with soft acrylate or Thiokol LP–2 resins.

V. Summary

1. A laboratory procedure is described for polymerizing acrylate monomers *in situ*. By use of small polymerization chambers, as much as 50-percent resin can be obtained in vegetable-tanned crust leather.

2. Specially prepared solution polymers have been made to impregnate leather. Up to 25-percent resin has been obtained in vegetable-tanned crust, and 50 percent in chrome retanned upper leather by this procedure.

3. Treatment with Thiokol LP–2 can be controlled to give a very stiff sole or to produce a soft shoe upper leather.

4. Abrasion resistance of vegetable-tanned crust leather is improved about 75 percent by *n*-butyl methacrylate polymerized *in situ*. Treatment with Thiokol LP–2 improves abrasion resistance by about 30 percent, whereas solution-copolymers of *n*-butyl methacrylate and ethyl acrylate contributed no improvement.

5. Half-hour water absorption data on vegetable-tanned crust leather indicate that treatment with *n*-butyl methacrylate, polymerized *in situ*, shows 95-percent reduction over untreated leather. On the same basis, solution-copolymers of *n*-butyl methacrylate and ethyl acrylate as well as Thiokol LP–2 are all about equally effective. For degreased chrome-retan leather, polyethyl acrylate solution polymer reduces ½-hr water absorption about one-half, and Thiokol LP–2 reduces ½-hr water absorption about one-third.

6. Water vapor permeability of degreased chrome-retan upper leather is reduced by 60 percent. However, the reduced value of about 400 $g/m^2/24$ hr is considered ample for comfort.

7. Stiffness of vegetable-tanned crust leather treated with *n*-butyl methacrylate polymerized *in situ* is not appreciably different from untreated leather. Vegetable-tanned crust leather treated with Thiokol LP–2 has a stiffness factor somewhat more than double that of untreated leather. Degreased chrome-retan upper leather shows no appreciable change in flexibility when treated with soft acrylate or Thiokol LP–2 resin. However, a different cure for Thiokol LP–2 in treated chrome retan upper leather reduces the stiffness slightly, as does polyethyl acrylate solution-polymer.

VI. References

[1] J. C. Niedercorn and F. D. Thayer, J. Am. Leather Chem. Assoc. **40,** 242 (1945).
[2] E. Chadwick, J. Intern. Soc. Leather Trades Chem. **30,** 53 (1946).
[3] George Virtue, U. S. Patent 2,413,806 (1947).
[4] D. E. Strain, R. G. Kennelley, and H. R. Dittmar, Ind. Eng. Chem. **31,** 382 (1939).
[5] Carl E. Barnes, J. Am. Chem. Soc. **67,** 217 (1945).
[6] Claus Heuck, Modern Plastics **24,** 158 (1946).
[7] I. M. Kolthoff, J. Am. Chem. Soc. **69,** 441, 2143 (1947).
[8] D. E. Strain, Ind. Eng. Chem. **30,** 345 (1938).

WASHINGTON, July 30, 1948.

U. S. Department of Commerce
National Bureau of Standards

Research Paper RP1952
Volume 42, January 1949

Part of the Journal of Research of the National Bureau of Standards

Noise Spectrum of a Diode With a Retarding Field[1]

By Jacob J. Freeman

A general expression for the noise-power spectrum generated by the random emission of electrons of arbitrary trajectories within a waveguide is obtained. A numerical solution of the potential distribution within a plane diode is effected, and a family of curves from which the potential distribution may be obtained is graphed. A graphical comparison between several actual potential distributions and Von Laue's solution is given. The above results are utilized to derive the equivalent mean-square fluctuation current due to the space charge within a diode for two cases of potential distribution, namely, the linear distribution, and that distribution which occurs at the neighborhood of the beginning of the retarding field. For the case of the linear potential distribution, the equivalent noise temperature of the diode conductance is shown to be equal to the cathode temperature.

I. Introduction

A considerable increase at high frequencies in both the shot noise and conductance of a negatively biased diode over the theoretical values computed on the basis of zero transit angle has been reported in the recent literature by several investigators. C. N. Smyth [1][2] observed excessive damping and noise from a negatively biased diode at 3,300 Mc/s, and suggested it was due to currents induced by space charge. A. Van der Ziel [2] and A. Versnel [3] reported preliminary measurements on the equivalent noise current, and on the conductance of a negatively biased diode at wavelengths of 5.8 and 7.25 m, over a range of anode voltages.

In this paper the noise-power spectrum of a diode with a retarding field [3] will be investigated theoretically, taking into account only the noise power generated by those electrons with insufficient energy to reach the plate, in order to be able to evaluate the equivalent mean square current fluctuations due to space charge alone.[4] Because of the mathematical intractability of the potential distribution, the analysis is carried out only for the case of large saturation current, when the slope of the potential curve at the anode is small, and the case of small saturation current, when the potential distribution is essentially linear. For the latter case, the equivalent temperature of the conductance is shown to be equal to the cathode temperature.

Coincidentally, the noise power spectrum generated by electrons of prescribed trajectory within a waveguide of arbitrary cross section is developed, partly because the results can be immediately applied to the specific problem of a diode across a transmission line, and partly because the results are necessary for intended investigations of noise from transit-time devices within waveguides.

II. Noise Spectrum

In this section [5] will be derived an expression for the noise power generated by random emission within a waveguide, or a transmission line. The latter is to be regarded as a special case of the former, in which the particular mode propagated is the TEM mode, and the word "guide" will be used to designate both. Although in this paper only the particular case of a retarding-field diode

[1] A dissertation submitted to the faculty of the Graduate School of Arts and Sciences of the Catholic University of America in partial fulfillment of the requirements for the degree of Doctor of Philosophy.

[2] Figures in brackets indicate the literature references at the end of this paper.

[3] By a retarding field is meant one in which the slope of the potential curve is always negative.

[4] For brevity, the term "space charge" will henceforth be used to designate the aggregate of electrons that have insufficient energy to reach the plate.

[5] MKS units are employed throughout this paper.

connected to a transmission line will be considered in detail, the noise spectrum of a diode inserted within a cylindrical guide of arbitrary cross section will be treated, since the generalization involves little further complication, and it seems desirable to have an explicit treatment of the problem for purposes of future reference (e. g., computation of the noise power generated by electronic transit-time devices within waveguides). It is assumed that the cathode and anode surfaces of the diode coincide with parts of the guide surface, so that there are no discontinuities due to the electrode structure. In other words, electrons emitted from a given portion of the guide surface describe a trajectory that is prescribed for electrons with given initial velocity by a given direct-current potential and impinge on another portion of the guide surface. It is assumed that the given direct-current potential has no minimum, so that the results of this section will apply either to the case of a temperature-saturated diode, or one with a retarding field, in which the anode voltage is sufficiently below the cathode, so that the slope of the potential curve at the anode is negative. If no direct-current potential minimum exists, the perturbations of the trajectory of electrons with a given initial velocity due to small fluctuations in the space-charge potential will be small, and it is assumed that they can be neglected. If a potential minimum exists (fig. 1), there is a discontinuous change in trajectory for electrons having just enough initial energy to reach the potential minimum, so that a small fluctuation of potential may cause a large fluctuation of trajectory for this class of electrons.

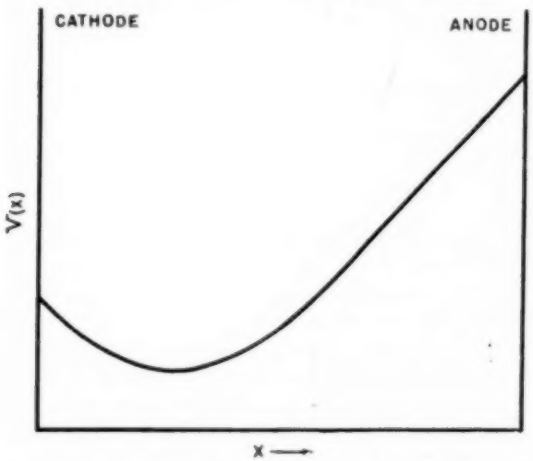

FIGURE 1. *Voltage distribution of diode with minimum.*

Accordingly, then, it may reasonably be assumed that each electron with a given initial velocity traverses a fixed trajectory independently of all other electrons; thus, one may regard the resulting electromagnetic pulses generated by each electron as random events.

The guide is considered to have its axis in the z-direction, and to be terminated at either end by a matched load, with the diode in the center. The immediate problem is to compute the average noise energy absorbed by each load, due to electrons having an arbitrary trajectory. Only the case where the range in frequency is such that the guide supports only the dominant mode will be considered.

Then if $\boldsymbol{E}=\boldsymbol{E}_0 \exp(j\omega t)$ represents the electric field of the dominant mode generated by a current density $\boldsymbol{J}=\boldsymbol{J}_0 \exp(j\omega t)$, it is shown in appendix 1 that

$$\boldsymbol{E}_0=-\frac{\mu\omega}{2\alpha}\boldsymbol{b}(\boldsymbol{r})\int \boldsymbol{J}(\boldsymbol{r}')\cdot\boldsymbol{b}(\boldsymbol{r}')\exp(-j\alpha|z'-z|)d\tau'. \tag{1}$$

Here μ is the magnetic permeability, and $d\tau'$ is an element of volume occupied by the current density. $\omega=2\pi f$ is the angular frequency, α the phase constant for the dominant mode, and $\boldsymbol{b}$ is the corresponding normal mode [4]. Some properties of $\boldsymbol{b}$ are briefly discussed in appendix 1. $\boldsymbol{r}(x,y,z)$ and $\boldsymbol{r}'(x',y',z')$ are the coordinate vectors of the field and source points, respectively. If the current density $\boldsymbol{J}(\boldsymbol{r}')$ has negligible cross section, $\boldsymbol{J}(\boldsymbol{r}')d\tau'=I(\boldsymbol{r}')d\boldsymbol{s}'$, where $I(\boldsymbol{r}')$ is the current flowing at (x',y',z'), and $d\boldsymbol{s}'$ is the incremental displacement along the path of current flow, s', corresponding to $d\tau'$. Equation 1 then becomes

$$\boldsymbol{E}_0(\boldsymbol{r})=-\frac{\mu\omega}{2\alpha}\boldsymbol{b}(\boldsymbol{r})\int I(\boldsymbol{r}')d\boldsymbol{s}'\cdot\boldsymbol{b}(\boldsymbol{r}')\exp[j\alpha(z'-z)],z>z'. \tag{2}$$

When the current $I(x',y',z')$ consists of an electron of charge e following the trajectory s',

$$I=e\delta(t-t')=\frac{e}{2\pi}\int_{-\infty}^{\infty}\exp[j\omega(t-t')]d\omega, \tag{3}$$

where t' represents the time at which the electron is at $(x',\ y',\ z')$, and $\delta(t-t')=0$, for $t\neq t'$, and $\int\delta(t-t')dt=1$. Accordingly, the field generated by an electron is

$$\boldsymbol{E}(t)=-\frac{\mu\epsilon\boldsymbol{b}}{2}\int_{-\infty}^{\infty}\frac{d\omega}{2\pi}\exp\left[j(\omega t-\alpha z)\right]\frac{\omega}{\alpha}$$
$$\int_0^{t_0}\boldsymbol{v}(t')\cdot\boldsymbol{b}\exp\left[j(\alpha z'-\omega t')\right]dt', \qquad (4)$$

where the variable of integration is changed from s' to t', $\boldsymbol{v}(t')=d\boldsymbol{s}'/dt'$, and t_0 is the transit time of the electron.

Let

$$s(\omega)=\int_0^{t_0}\boldsymbol{v}(t')\cdot\boldsymbol{b}\exp\left[j(\alpha z'-\omega t')\right]dt'. \qquad (5)$$

Then,

$$\boldsymbol{E}(t)=-\frac{\mu\epsilon\boldsymbol{b}}{4\pi}\int_{-\infty}^{\infty}\frac{\omega}{\alpha}\exp\left[j(\omega t-\alpha z)\right]s(\omega)d\omega. \qquad (6)$$

Since $\boldsymbol{H}=j/\mu\omega$ curl $\boldsymbol{E}$, one finds similarly that

$$\boldsymbol{H}=-\frac{je}{4\pi}\int_{-\infty}^{\infty}\exp\left[j(\omega t-\alpha z)\right]s(\omega)d\omega$$
$$\left[\frac{-j\alpha\boldsymbol{k}\times\boldsymbol{b}+\text{curl }\boldsymbol{b}}{\alpha}\right]. \qquad (7)$$

Since it is desired that $\boldsymbol{E}(t)$ be real, α is defined as an odd function of ω, so that the imaginary parts of the integrals in eq. 6 and 7 vanish, since they are odd functions of ω.

The instantaneous power flow due to the passage of a single electron, is, by Poynting's Theorem,

$$P(t)=\int_{S'}\boldsymbol{E}\times\boldsymbol{H}\cdot\boldsymbol{n}\,da, \qquad (8)$$

where $\boldsymbol{n}$ is a unit normal to the surface S'.

If one utilizes the orthogonality properties of the normal modes, as stated in eq. 94 and 95 in appendix 1, namely,

$$\int_{S'}\boldsymbol{b}_j\cdot\boldsymbol{b}_k da=\delta_{jk},$$

and

$$\int_{S'}\left[\boldsymbol{b}_j\times(\nabla x\boldsymbol{b}_k\right]\cdot k da=0,$$

it is found on substituting eq 6 and 7 in eq 8, that

$$P(t)=\frac{\mu e^2}{16\pi^2}\int_{-\infty}^{\infty}\frac{\omega}{\alpha}\exp\left(j(\omega t-\alpha z)\right)s(\omega)d\omega$$
$$\int_{-\infty}^{\infty}\exp\left[j(\omega t-\alpha z)\right]s(\omega)d\omega. \qquad (9)$$

Since the pulses of energy are random, or statistically independent, the average power flow, by Campbell's Theorem [5], is

$$\overline{P}=\overline{P(t)}=\lambda\int_{-\infty}^{\infty}P(t)dt,$$

where λ is the average number of electrons emitted per second, and $\lambda e=I$, the direct current.

$$\overline{P}=\frac{\lambda e^2\mu}{16\pi_2}\int_{-\infty}^{\infty}\int_{-\infty}^{\infty}\frac{\omega}{\alpha}\exp\left[j(\omega t-\alpha z)\right]s(\omega)d\omega$$
$$\int_{-\infty}^{\infty}s(\omega)\exp\left[j(\omega t-\alpha z)\right]d\omega dt. \qquad (10)$$

By Parseval's Theorem [6],

$$\int_{-\infty}^{\infty}f_1(t)f_2(\mp t)dt=\int_{-\infty}^{\infty}F_2(f)F_1(\pm f)df, \qquad (11)$$

where f_1 and f_2 are the Fourier transforms of F_1 and F_2.

Substituting eq 11 in eq 10,

$$\overline{P}=\frac{\lambda e^2\mu}{8\pi}\int_{-\infty}^{\infty}\frac{\omega}{\alpha}s(\omega)s(-\omega)d\omega.$$

Or, since $s(-\omega)=s^*(\omega)$ where s^* is the complex conjugate of s, and since s^*s is even in ω,

$$\overline{P}=\frac{eI\mu}{4\pi}\int_0^{\infty}\frac{\omega}{\alpha}|s(\omega)|^2d\omega. \qquad (12)$$

If one defines $\omega\mu/\alpha=Z$, the wave impedance, then

$$\overline{P}=\frac{eI}{4\pi}\int_0^{\infty}Z(\omega)|s(\omega)|^2d\omega. \qquad (13)$$

We consider now a plane parallel transmission line, with planes a distance a apart, and of width d (fig. 2). For this case, $\boldsymbol{b}=\boldsymbol{i}/\sqrt{ad}$, and $\alpha=\omega\sqrt{\mu\epsilon}$, where $\boldsymbol{i}$ is a unit vector in the x-direction, and ϵ is the specific inductive capacity of free space. Hence,

$$\overline{P}=\frac{eI}{4\pi}\sqrt{\frac{\mu}{\epsilon}}\int_0^{\infty}|s(\omega)|^2d\omega, \qquad (14)$$

where

$$s(\omega)=\int_0^{t_0}\frac{\boldsymbol{v}(t')\cdot\boldsymbol{i}\exp j(\omega\sqrt{\mu\epsilon}\,z'-\omega t')}{\sqrt{ad}}dt' \qquad (15)$$

If the trajectory is considered to be in the x,y, plane, and the linear dimensions of the cathode small compared to the wavelength corresponding to any frequency in the range considered, then one may take $z'=0$ and let the origin of coordinates be at the cathode. Equation 15 becomes

$$s(\omega)=\int_0^{t_0}\frac{\boldsymbol{v}(t')\cdot\boldsymbol{i}\exp\ (-j\omega t')dt'}{\sqrt{ad}}. \qquad (16)$$

In order to compute the power spectrum from a diode with a retarding field the trajectories must be computed, and this requires that the potential distribution for the case of a retarding field be determined. This is indicated in the next section.

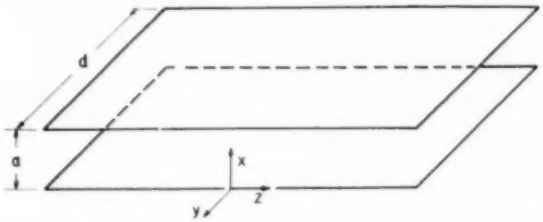

FIGURE 2. *Schematic of parallel-plane transmission line.*

III. Potential Within a Plane Parallel Diode Subject to a Retarding Field

1. Rigorous Solution

The potential distribution within a conducting diode has been thoroughly investigated by Fry [7] and Langmuir [8], among others. However, Fry limited his investigations to the case where the potential has a minimum. Von Laue [9] has exhaustively treated the potential distribution of a diode for the case of a retarding field, where it is assumed that the plate current, I_p, makes a negligible contribution to the potential in comparison to the contribution made by those electrons that never reach the anode. In other words, Von Laue assumes that the electron gas between the two electrodes is in statistical equilibrium, and that the space-charge distribution is governed by the familiar relation,

$$\rho=\rho_0\exp\left(-\frac{eV}{kT}\right),$$

where ρ is the space charge per unit volume. Since the rigorous potential distribution for the case of a retarding field has never been investigated, it was believed desirable that this be done, in order to check the accuracy and range of Von Laue's solution.

The separation, a, between cathode and anode (fig. 3) is considered to be sufficiently small with respect to the area of the electrodes so that edge effects may be neglected, and the potential distribution is governed by

$$\frac{d^2V}{dx^2}=-\frac{\rho}{\epsilon}, \qquad (17)$$

where V is the potential, ρ the charge density, and

$$\epsilon=1/36\pi.10^{-9}\text{ farad per meter.}$$

The anode is assumed to be at a voltage V_1 sufficiently negative with respect to the cathode

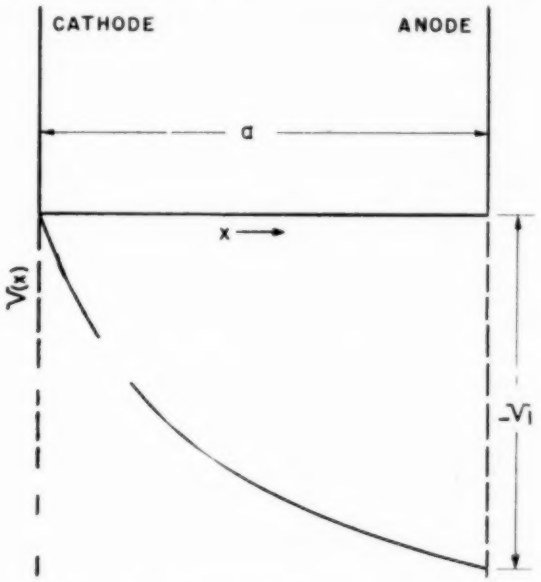

FIGURE 3. *Voltage distribution of diode with retarding field.*

so that the slope of the potential $V(x)$ is always negative.

The following analysis follows Fry's analysis of the α-space precisely, and is outlined here for completeness. The only difference, of course, is that here the constant of integration is not zero, as it is when one has a potential minimum. If v_0 represents the initial velocity of an electron, and v is its velocity at position x,

$$\frac{1}{2}Mv^2+eV=\frac{1}{2}Mv_0^2, \qquad (18)$$

where $e=-1.60\ 10^{-19}$ coulomb, is the charge of the electron, and $M=9.10^{-31}$, is the mass of the electron in kilograms.

At a given position x, those electrons having initial velocities such that $1/2Mv_0^2<eV$ never reach x; those having initial velocities such that $eV<1/2Mv_0^2<eV_1$ pass by x twice, going and

returning. Those having initial velocitis such that $1/2Mv_0^2 > eV_1$ are captured by the plate and pass the point only once. Accordingly, the charge density is given by

$$\rho(x) = e\int_{\sqrt{rV_1}}^{\infty} \frac{n(v_0)}{v} dv_0 + 2e\int_{\sqrt{rV(x)}}^{\sqrt{rV_1}} \frac{n(v_0)}{v} dv_0, \quad (19)$$

where $n(v_0)$ is the number of electrons emitted per second per square meter with initial velocities between v_0 and v_0+dv_0, and $r=2e/M$. Substituting eq 19 and 18 in eq 17,

$$\frac{d^2V}{dx^2} = -\frac{e}{\epsilon}\left[\int_{\sqrt{rV_1}}^{\infty} \frac{n(v_0)dv_0}{\sqrt{v_0^2-rV}} + 2\int_{\sqrt{rV}}^{\sqrt{rV_1}} \frac{n(v_0)dv_0}{\sqrt{v_0^2-rV}}\right]. \quad (20)$$

Integrating eq 20 between the limits x and a, we get

$$\left(\frac{dV}{dx}\right)_a^2 - \left(\frac{dV}{dx}\right)^2 = \frac{2M}{\epsilon}\left[\int_{\sqrt{rV_1}}^{\infty} n(v_0)\sqrt{v_0^2-rV_1}\, dv_0 - \int_{\sqrt{rV_1}}^{\infty} n(v_0)\sqrt{v_0^2-rV}\, dv_0 - 2\int_{\sqrt{rV}}^{\sqrt{rV_1}} n(v_0)\sqrt{v_0^2-rV}\, dv_0\right]. \quad (21)$$

Since the initial velocities are distributed according to the Maxwell-Boltzmann distribution,

$$n(v_0) = \frac{NM}{kT} v_0 \exp\left(-\frac{Mv_0^2}{2kT}\right), \quad (22)$$

in which N is the total number of electrons emitted per square meter per second, k is Boltzmann's constant, $k=1.38\ 10^{-23}$, and T is the absolute temperature.

$$I_0 = Ne, \quad (23)$$

where I_0 is the saturation current density. If one changes to reduced variables,

$$\xi = \sqrt{\zeta}(x-a), \quad (24)$$

and

$$\eta = \frac{e(V_1-V)}{kT}, \quad (25)$$

where

$$\alpha = \frac{\sqrt{2\pi M}}{\epsilon}\frac{eI_p}{(kT)^{3/2}}, \quad (25a)$$

and I_p is the plate current, then eq 21 reduces, when $n(v_0)$ is replaced by its value, (eq 22), to the following:

$$\left(\frac{d\eta}{d\xi}\right)^2 = \left(\frac{d\eta}{d\xi}\right)_0^2 + e^{\eta}(1+\operatorname{erf}\sqrt{\eta}) - \left(1+2\frac{\sqrt{\eta}}{\sqrt{\pi}}\right). \quad (26)$$

Here erf η is the error function,

$$\operatorname{erf} x = \frac{2}{\sqrt{\pi}}\int_0^x \exp(-t^2)dt, \quad (27)$$

and $(d\eta/d\xi)_0^2$ is the value of $(d\eta/d\xi)^2$ at $\xi=0$, that is, at the anode, $x=a$.

For brevity, let

$$f(\eta) = (1+\operatorname{erf}\sqrt{\eta})e^{\eta} - \left(1+\frac{2}{\sqrt{\pi}}\sqrt{\eta}\right), \quad (28)$$

and

$$\left(\frac{d\eta}{d\xi}\right)_0 = -m. \quad (29)$$

Accordingly, eq 26 may be written as

$$\left(\frac{d\eta}{d\xi}\right)^2 = m^2 + f(\eta). \quad (30)$$

Since ξ is always negative,

$$\xi = -\int_0^{\eta} \frac{d\eta}{\sqrt{f(\eta)+m^2}}. \quad (31)$$

The value of m is determined by the boundary condition at the cathode.

At the cathode, $x=0, \xi=-a\sqrt{\zeta}=\xi_1, \eta=eV_1/kT=\eta_1$, so that

$$\xi_1 = -\int_0^{\eta_1} \frac{d\eta}{\sqrt{f(\eta)+m^2}}. \quad (32)$$

fixes the value of m^2.

Since for large values of η, $f(\eta)\to 2e^{\eta}$, the upper limit of the integral in eq 32 may be replaced by infinity, so that one has, approximately,

$$\xi = -\int_0^{\infty} \frac{d\eta}{(f(\eta)+m^2)^{\frac{1}{2}}}.$$

Since ξ_1 is proportional to $I_p^{\frac{1}{2}}$, it may be inferred from the above equation that a large value of m^2 implies a small value of plate current, and that a small value of m^2 implies a relatively large value of plate current.

North's paper [10] tabulates $f(\eta)$ (his $\phi_a(\eta)$), and tabulates the solution of eq 14, for the case $m^2=0$, (his ξ_a). Using the computed values of

$f(\eta)$ from North's paper, ξ was determined as a function of η by numerical integration, for selected values of m^2, and the results are tabulated in table 1 for $0 \leq \eta \leq 20$, and are graphed in figure 4 for $0 \leq \eta \leq 10$. To determine ξ for $\eta > 9$, one observes that for the tabulated values of m^2, $f(\eta) + m^2 \simeq 2e^{\eta}$, for $\eta > 9$. Accordingly for $\eta > 9$, eq 14 yields

$$\xi(\eta) = \xi(9) + \sqrt{2}(e^{-4.5} - e^{-\eta/2}), \tag{33}$$

from which $\xi(\eta)$ may be calculated for larger values of η than are tabulated in table 1.

To determine the potential distribution of a given tube, one first determines ξ_1 and η_1 from the given values of cathode temperature, plate current, or saturation current, plate voltage, and plate-cathode separation, a. Then, from the family of ξ, η curves plotted in figure 4, one determines the particular curve of the family that passes through the point ξ_1, η_1. From this curve $\eta(\xi), (\eta < \eta_1, \xi < \xi_1)$, the potential $V(x)$ within the diode may be determined from

$$\frac{V(x)}{V_1} = \frac{\eta_1 - \eta}{\eta_1}, \tag{34}$$

$$\frac{x}{a} = \frac{\xi_1 - \xi}{\xi_1}, \tag{35}$$

according to the definitions of ξ and η (eq 24 and 25).

2. Approximate Analytic Expressions for the Potential

In order to obtain an analytic approximation for the potential, one must examine approximations to $f(\eta)$ that will make the equation

TABLE 1. *Values of* $\xi = -\int_0^{\eta} \frac{dx}{\sqrt{f(x) + m^2}}$ *as a function of* η, *for selected values of* m^2

η	$m^2=0-\xi$	$m^2=0.05-\xi$	$m=0.1-\xi$	$m^2=0.2-\xi$	$m^2=0.3-\xi$	$m^2=0.5-\xi$	$m^2=1-\xi$	$m^2=3-\xi$	$m^2=10-\xi$	$m^2=20-\xi$
0	0	0	0	0	0	0	0	0	0	0
0.01	.....	0.0426	0.0309	0.0221	0.0181	0.0141	.....	.....	.....	.....
.02	.....	.0814	.0601	.0437	.0359	.0280	0.0199	0.0115	.....	.....
.03	.....	.1171	.0880	.0652	.0533	.0418	.....	.....	.....	.....
.04	.....	.1503	.1147	.0858	.0704	.0554	.0396	.0230	.....	.....
.05	0.4281	.1814	.1402	.1057	.0873	.0688	.....	.....	.....	.....
.06	.....	.2108	.1648	.1252	.1038	.0821	.0590	.0344	.....	.....
.07	.....	.2386	.1884	.1443	.1200	.0952	.....	.....	.....	.....
.08	.....	.2650	.2111	.1628	.1360	.1082	.0782	.0458	.....	.....
.09	.....	.2902	.2337	.1808	.1516	.1210	.....	.....	.....	.....
.10	.5941	.3141	.2542	.1984	16.70	.1337	.0971	.0572	.....	.....
.20	.8170	.5171	.434	.3565	.3080	.2528	.1881	.1130	.....	.....
.30	.9785	.6677	.578	.4887	.4285	.3580	.2730	.1673	.....	.....
.40	1.1081	.7918	.697	.6006	.5339	.4545	.3521	.2200	.....	.....
.50	1.2173	.9077	.801	.6985	.6277	.5409	.4258	.2710	0.1545	0.1105
.60	1.3120	.9993	.891	.7866	.7116	.6195	.4945	.3203	.....	.....
.70	1.3956	1.072	.972	.8638	.7876	.6914	.5586	.3678	.....	.....
.80	1.4704	1.146	1.045	.9348	.8568	.7574	.6184	.4133	.....	.....
.90	1.5380	1.213	1.111	.9994	.9201	.8184	.6744	.4574	.....	.....
1.0	1.5996	1.273	1.171	1.059	.9786	.8756	.7269	.4995	.2997	.2174
2.0	2.0134	1.714	1.610	1.488	1.402	1.302	1.120	.8355	.5461	.4106
3.0	2.2338	1.933	1.829	1.701	1.615	1.530	1.331	1.040	.7259	.5654
4.0	2.3615	2.059	1.954	1.837	1.741	1.647	1.456	1.164	.8454	.6762
5.0	2.4376	2.134	2.029	1.903	1.817	1.722	1.531	1.239	.9206	.7490
6.0	2.4834	2.179	2.075	1.947	1.864	1.769	1.577	1.282	.9669	.7946
7.0	2.5112	2.206	2.103	1.976	1.891	1.795	1.605	1.312	.9951	.8227
8	2.5280	2.224	2.119	1.992	1.907	1.812	1.621	1.329	1.0122	.8398
9	2.5382	2.234	2.129	2.002	1.918	1.822	1.631	1.339	1.0227	.8502
10	2.5444	2.2402	2.1352	2.0082	1.9242	1.8282	1.6372	1.3452	1.0289	.8564
12	2.5504	2.2462	2.1412	2.0142	1.9302	1.8342	1.6432	1.3512	1.0349	.8624
14	2.5526	2.2484	2.1434	2.0164	1.9324	1.8364	1.6454	1.3534	1.0371	.8646
16	2.5534	2.2492	2.1361	2.0172	1.9332	1.8372	1.6462	1.3542	1.0379	.8654
18	2.5537	2.2495	2.1445	2.0175	1.9335	1.8375	1.6465	1.3545	1.0382	.8657
20	2.5538	2.2496	2.1446	2.0176	1.9336	1.8376	1.6466	1.3546	1.0383	.8658

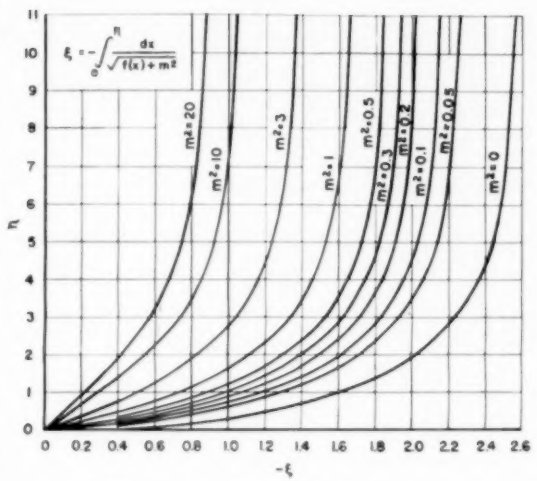

FIGURE 4. *Family of ξ, η curves.*

$$-\xi=\int_0^\eta \frac{dx}{\sqrt{f(x)+m^2}},$$

integrable in terms of tabulated functions. For η large, $f(\eta)\simeq 2e^\eta$, and as $\eta\to 0$, $f(\eta)\to\eta$.

For $T=1{,}000°\ K$, $\frac{e}{kT}=11.7$, and $\eta=11.7(V_1-V)$.

For negative plate voltages of one volt or more, η will be larger than, say 2, over most of the voltage range, so that the approximation $f(\eta)\simeq 2(e^\eta-1)$ will be fairly good over most of the range of η. This is illustrated in table 2, where $f(\eta)$ and $2(e^\eta-1)$ are tabulated for $0<\eta<9$. For large values of η the approximation is quite good, but becomes poor for $0<\eta<2$. On the other hand, the error in ξ due to the approximation is reduced by the addition of m^2, especially for larger values of m^2. Accordingly, let

$$-\xi=\int_0^\eta \frac{dx}{\sqrt{2e^x+m^2-2}}=\frac{1}{\sqrt{2}}\int_0^\eta \frac{dx}{\sqrt{e^x+A^2}}, \quad (36)$$

where

$$A^2=\frac{m^2}{2}-1. \quad (37)$$

Equation 36 is a solution of

$$\frac{d_2\eta}{d\xi^2}=e^\eta, \quad (38)$$

which is Von Laue's expression [9], inferred from the assumption that equilibrium exists. It is equivalent to

$$\frac{d^2V}{dx^2}=-\frac{I_0\sqrt{\frac{2\pi M}{kT}}}{\epsilon}\,e^{-\frac{eV}{kT}}, \quad (39)$$

which in turn implies that the space charge distribution is

$$\rho=\rho_0 e^{-\frac{eV}{kT}}, \quad (40)$$

where

$$\rho_0=I_0\sqrt{\frac{2\pi M}{kT}}. \quad (41)$$

If one integrates the rigorous expression for ρ in eq 19, one gets

$$\rho=I_0\sqrt{\frac{2\pi M}{kT}}\,e^{-\frac{eV}{kT}}\frac{\left(1+\operatorname{erf}\sqrt{\frac{e(V_1-V)}{kT}}\right)}{2}. \quad (42)$$

Since

$$\operatorname{erf}\sqrt{\frac{e}{kT}(V_1-V)}=\operatorname{erf}\sqrt{\eta}\approx 1,$$

for $\eta>2$, it is seen that the approximate expression for ρ approaches the rigorous expression fairly closely for $\eta>2$, and accordingly, the approximate expression for the potential must also approach the true potential in this region.

For $-1\leq A^2<0$, $(0\leq m^2<2)$, the integral of eq 36 is given by

TABLE 2. *A comparison of $f(\eta)$ and $2(e^\eta-1)$*

η	$f(\eta)$	$2(e^\eta-1)$
0	0	0
0.2	0.294	0.44
.4	.716	.98
.6	1.27	1.64
.8	1.98	2.46
1	2.88	3.44
2	11.8	12.78
3	36.9	38.18
4	106.6	107
5	293	295
6	803	804
7	2,190	2,191
8	5,960	5,960
9	16,200	16,204

$$-\xi=\frac{\sqrt{2}}{\sqrt{1-\frac{m^2}{2}}}\left[\cos^{-1}\left(\sqrt{1-\frac{m^2}{2}}\,e^{-\eta/2}\right)-\cos^{-1}\sqrt{1-\frac{m^2}{2}}\right]. \quad (43)$$

For $A^2=0$, $(m^2=2)$,

$$\xi-\xi_1=\sqrt{2}(e^{-\eta/2}-e^{-\eta_1/2}). \quad (44)$$

For $A^2>0$, $(m^2>2)$,

$$-\xi=\frac{\sqrt{2}}{\sqrt{\frac{m^2}{2}-1}}\left[\sinh^{-1}\sqrt{\frac{m^2}{2}-1}-\sinh^{-1}\left(e^{-\eta/2}\sqrt{\frac{m^2}{2}-1}\right)\right]. \quad (45)$$

The value of m^2 in the above equations is fixed by the boundary conditions at the cathode, namely, $\eta=\eta_1$ when $\xi=\xi_1$. For large values of m, eq 45 gives

$$m=-\frac{\eta_1}{\xi_1}, \quad (46)$$

and the resulting potential distribution is, of course, the same linear function of distance one gets in the absence of space charge.

In order to compare eq 43, 44, and 45, which are Von Laue's solutions, with the rigorous solutions of eq 32 obtained numerically, values of the two solutions are tabulated in table 3, for $\eta_1=10$, and for $m^2=0$, and $m^2=3$. For $m^2=3$, the agreement between the two solutions is excellent, and even for $m^2=0$, the worst possible case for a given value of η_1, the agreement is fair.

Unfortunately, the expressions for the potential obtained from eq 43 and 45 do not permit the time of transit of an electron as a function of its position to be calculated explicitly, which is necessary for an evaluation of the noise power spectrum.

However, the potential distribution given by eq 44 approximates fairly well the shape of the potential curve for small m^2, that is, $0<m^2<20$ (large I_0). In figure 5 graphs are plotted of the true reduced potential distribution, $V/V_1=(\eta_1-\eta)/\eta_1$ as a function of the reduced distance $x/a=(\xi_1-\xi)/\xi_1$, for $m^2=0$, $m^2=10$, and $m^2=20$, for $\eta_1=10$. Also, the relative potential distribution obtained from eq 44 is plotted and is seen to fall about midway between the curves $m^2=0$ and $m^2=20$. Accordingly, for the case of large plate currents, one may use eq 44 for obtaining an approximate potential distribution and thence calculating the noise spectrum.

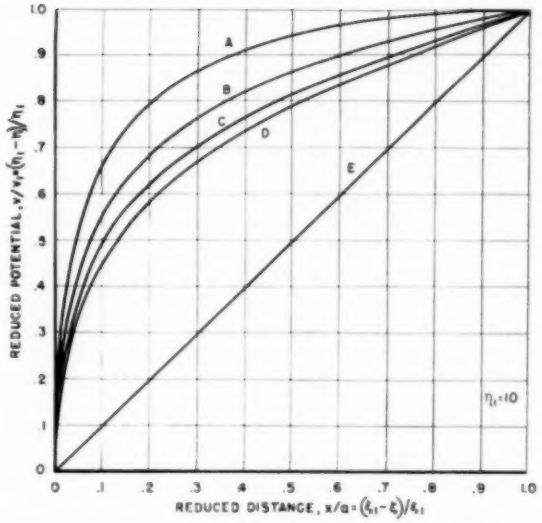

FIGURE 5. *Comparison between approximate and rigorous potential distributions.*

A, $m^2=0$; B, approximate formula; C, $m^2=10$; D, $m^2=20$; E, $m=-\eta_1/\xi_1$.

TABLE 3. *A comparison of the reduced potential, $V/V_1=1-\eta/\eta_1$, as a function of the reduced distance, $x/a=1-\xi/\xi_1$, obtained from the rigorous solution (eq 14), and from Von Laue's approximation (eq 43, 45)*

$m^2=0$			$m^2=3$	
	Rigorous	Approximate	Rigorous	Approximate
$1-v/v_1$	$1-i/i_1$	$1-i/i_1$	$1-i/i_1$	$1-i/i_1$
0	0	0	0	0
0.1	0.0025	0.0015	0.0045	0.0048
.2	.0064	.0061	.0120	.0125
.3	.0130	.0138	.0247	.0254
.4	.0240	.0264	.0470	.0466
.5	.0420	.0470	.0789	.0814
.6	0719	.0814	.135	.139
.7	.1221	.1385	.227	.233
.8	.209	.234	.379	.386
.9	.371	.412	.629	.630
.95	.522	.566	.799	.798
.98	.679	.719	.916	.915
1.0	1.000	1.000	1.000	1.000

For the case of small plate currents, and large negative anode voltages, the reduced potential distribution approaches a straight line of unit

slope, also graphed in figure 5 under the label $m=-\eta_1/\xi_1$. Accordingly, the following section proceeds with the calculation of the noise-power spectrum for the two cases, large plate current (m^2 small) and small plate current (m^2 large).

IV. Noise Power Spectrum for a Diode

1. Case 1: Noise Power Spectrum for Large Plate Current (m^2 small)

If one substitutes the values of ξ and η from eq 34 and 35 into eq 44, one gets for the potential energy of an electron, U,

$$U=Ve=2kT\ln(1+bx), \tag{47}$$

where

$$b=\frac{e^{\frac{eV_1}{2kT}}-1}{a}\simeq\frac{e^{\frac{eV_1}{2kT}}}{a}. \tag{48}$$

In this paper only the contribution to the noise spectrum made by those electrons that never reach the plate, but which return to the cathode will be considered, since the effect of those electrons which constitute the plate current has been treated by Rack [11]. Accordingly, one considers only electrons whose initial kinetic energy, E, is less than eV_1.

For an electron emitted at $t=0$, the time at which it has position x is given by

$$t=\int_0^x\frac{dx}{\sqrt{2/M}\sqrt{E-U(x)}}. \tag{49}$$

If one substitutes for $U(x)$ its value given by eq 47 and integrates

$$t=\sqrt{\frac{\pi M}{kT}}\frac{\exp(E/2kT}{2b}\left[\operatorname{erf}\sqrt{\frac{E}{2kT}}-\operatorname{erf}\sqrt{\frac{E}{2kT}}-\ln(1+bx)\right], \tag{50}$$

for $0\leq t\leq t_0/2$, where t_0 is the transit time of the electron.

$$t_0=\sqrt{\frac{\pi M}{kT}}\frac{\exp\left(\frac{E}{kT}\right)}{b}\operatorname{erf}\sqrt{\frac{E}{2kT}}, \tag{51}$$

so that

$$t=\frac{t_0}{2}\left[1-\frac{\operatorname{erf}\sqrt{\frac{E}{2kT}}-\ln(1+bx)}{\operatorname{erf}\sqrt{\frac{E}{2kT}}}\right], \tag{52}$$

for $0\leq t\leq t_0/2$.

According to eq 14 and 16, the noise power, P_E, absorbed by each load in the frequency range Δf, due to electrons with initial energy E, is

$$P_E=\frac{eI_E}{2}\sqrt{\frac{\mu}{e}}|s(\omega)|^2\frac{\Delta\omega}{2\pi}, \tag{53}$$

where

$$s(\omega)=\int_0^{t_0}v\cdot t\exp(-j\omega t)dt\Big/\sqrt{ad}, \tag{54}$$

and where I_E is that portion of the saturation current composed of electrons of energy E.

Since $t(x)$ and $t'(x)$, the first and second times at which the electron passes the point x, respectively, are related by

$$t'=t_0-t,$$

and since

$$v(t_0-t)=-v(t), \tag{55}$$

$$s(\omega)=\frac{1}{\sqrt{ad}}\left\{\int_0^{t_0/2}v(t)\exp(-j\omega t)dt-\int_0^{t_0/2}v(t)\exp[j\omega(t-t_0)]dt\right\}. \tag{56}$$

Letting

$$s_1(\omega)=\int_0^{t_0/2}v(t)\exp(-j\omega t)dt=\int_0^{x_m}\exp(-j\omega t)dx \tag{57}$$

where x_m is the maximum value of x,

$$s(\omega)=\frac{1}{\sqrt{ad}}[s_1(\omega)-\exp(-j\omega t_0)s_1(-\omega)]. \tag{58}$$

Substituting eq 52 in eq 57 and 58,

$$s(\omega)=\frac{2i\exp\left(\frac{-j\omega t_0}{2}\right)}{\sqrt{ad}}\int_0^{x_m}\sin\left\{\frac{\omega t_0\operatorname{erf}\sqrt{\frac{E}{2kT}}-\ln(1+bx)}{2\operatorname{erf}\sqrt{\frac{E}{2kT}}}\right\}dx. \tag{59}$$

To simplify the above somewhat, the substitution

$$y=\sqrt{\frac{E}{2kT}-\ln(1+bx)}, \tag{60}$$

is made, and one obtains

$$s(\omega)=\frac{4i\exp\left(\frac{E}{2kT}-\frac{j\omega t_0}{2}\right)}{b\sqrt{ad}}\int_0^{\sqrt{\frac{E}{2kT}}} ye^{-y^2}\sin\left\{\frac{\omega t_0\ \mathrm{erf}\ y}{2\ \mathrm{erf}\sqrt{\frac{E}{2kT}}}\right\}dy. \tag{61}$$

Let

$$A\left(\sqrt{\frac{E}{2kT}}\right)=\int_0^{\sqrt{\frac{E}{2kT}}} ye^{-y^2}\sin\left\{\frac{\omega t_0\ \mathrm{erf}\ y}{2\ \mathrm{erf}\sqrt{\frac{E}{2kT}}}\right\}dy. \tag{62}$$

Then

$$|s(\omega)|^2=\frac{16a}{d}\exp\left(\frac{E-eV_1}{kT}\right)A^2\left(\sqrt{\frac{E}{2kT}}\right), \tag{63}$$

where the value for b given by eq 48 has been substituted.

Since the energy distribution of the electrons is Maxwellian,

$$I_E=\frac{I_0}{kT}\exp(-E/kT)dE, \tag{64}$$

and since the resultant noise power due to uncorrelated noise sources is simply the sum of the powers of the individual sources [5], the resultant noise power spectrum due to all the electrons that return to the cathode is

$$P=\frac{8eI_P}{kT}\frac{a}{d}\sqrt{\frac{\mu}{\epsilon}}\int_0^{V_1} A^2\left(\sqrt{\frac{E}{2kT}}\right)dE\Delta f, \tag{65}$$

where P represents the noise power absorbed by each matched load in the interval $\Delta f=\Delta\omega/2\pi$.

The diode shunted by two matched transmission lines is now replaced by its equivalent circuit, namely, a diode shunted by impedance $Z_0/2$. The equivalent mean square fluctuation current, $\bar{i}^2$ is defined by

$$2P=Z_0/2\bar{i}^2, \tag{66}$$

where $Z_0=\sqrt{\mu/\epsilon}\,a/d$ is the characteristic impedance of the line. If the impedance of the diode is large compared to Z_0, which is assumed to be true, $\bar{i}^2$ represents the equivalent mean square fluctuation current that would flow through a diode short-circuited at frequency f.

From eq 65 and 66,

$$\bar{i}^2=\frac{32eI_P}{kT}F(V_1,f)\Delta f, \tag{67}$$

where

$$F(V_1,f)=\int_0^{eV_1} A^2(\sqrt{E/2kT})dE, \tag{68}$$

Since

$$\frac{\omega t_0}{2\ \mathrm{erf}\sqrt{E/2kT}}=a\omega\sqrt{\pi}M/4kT\exp\left(\frac{E-eV_1}{2kT}\right)$$

from eq 48 and 51, letting

$$c=a\omega\sqrt{\pi}M/4kT, \tag{69}$$

$$A(\sqrt{E/2kT})=\int_0^{\sqrt{E/2kT}} ue^{-u^2}\sin\left\{c\exp\left(\frac{E-eV_1}{2kT}\right)\mathrm{erf}\ u\right\}du. \tag{70}$$

Integrating the above equation by parts,

$$A(\sqrt{E/2kT})=\frac{\sqrt{\pi}}{2c\exp\left(\frac{E-eV_1}{2kT}\right)}\left[\int_0^{\sqrt{E/2kT}}\cos\left\{c\exp\left[\frac{E-eV_1}{2kT}\right]\mathrm{erf}\ u\right\}du-\sqrt{E/2kT}\cos\left\{c\exp\left[\frac{E-eV_1}{2kT}\right]\mathrm{erf}\sqrt{E/2kT}\right\}\right]. \tag{71}$$

One observes that $A(\sqrt{E/2kT})=0$, for $c=0$ and $c=\infty$. Since the expression within brackets is always less than $2\sqrt{E/2kT}$ in absolute value,

$$A(\sqrt{E/2kT})<\frac{\sqrt{\pi}\sqrt{E/2kT}}{c\exp\left[\frac{E-eV_1}{2kT}\right]} \tag{72}$$

and

$$F(V_1,f)=\int_0^{V_1e}A^2(\sqrt{E/2kT})dE<\frac{\pi kT}{2c^2\exp(-eV_1/kT)}, \tag{73}$$

which gives an upper limit to $F(V_1,f)$ for very high frequencies.

Since $A^2(\sqrt{E/2kT})$ approaches zero as E/kT for E/kT small, and increases exponentially as $\exp(E/kT)$ for $E/kT>1$, and since one is interested in $\int_0^{eV_1}A^2dE$ for an upper limit $E/kT=eV_1/kT>10$, the contribution to the integral from large values of the argument far overshadows the contribution from small values of the argument. Hence, we may replace the value of $A(\sqrt{E/2kT})$ by its asypmtotic value for large values of the argument,

$$A(\sqrt{E/2kT})=\frac{c}{2\sqrt{2}}\exp\left(\frac{E-eV_1}{2kT}\right). \tag{77}$$

Physically, this means that despite their preponderance in numbers, the low-energy electrons, because of their small excursions toward the plate and consequent short transit times, contribute practically nothing toward the low-frequency noise spectrum.
Accordingly,

$$\int_0^{eV_1}A^2dE=\frac{kTc^2}{8},$$

(a) Low-Frequency Approximation

For a cathode temperature of about 1,000°K, and with a, the cathode-anode spacing expressed in millimeters as a_m, one has

$$c<5\times10^{-8}fa_m. \tag{74}$$

Since $E\leq eV_1$, one may approximate the sine of the argument in eq 71 by the argument for frequencies such that $c<0.3$.

$$A(\sqrt{E/2kT})=c\exp\left[\frac{E-eV_1}{2kT}\right]\int_0^{\sqrt{\frac{E}{2kT}}}ue^{-u^2}\operatorname{erf}u\,du. \tag{75}$$

Or, integrating by parts,

$$A(\sqrt{E/2kT})=\frac{c\exp\left(-\frac{eV_1}{2kT}\right)}{2}\left[\frac{\exp(E/2kT)}{\sqrt{2}}\operatorname{erf}\sqrt{E/2kT}-\operatorname{erf}\sqrt{E/2kT}\right]. \tag{76}$$

and

$$\overline{i^2}=eI_Pa^2\omega^2\frac{\pi M}{kT}\Delta f. \tag{78}$$

(The above formula holds only for

$$c=a\omega\sqrt{\pi M/4kT}<0.3).$$

2. Case 2: m^2 Large (I_p Small)

For this case, the potential energy of the electron is

$$U(x)=\frac{eV_1x}{a},$$

and the time, t, an electron reaches a point x, is given by

$$t=\sqrt{M/2}\,\frac{2a\sqrt{E}}{eV_1}\left[1-\sqrt{1-\frac{eV_1x}{Ea}}\right],\quad 0\leq t\leq t_0/2.$$

Following the same procedure as in case 1, one finds for the noise power absorbed by each load in the frequency interval Δf,

$$P=\frac{I_0eZ_0}{2kT}(4/eV_1)^2\int_0^{eV_1}E^2e^{-\frac{E}{kT}}\left\{\frac{\cos\sigma\sqrt{E}}{\sigma\sqrt{E}}-\frac{\sin\sigma\sqrt{E}}{\sigma^2E}\right\}^2dE\Delta f, \tag{79}$$

where

$$\sigma=\omega\sqrt{2M}\,a/eV_1.$$

The equivalent mean square fluctuation current through the diode is

$$\overline{i^2}=\frac{2I_0e}{kT}(4/eV_1)^2\int_0^{eV_1}E^2e^{-\frac{E}{kT}}\left\{\frac{\cos\sigma\sqrt{E}}{\sigma\sqrt{E}}-\frac{\sin\sigma\sqrt{E}}{\sigma^2E}\right\}^2dE\Delta f. \tag{80}$$

For low enough frequencies, such that $\sigma\sqrt{eV_1}<0.3$, the expression in brackets approximately equals $\sigma^2E/9$. Since also,

$$\int_0^{eV_1} E^3 e^{\frac{-E}{kT}} dE \simeq 6(kT)^4, \text{ for } eV_1/kT>10, \quad (81)$$

$$\overline{i^2}=\frac{128Ma^2\omega^2eI_0}{3\left(\frac{eV_1}{kT}\right)^4 kT}\Delta f. \quad (82)$$

For large values of V_1, or for high frequencies, the upper limit in eq 80 may be taken as infinity with negligible error. Accordingly, eq 80 may be rewritten as

$$\overline{i^2}=\frac{2I_0e}{kT}\left(\frac{4}{eV_1}\right)^2\int_0^\infty E^2 e^{\frac{-E}{kT}}\left\{\frac{\cos\sigma\sqrt{E}}{\sigma\sqrt{E}}-\frac{\sin\sigma\sqrt{E}}{\sigma^2E}\right\}^2 dE\Delta f. \quad (83)$$

In appendix 2 it is shown that

$$\int_0^\infty E^2 e^{\frac{-E}{kT}}\left\{\frac{\cos\sigma\sqrt{E}}{\sigma\sqrt{E}}-\frac{\sin\sigma\sqrt{E}}{\sigma^2E}\right\}^2 dE=\frac{(kT)^3}{2}\left\{(1+2w)e^{-w}F\left(\frac{1}{2},\frac{3}{2},w\right)-1\right\}, \quad (84)$$

where

$$w=\sigma^2kT, \quad (85)$$

and F is Kummer's function [12], also known as the confluent hypergeometric function.

Accordingly, the expression for $\overline{i^2}$ may be written,

$$\overline{i^2}=\frac{16I_0e}{\left(\frac{eV_1}{kT}\right)^2}\left\{(1+2w)e^{-w}F\left(\frac{1}{2},\frac{3}{2},w\right)-1\right\}\Delta f. \quad (86)$$

V. Equivalent Temperature of the Conductance Due to Space-Charge

The shunt conductance, g, of the space-charge within a diode has recently been calculated by Begovich [13], who finds[6]

$$g=\frac{4I_0e}{kT\left(\frac{eV_1}{kT}\right)^2}\left\{(1+2w)e^{-w}F\left(\frac{1}{2},\frac{3}{2},w\right)-1\right\}, \quad (87)$$

where w is defined above (eq 85) and $F\left(\frac{1}{2},\frac{3}{2},w\right)$ is the confluent hypergeometric function [12].

If the above value of g, and the value of $\overline{i^2}$ given by eq 86 are substituted in the Nyquist formula [24],

$$\overline{i^2}=4kT_{eq}g\Delta f,$$

where T_{eq} is the equivalent temperature of the conductance, it is immediately found that

$$T_{eq}=T, \quad (88)$$

in agreement with the experimental results obtained by Van der Ziel [3].

VI. Summary

1. A general expression for the noise power spectrum generated by the random emission of electrons of arbitrary trajectories within a waveguide is developed in section I.

2. A numerical solution of the potential distribution within a plane diode is effected in section II, and a family of curves from which the potential distribution may be obtained is graphed in figure 4. A graphical comparison between several actual potential distributions and their approximate representation is given in figure 5.

3. The results of sections I and II are utilized to derive the equivalent mean square fluctuation current due to the space charge within a diode for two types of a retarding potential distribution, namely, the linear distribution, and those distributions whose slope at the plate is small.

4. Utilizing the results of section III, and a recently computed value of the conductance due to the space charge within a diode, the equivalent noise temperature is shown to be equal to the cathode temperature.

The author is greatly indebted to K. F. Herzfeld for his many helpful discussions and generous guidance during the course of this work. Also, the writer is extremely grateful to H. Lyons, chief

[6] The writer is indebted to N. Begovich for a personal communication amplifying the material contained in reference [13].

of the Microwave Standards Section, National Bureau of Standards, for his wholehearted cooperation and valuable criticisms.

VIII. References

[1] C. N. Smyth, Nature **157**, 841 (1946).
[2] A. Van der Ziel, Nature **159**, 675 (1947).
[3] A. Versnel and A. Van der Ziel, Nature **159**, 640 (1947).
[4] For properties and applications of normal modes to waveguides, see H. Bethe, Formal theory of waveguides of arbitrary cross section, Radiation Laboratory Report 43–26 (Mar. 16, 1943).
[5] N. R. Campbell and V. J. Francis, J. Inst. Elec. Eng. **93**, 45, (1946).
[6] G. Campbell and R. Foster, Fourier integrals for practical applications, Bell Telephone System Monograph B–584, p. 39 (1931).
[7] T. C. Fry, Phys. Rev. **17**, 441 (1921).
[8] I. Langmuir, Phys. Rev. **21**, 419 (1923).
[9] M. Von Laue, Jahrbuch der Radioaktivitat und Electronik **15**, 204 (1918).
[10] B. J. Thompson, D. O. North, W. A. Harris, RCA Rev. **4**, 447 (Apr., 1940).
[11] A. J. Rack, Bell System Tech. J. **17**, 592 (Oct. 1938).
[12] T. M. MacRobert, Functions of a complex variable", p. 346, 3d ed. (1947).
[13] N. Begovich, High frequency loading, Bull. Am. Phys. Soc. **23**, No. 5 (June 24, 1948).
[14] H. Nyquist, Thermal agitation of electric charge in conductors, Phys. Rev. **32**, 110 (1928).
[15] J. W. Miles, The equivalent circuit for a plane discontinuity in a cylindrical waveguide, Inst. Radio Eng. **34**, 728 (Oct. 1946).
[16] T. M. MacRobert, Functions of a complex variable, 3d ed., p. 145 (Macmillian & Co., London, 1947).

VIII. Appendix 1

Let x,y be generalized coordinates suitable for describing the guide surface S, and z the usual cartesian coordinate which is parallel to the axis of the guide. The normal modes, $\boldsymbol{b}_j$ of electric type for a cylindrical guide are a doubly infinite set obtained by two independent processes [15,4].

$$\boldsymbol{b}_j=\nabla U_j\times\boldsymbol{k}, \tag{89}$$

where $\boldsymbol{k}$ is a unit vector in the z-direction, and where

$$\nabla^2U_j(x,y)+\beta_j^2U_j(x,y)=0, \tag{90}$$

and $\boldsymbol{n}\cdot\nabla U_j=0$ on S, the surface of the guide. $\boldsymbol{n}$ is normal to S.

$$\boldsymbol{b}_j=\beta_j^2v_j(x,y)\boldsymbol{k}\mp j\alpha\nabla v_j(x,y), \tag{91}$$[7]

[7] The v_j should not be confused with the letter v used in section I to represent velocity.

where $\nabla^2v_j+\beta_j^2v_j=0$, and $v_j=0$ on S, except for the TEM case for which $\beta_j=0$, and

$$\boldsymbol{n}\times\nabla v_j=0 \text{ on } S. \tag{92}$$

(The β_j are, in general, different for the U_j and v_j.)

If the U_j and v_j are normalized, that is,

$$\int_{S'}U_j^2da=\int_{S'}v_j^2da=1, \tag{93}$$

where the integral is taken over the transverse plane S' of the guide, then the following orthogonal properties may be demonstrated [15,4]:

$$\int_{S'}\boldsymbol{b}_j\cdot\boldsymbol{b}_hda=\delta_{jh}, \tag{94}$$

where $\delta_{jh}=0$, for $j\neq h$, and $\delta_{jh}=1$, for $j=h$.

$$\int_{S'}(\boldsymbol{b}_j\times\text{curl }\boldsymbol{b}_h)\cdot\boldsymbol{k}da=0 \text{ for all } j \text{ and } h. \tag{95}$$

The phase constant α corresponding to each $\boldsymbol{b}_j$ is given by

$$\alpha^2=\mu\epsilon\omega^2-\beta_j^2, \tag{96}$$

and $\boldsymbol{L}_j=\boldsymbol{b}_j\exp(\pm j\alpha z)$ satisfies the vector wave equation

$$\text{curl curl }\boldsymbol{L}_j=\mu\epsilon\omega^2\boldsymbol{L}_j. \tag{97}$$

Utilizing the above properties of the normal modes, the field within a guide excited by an arbitrary current distribution will be determined by a method due to Bethe [4].

Using Gauss' Theorem, if $\boldsymbol{A}$ and $\boldsymbol{D}$ are two arbitrary vectors,

$$\int_S[\boldsymbol{A}\times\text{curl }\boldsymbol{D}-\boldsymbol{D}\times\text{curl }\boldsymbol{A}]\cdot\boldsymbol{n}da=$$
$$\int_V(\boldsymbol{D}\cdot\nabla\times\nabla\times\boldsymbol{A}-\boldsymbol{A}\cdot\nabla\times\nabla\times\boldsymbol{D})d\tau, \tag{98}$$

where $\boldsymbol{n}$ is the outward drawn normal to S, enclosing the volume V whose element is $d\tau$. If one lets $\boldsymbol{A}=\boldsymbol{E}$, the electric field which satisfies

$$\text{curl curl }\boldsymbol{E}-\mu\epsilon\omega^2\boldsymbol{E}=-j\omega\mu\boldsymbol{J}, \tag{99}$$

where $\boldsymbol{J}$ is the current density, and lets $\boldsymbol{D}$ be a solution of

$$\nabla\times\nabla\times\boldsymbol{D}-\mu\epsilon\omega^2\boldsymbol{D}=0,$$

then eq 98 becomes

$$\int_S(\boldsymbol{E}\times\nabla\times\boldsymbol{D}-\boldsymbol{D}\times\nabla\times\boldsymbol{E})\cdot\boldsymbol{n}da=-\mu j\omega\int_V\boldsymbol{J}\cdot\boldsymbol{D}d\tau. \tag{100}$$

Consider a current element within the guide at $z=z'$, and take matched loads at the two planes, $z=0$ and $z=z_1$. Expanding the field E in terms of the normal modes, let

$$\left.\begin{aligned}\boldsymbol{E}&=\sum_j A_j\boldsymbol{b}_j \exp(-j\alpha_j z) z>z'\\ \boldsymbol{E}&=\sum C_j\boldsymbol{b}_j \exp(+j\alpha_j z) z<z'\end{aligned}\right\} \quad (101)$$

Since $\boldsymbol{E}$ is continuous at $z=z'$, and since the $\boldsymbol{b}_j$ are orthogonal,

$$A_j \exp(-j\alpha_j z')=C_j \exp(j\alpha_j z'). \quad (102)$$

If one substitutes the value of $\boldsymbol{E}$ given by eq 101 in eq 100, and lets $\boldsymbol{D}=\boldsymbol{b}_j \exp(-j\alpha_j z)$, and integrates the left side of eq 100 over the plane $z=0$, one gets

$$-\int_{z=0}\sum_h C_h[\boldsymbol{b}_h\times\nabla\times(\boldsymbol{b}_j \exp(-j\alpha_j z))$$
$$-\boldsymbol{b}_j\times\nabla\times(\boldsymbol{b}_h \exp(+j\alpha_h z)]\cdot\boldsymbol{k}da,$$

or,

$$-\sum_h C_h\int[\boldsymbol{b}_h\times\nabla\times\boldsymbol{b}_j-j\alpha_j\boldsymbol{b}_h\times(\boldsymbol{k}\times\boldsymbol{b}_j$$
$$-\boldsymbol{b}_j\times\nabla\times\boldsymbol{b}_h-j\alpha_h\boldsymbol{b}_j\times(\boldsymbol{k}\times\boldsymbol{b}_h)]\cdot\boldsymbol{k}da.$$

Because of the orthogonality relation (eq 96), the above simplifies to

$$-\sum_h C_h[-j\alpha_j\int\boldsymbol{b}_h\cdot\boldsymbol{b}_j da-j\alpha_h\int\boldsymbol{b}_j\cdot\boldsymbol{b}_h da=2C_j\alpha_j j.$$

The surface integral over the plane $z=z_1$ vanishes, and one has, from eq 100,

$$C_j=-\frac{\mu\omega}{2\alpha_j}\int_V \boldsymbol{J}\cdot\boldsymbol{b}_j \exp(-j\alpha_j z')d\tau. \quad (103)$$

Substituting eq 103 and eq 102 in eq 101, one finally gets

$$\boldsymbol{E}=-\frac{\mu\omega}{2}\sum_j\boldsymbol{b}_j\int\frac{\boldsymbol{J}\cdot\boldsymbol{b}_j \exp(-j\alpha_j|z'-z|)}{\alpha_j}d\tau. \quad (104)$$

IX. Appendix 2

Let

$$I=\int_0^\infty E^2 e^{-\frac{E}{kT}}\left\{\frac{\cos\sigma\sqrt{E}}{\sigma\sqrt{E}}-\frac{\sin\sigma\sqrt{E}}{\sigma^2 E}\right\}^2 dE, \quad (104)$$

$$\left\{\frac{\cos x}{x}-\frac{\sin x}{x^2}\right\}^2=2\sum_{j=1}^\infty(-1)^j\frac{(2x)^{2j-2}}{(2j)!}\frac{(j-1)}{(j+1)}, \quad (105)$$

which may be verified by performing the square, expressing the result in trigonometric functions of $2x$, and then substituting for each trigonometric function its corresponding infinite series and combining.

If we substitute, eq 105 in eq 104, we obtain

$$I=(kT)^3\sum_{j=1}^\infty(-1)^j 2^{2j-1}(\sigma^2 kT)^{j-1}\frac{(j-1)\gamma(j+2)}{(2j)!(j+1)}, \quad (106)$$

where we have utilized the formula for the gamma function,

$$\int_0^\infty x^{n-1}e^{-ax}dx=\frac{\gamma(n)}{a^n}. \quad (107)$$

Using the duplication formula [16] for the γ-function,

$$(2j)!=2^j\gamma(2j)=\frac{2^{2j}}{\sqrt{\pi}}\gamma(j+1)\gamma\left(j+\frac{1}{2}\right),$$

eq 106 simplifies to

$$I=\frac{(kT)^3}{2}\left\{\gamma\left(\frac{3}{2}\right)\sum_{j=0}^\infty\frac{(-\sigma^2 kT)^j}{\gamma\left(j+\frac{3}{2}\right)}-\gamma\left(\frac{1}{2}\right)\sum_{j=0}^\infty\frac{(-\sigma^2 kT)^j}{\gamma\left(j+\frac{1}{2}\right)}\right\}. \quad (108)$$

From MacRobert's definition of the confluent hypergeometric function, it follows that

$$F(\alpha,\rho,w)=\frac{\gamma(\rho)}{\gamma(\alpha)}\sum_{n=0}\frac{w^n\gamma(\alpha+n)}{\gamma(n+1)\gamma(\rho+n)}. \quad (109)$$

Accordingly, eq A 109 may be written

$$I=\frac{(kT)^3}{2}\left\{-F\left(1,\frac{1}{2},-w\right)+F\left(1,\frac{3}{2},-w\right)\right\}, \quad (110)$$

where $w=\sigma^2 kT$

However, since

$$F(1,\rho-1,-w)=1-\frac{\gamma(\rho-1)}{\gamma(\rho)}wF(1,\rho,-w), \quad (111)$$

$$I=\frac{(kT)^3}{2}\left\{(1+2w)F\left(1,\frac{3}{2},-w\right)-1\right\}. \quad (112)$$

Finally since

$$F(\alpha,\rho,w)=e^w F(\rho-\alpha,\rho,-w), \quad (113)$$

$$I=\frac{(kT)^3}{2}\left\{(1+2w)e^{-w}F\left(\frac{1}{2},\frac{3}{2},w\right)\right\}. \quad (114)$$

WASHINGTON, October 6, 1948.